

MODELING AND CONTROL OF QUADROTOR FORMATIONS CARRYING A
SLUNG LOAD

A THESIS SUBMITTED TO
THE GRADUATE SCHOOL OF NATURAL AND APPLIED SCIENCES
OF
MIDDLE EAST TECHNICAL UNIVERSITY

BY

SEGUN ARIYIBI

IN PARTIAL FULFILLMENT OF THE REQUIREMENTS
FOR
THE DEGREE OF DOCTOR OF PHILOSOPHY
IN
AEROSPACE ENGINEERING

JUNE 2019

Approval of the thesis:

**MODELING AND CONTROL OF QUADROTOR FORMATIONS
CARRYING A SLUNG LOAD**

submitted by **SEGUN ARIYIBI** in partial fulfillment of the requirements for the degree of **Doctor of Philosophy in Aerospace Engineering Department, Middle East Technical University** by,

Prof. Dr. Halil Kalipçılar Özgen
Dean, Graduate School of **Natural and Applied Sciences**

Prof. Dr. Ismail H. Tuncer
Head of Department, **Aerospace Engineering**

Prof. Dr. Ozan Tekinalp
Supervisor, **Aerospace Engineering, METU**

Examining Committee Members:

Prof. Dr. Ozan Tekinalp
Aerospace Engineering, METU

Prof. Dr. Mehmet Onder Efe
Computer Engineering, HACETTEPE

Assist. Prof. Dr. Ilkay Yavrucuk
Aerospace Engineering, METU

Date:

I hereby declare that all information in this document has been obtained and presented in accordance with academic rules and ethical conduct. I also declare that, as required by these rules and conduct, I have fully cited and referenced all material and results that are not original to this work.

Name, Surname: Segun Ariyibi

Signature :

ABSTRACT

MODELING AND CONTROL OF QUADROTOR FORMATIONS CARRYING A SLUNG LOAD

Ariyibi, Segun

Ph.D., Department of Aerospace Engineering

Supervisor: Prof. Dr. Ozan Tekinalp

June 2019, 140 pages

In this thesis, an algorithm for the autonomous formation flight of quadrotors carrying a slung load is developed. Full nonlinear models for a single quadrotor carrying a slung load as well as two and three quadrotors carrying a slung load problems are addressed. For the two and three quadrotor slung load systems, a leader-follower approach is employed to make the quadrotors fly in a fixed geometrical formation. The overall control algorithm employs a loop structure with a Lyapunov based formation guidance controller on the outermost loop. In the inner loop, two different approaches are employed. One approach uses linear quadratic tracking controllers to track the velocity commands to the quadrotors and the other approach utilizes a two-loop architecture where a linear quadratic tracking controller outputs a desired thrust vector direction which is then sent a Lyapunov function based quaternion parameterized nonlinear attitude controller. Simulations of our proposed algorithms is then carried out using the MATLAB/SIMULINK platform to test the efficacy of the control approaches employed.

Keywords: Unmanned Aerial Vehicle, Autonomous Formation flight, Lyapunov, Leader-follower approach, Quaternion attitude control, Slung Load, Quadrotors.

ÖZ

KOL UÇUŞUNDA SARKAN YÜK TAŞIYAN DÖRT PERVANELİLERİN MODELLEMESİ VE KONTROLÜ

Ariyibi, Segun

Doktora, Havacılık ve Uzay Mühendisliği Bölümü

Tez Yöneticisi: Prof. Dr. Ozan Tekinalp

Haziran 2019 , 140 sayfa

Bu tez çalışmasında otonom kol uçuşu yaparak birlikte yük taşıyan dört pervanelilerin (quadrotor) için uçuş kontrol algoritmaları geliştirilmiştir. Tek başında, veya iki üç dört pervanelinin birlikte yük taşımalarının doğrusal olmayan modelleri oluşturulmuştur. İkili ve üçlü sarkan yük taşıyan sistemlerin kol uçuşunda lider ve takipçi yaklaşımı kullanılmıştır. Kontrol algoritması çoklu kapalı döngü kullanmaktadır. En dış döngüde kol uçuşunun kontrolü için gerekli komutalar Lyapunov fonksiyonu temelli bir kontrolcü dört pervanelilere gerekli hız vektörü komutları üretilmektedir. İç döngüde ise iki farklı yaklaşım kullanılmıştır. Birinci yaklaşımda komut takip eden doğrusal karesel kontrolcü dış döngüden gelen hız komutları takip etmektedir. İkinci yaklaşımda ise iç içe iki döngü mevcuttur. Dış döngüde komut takip eden doğrusal karesel kontrolcü hız komutlarını itki vektörü komutlarına çevirmekte, iç döngüde ise dörtlük (quaternion) kullanan Lyapunov fonksiyonu temelli doğrusal olmayan yönelim kontrolcüsü kullanılmıştır. Kontrolcülerin etkinliğini ortaya koymak üzere yapılan benzetimler MATLAB/SIMULINK ortamında gerçekleştirilmiştir.

Anahtar Kelimeler: İnsansız Hava Aracı, Otonom Kol Uçuşu, Lider-Takipçi Yaklaşımı, Dörtlük Temelli Yönelim Kontrolü, Sarkan Yük, Dört Pervaneli.

To my family

ACKNOWLEDGMENTS

I would like to express my deepest and sincerest gratitude to my thesis supervisor, Prof. Dr. Ozan Tekinalp. Without his devotion, I would not have been able to complete this thesis. He provided invaluable ideas and shared with me his wealth of knowledge which facilitated the completion of the thesis.

TABLE OF CONTENTS

ABSTRACT	v
ÖZ	vii
ACKNOWLEDGMENTS	x
TABLE OF CONTENTS	xi
LIST OF TABLES	xv
LIST OF FIGURES	xvi
LIST OF ABBREVIATIONS	xxiv
CHAPTERS	
1 INTRODUCTION	1
1.1 Aim of the Thesis	1
1.2 Literature Survey	1
1.3 Contribution of the Thesis	7
1.4 Content of the Thesis	7
2 ONE QUADROTOR SLUNG LOAD SYSTEM	9
2.1 Equation of Motion for the Quadrotor Slung load System	9
2.2 Quadrotor Modelling	13
2.2.1 Control of Quadrotor	13
2.2.2 Dynamical Model of the Quadrotor	15

2.3	LQT Controller Design	17
2.3.1	Linearization of the Nonlinear Quadrotor Model	18
2.3.2	Velocity_x and Velocity_z LQT Controller Design	21
2.3.3	Velocity_y and Heading LQT Controller Design	22
2.4	One Quadrotor Slung Load System Results and Discussion	23
3	TWO QUADROTOR SLUNG LOAD SYSTEM	27
3.1	Equation of Motion for the Two Quadrotor Slung Load System	27
3.2	Formation-Hold Control System Approach	32
3.2.1	Lyapunov function based Formation Guidance Controller	33
3.3	Two Quadrotor Slung Load System Results and Discussion	35
4	THREE QUADROTOR SLUNG LOAD SYSTEM	41
4.1	Equation of Motion for the Three Quadrotor Slung Load System	41
4.2	Three Quadrotor Slung Load System Result and Discussion	45
5	TWO QUADROTOR SLUNG LOAD SYSTEM: QUATERNION BASED ATTITUDE CONTROL APPROACH	53
5.1	Problem Formulation and Implementation	54
5.1.1	Definition of the to-go quaternion	54
5.1.2	Mechanization of the Attitude Control	55
5.1.3	LQT Velocity Controller Design (Middle Loop)	57
5.1.4	Quaternion based Attitude Controller Design (Innermost Loop)	59
5.2	Two Quadrotor Slung Load System Result and Discussion (New Approach)	60
5.3	Alternative Approach: Full Nonlinear Control Algorithm for a Two Quadrotor Slung Load System	66

5.3.1	Alternative Approach: Full Nonlinear Control Algorithm Problem Formulation and Implementation	66
5.3.2	Guidance and Control Loop	67
5.3.3	Result and Discussion	68
6	ROBUSTNESS TEST FOR THE FULL NONLINEAR CONTROL ALGORITHM DESIGNED IN SECTION 5.3	79
6.1	Stability Robustness Test of the Nonlinear Controller	79
6.1.1	Stability Robustness of the Inner Loop Attitude Controller	80
6.1.2	Stability Robustness of the Outer Loop Formation Guidance Controller	82
6.1.3	Derivative of the Innerloop and Outerloop Lyapunov functions for a range of reaction force and torque	85
6.2	Performance Robustness Test of the Nonlinear Controller	87
6.2.1	Effects of Sensor Noise and Atmospheric Disturbances	87
6.2.2	Effects of Varying Load Weight	94
7	FULL NONLINEAR CONTROL ALGORITHM FOR A TWO QUADROTOR SLUNG LOAD SYSTEM WITH SLUNG DYNAMICS DISTURBANCE CANCELLATION	99
7.1	Outer loop Formation Guidance Algorithm with Disturbance Cancellation	99
7.2	Inner loop Attitude Control Algorithm with Disturbance Cancellation	100
7.3	Performance Comparison of the Control System with and without Disturbance Cancellation	101
8	MODELLING OF A TWO QUADROTOR SLUNG SYSTEM WITH FLEXIBLE BARS USING THE MSC ADAMS SOFTWARE	105
8.1	Two Quadrotor SLung Load System with Flexible Bar with MSC ADAMS	105
8.2	Two Quadrotor Slung Load System with Flexible Bar: Result and Discussion For the Control System designed in chapter 3	107

8.3	Two Quadrotor Slung Load System with Flexible Bar: Result and Discussion For the Control System designed in section 5.3	112
8.4	Performance Effects of Different Beam Stiffness on the Control System in section 8.3	117
8.4.1	Results and Discussion For Varying Beam Stiffness	117
9	SUMMARY AND CONCLUSIONS	121
9.1	Conclusion	121
9.2	Future Work	123
	REFERENCES	125
APPENDICES		
A	PERFORMANCE COMPARISON BETWEEN THE MSC ADAMS MODEL AND THE SIMULINK MODEL DESIGNED USING EQUATIONS OF MOTION	131
B	TWO QUADROTOR SLUNG LOAD SYSTEM EQUATION OF MOTION DERIVATION	135
	CURRICULUM VITAE	139

LIST OF TABLES

TABLES

Table 2.1 Definition of Symbols used in the Derivation of the Equations of Motion	11
Table 2.2 Properties of the Quadrotor, Load and Stiff Cable	20
Table 2.3 LQT Gains for the Velocity_x and Velocity_z Controller	21
Table 2.4 Eigenvalues of the Velocity_x and Velocity_z Controller	22
Table 2.5 LQT Gains for the Velocity_x and Heading Controller	23
Table 2.6 Eigenvalues of the Velocity_y and Heading Controller	23
Table 5.1 LQT Gains for the Velocity Controller with Thrust vector output . . .	58
Table 5.2 Eigenvalues of the Velocity_x and Velocity_z Controller	58
Table 5.3 Controller Settling Times	60
Table 5.4 Controller Settling Times (Full Nonlinear)	68
Table 8.1 Controller Settling Times (Full Nonlinear, Flexible Bar)	112
Table 8.2 Aluminium Beam Properties	117
Table B.1 Reference frames for the expression of components of dynamic entities	136

LIST OF FIGURES

FIGURES

Figure 1.1	Various Formation Geometries	3
Figure 2.1	One Quadrotor Slung Load System	10
Figure 2.2	Quadrotor Rotor Configuration	14
Figure 2.3	Velocity _x ,Velocity _z control system schematic	21
Figure 2.4	Velocity _y and Heading control system schematic	22
Figure 2.5	Quadrotor Velocity in x, y and z directions respectively (One Quadrotor)	25
Figure 2.6	Quadrotor and Load Position (One Quadrotor)	25
Figure 2.7	Swing, Rock and Heading Angles of the Load (One Quadrotor) .	26
Figure 2.8	Propeller Speeds of the Quadrotor (One Quadrotor)	26
Figure 3.1	Two Quadrotor Slung Load System	28
Figure 3.2	Two Quadrotor Slung Load System Rock Angle	31
Figure 3.3	Two Quadrotor Slung Load system Swing Angle (Left) and Heading Angle (Right)	32
Figure 3.4	Formation-Hold Control System Schematic	33
Figure 3.5	Leader Quadrotor Velocity in x, y and z directions respectively (Two Quadrotor)	37

Figure 3.6	Leader and Follower Quadrotor position and Load Position (Two Quadrotor)	38
Figure 3.7	Leader and Follower Quadrotor position and Load Position (Two Quadrotor, 40 secs simulation)	38
Figure 3.8	Leader and Follower Quadrotor relative positions (Two Quadrotor)	39
Figure 3.9	Swing, Rock and Heading Angles of the Load (Two Quadrotor)	39
Figure 3.10	Propeller Speeds of the Leader Quadrotor (Two Quadrotor)	40
Figure 3.11	Propeller Speeds of the Follower Quadrotor (Two Quadrotor)	40
Figure 4.1	Three Quadrotor Slung Load System	42
Figure 4.2	Three quadrotor formation geometry	45
Figure 4.3	Leader Quadrotor Velocity in x, y and z directions respectively (Three Quadrotor)	47
Figure 4.4	Leader and Follower Quadrotor position and Load Position (Three Quadrotor)	47
Figure 4.5	Leader and Follower Quadrotor position and Load Position (Three Quadrotor, 40 secs simulation)	48
Figure 4.6	Leader and 1st Follower Quadrotor relative positions (Three Quadrotor)	48
Figure 4.7	Leader and 2nd Follower Quadrotor relative positions (Three Quadrotor)	49
Figure 4.8	Swing, Rock and Heading Angles of the Load (Three Quadrotor)	49
Figure 4.9	Propeller Speeds of the Leader Quadrotor (Three Quadrotor)	50
Figure 4.10	Propeller Speeds of the 1st Follower Quadrotor (Three Quadrotor)	50

Figure 4.11	Propeller Speeds of the 2nd Follower Quadrotor (Three Quadrotor)	51
Figure 5.1	Two quadrotor slung load control system schematic: new approach	54
Figure 5.2	Current Thrust Vector, γ^B , Desired Thrust Vector, λ^B , Rotation Axis, η^B , Rotation Angle, β	56
Figure 5.3	LQT Velocity Control System with Thrust vector output	58
Figure 5.4	Leader Quadrotor Velocity in x, y and z directions respectively (Two Quadrotor, New Approach)	62
Figure 5.5	Leader and Follower Quadrotor position and Load Position (Two Quadrotor, New Approach)	62
Figure 5.6	Leader and Follower Quadrotor position and Load Position (Two Quadrotor, New Approach, 40 secs Simulation)	63
Figure 5.7	Leader and Follower Quadrotor relative positions (Two Quadrotor, New Approach)	63
Figure 5.8	Swing, Rock and Heading Angles of the Load (Two Quadrotor, New Approach)	64
Figure 5.9	Propeller Speeds of the Leader Quadrotor (Two Quadrotor, New Approach)	64
Figure 5.10	Propeller Speeds of the Follower Quadrotor (Two Quadrotor, New Approach)	65
Figure 5.11	Follower quadrotor guidance and control using a two loop approach	66
Figure 5.12	Leader Quadrotor Velocity in x, y and z directions respectively (Two Quadrotor, Alternative Approach)	70

Figure 5.13	Leader and Follower Quadrotor position and Load Position (Two Quadrotor, Alternative Approach)	70
Figure 5.14	Leader and Follower Quadrotor position and Load Position (Two Quadrotor, Alternative Approach, 40 secs simulation)	71
Figure 5.15	Leader and Follower Quadrotor relative positions (Two Quadrotor, Alternative Approach)	71
Figure 5.16	Swing, Rock and Heading Angles of the Load (Two Quadrotor, Alternative Approach)	72
Figure 5.17	Propeller Speeds of the Leader Quadrotor (Two Quadrotor, Alternative Approach)	72
Figure 5.18	Propeller Speeds of the Follower Quadrotor (Two Quadrotor, Alternative Approach)	73
Figure 5.19	Leader Quadrotor Velocity in x, y and z directions respectively (circular trajectory, Alternative Approach)	75
Figure 5.20	Leader and Follower Quadrotor position and Load Position (circular trajectory, Alternative Approach)	75
Figure 5.21	Leader and Follower Quadrotor relative positions (circular trajectory, Alternative Approach)	76
Figure 5.22	Swing, Rock and Heading Angles of the Load (circular trajectory, Alternative Approach)	76
Figure 5.23	Propeller Speeds of the Leader Quadrotor (circular trajectory, Alternative Approach)	77
Figure 5.24	Propeller Speeds of the Follower Quadrotor (circular trajectory, Alternative Approach)	77
Figure 6.1	Innerloop Lyapunov function derivative without slung load torque effect	81

Figure 6.2	Innerloop Lyapunov function derivative with slung load torque effect	81
Figure 6.3	Retuned Innerloop Lyapunov function derivative with slung load torque effect	82
Figure 6.4	Outerloop Lyapunov function derivative without slung load force effect	84
Figure 6.5	Outerloop Lyapunov function derivative with slung load force effect	84
Figure 6.6	Retuned Outerloop Lyapunov function derivative with slung load force effect	85
Figure 6.7	Retuned Outerloop Lyapunov function derivative with increasing slung load force effect	86
Figure 6.8	Retuned Innerloop Lyapunov function derivative with increasing slung load torque effect	86
Figure 6.9	Wind shear velocity profile in the 3-directions	89
Figure 6.10	Wind Gust velocity profile in the 3-directions	89
Figure 6.11	Combined Wind Shear and Gust velocity profile in the 3-directions	90
Figure 6.12	Leader Quadrotor Velocity in x, y and z directions respectively (Sensor noise, wind disturbance)	91
Figure 6.13	Leader and Follower Quadrotor position and Load Position (Sensor noise, wind disturbance)	91
Figure 6.14	Leader and Follower Quadrotor relative positions (Sensor noise, wind disturbance)	92
Figure 6.15	Swing, Rock and Heading Angles of the Load (Sensor noise, wind disturbance)	92

Figure 6.16	Propeller Speeds of the Leader Quadrotor (Sensor noise, wind disturbance)	93
Figure 6.17	Propeller Speeds of the Follower Quadrotor (Sensor noise, wind disturbance)	93
Figure 6.18	Leader Quadrotor Velocity in x, y and z directions respectively (Varying load)	95
Figure 6.19	Leader and Follower Quadrotor relative positions (Varying load)	95
Figure 6.20	Swing, Rock and Heading Angles of the Load (Varying load) . .	96
Figure 6.21	Propeller Speeds of the Leader Quadrotor (Varying load)	96
Figure 6.22	Propeller Speeds of the Follower Quadrotor (Varying load) . . .	97
Figure 6.23	Leader and Follower Quadrotor relative positions (Varying load, Retuned)	97
Figure 6.24	Swing, Rock and Heading Angles of the Load (Varying load, Retuned)	98
Figure 7.1	Leader Quadrotor Velocity in x, y and z directions respectively (Disturbance Cancellation)	102
Figure 7.2	Leader and Follower Quadrotor relative positions (Disturbance Cancellation)	103
Figure 7.3	Swing, Rock and Heading Angles of the Load (Disturbance Cancellation)	103
Figure 7.4	Propeller Speeds of the Leader Quadrotor (Disturbance Cancellation)	104
Figure 7.5	Propeller Speeds of the Follower Quadrotor (Disturbance Cancellation)	104

Figure 8.1	Two Quadrotor Slung Load System with Flexible Bar ADAMS Model	106
Figure 8.2	Two Quadrotor Slung Load System with Flexible Bar ADAMS to SIMULINK Model	106
Figure 8.3	Leader Quadrotor Velocity in x, y and z directions respectively (Two Quadrotor, Flexible Bar)	108
Figure 8.4	Leader and Follower Quadrotor position and Load Position (Two Quadrotor, Flexible Bar)	108
Figure 8.5	Leader and Follower Quadrotor position and Load Position (Two Quadrotor, Flexible Bar, 40 secs simulation)	109
Figure 8.6	Leader and Follower Quadrotor relative positions (Two Quadrotor, Flexible Bar)	109
Figure 8.7	Swing, Rock and Heading Angles of the Load (Two Quadrotor, Flexible Bar)	110
Figure 8.8	Swing, Rock and Heading Angles of the Load (Two Quadrotor, Rigid Bar)	110
Figure 8.9	Propeller Speeds of the Leader Quadrotor (Two Quadrotor, Flexible Bar)	111
Figure 8.10	Propeller Speeds of the Follower Quadrotor (Two Quadrotor, Flexible Bar)	111
Figure 8.11	Leader Quadrotor Velocity in x, y and z directions respectively (Flexible Bar, Alternative Approach)	113
Figure 8.12	Leader and Follower Quadrotor position and Load Position (Flexible Bar, Alternative Approach)	114
Figure 8.13	Leader and Follower Quadrotor position and Load Position (Flexible Bar, Alternative Approach, 40 secs simulation)	114

Figure 8.14	Leader and Follower Quadrotor relative positions (Flexible Bar, Alternative Approach)	115
Figure 8.15	Swing, Rock and Heading Angles of the Load (Flexible Bar, Alternative Approach)	115
Figure 8.16	Propeller Speeds of the Leader Quadrotor (Flexible Bar, Alternative Approach)	116
Figure 8.17	Propeller Speeds of the Follower Quadrotor (Flexible Bar, Alternative Approach)	116
Figure 8.18	Leader Quadrotor Velocity in x, y and z directions respectively (Flexible Bar, Stiffness Variation)	118
Figure 8.19	Leader and Follower Quadrotor relative positions (Flexible Bar, Stiffness Variation)	119
Figure 8.20	Swing, Rock and Heading Angles of the Load (Flexible Bar, Stiffness Variation)	119
Figure 8.21	Propeller Speeds of the Leader Quadrotor (Flexible Bar, Stiffness Variation)	120
Figure 8.22	Propeller Speeds of the Follower Quadrotor (Flexible Bar, Stiffness Variation)	120
Figure A.1	Comparison between leader quadrotor velocities	132
Figure A.2	Comparison between follower quadrotor velocities	132
Figure A.3	Comparisons between load angle deflections	133
Figure B.1	Two Quadrotor Slung Load System Free Body Diagram	135
Figure B.2	Free body Diagram of the Individual dynamic entities	136

LIST OF ABBREVIATIONS

VTOL	Vertical Take-off and Landing
LQT	Linear Quadratic Tracking
UAV	Unmanned Aerial Vehicle
ARE	Algebraic Ricatti Equation
ADAMS	Automated Dynamic Analysis of Mechanical Systems
c.g	Centre of Gravity

LIST OF UNITS

kg	Kilogram
deg	degree
m/s	Meter per Second
rpm	revolutions per minute
rad/s	radian per second
N	Newton

LIST OF SYMBOLS

g	Gravitational Acceleration
J_i	Inertia Matrix of the i th Quadrotor
J_{ci}	Inertia Matrix of i th Cable
J_L	Inertia Matrix of the Load
I_x, I_y, I_z	Moment of Inertia along the x,y and z axis respectively
F_i, T_i	Force and Torque of the i th Quadrotor
F_{ci}, T_{ci}	Force and Torque of the i th Cable

F_L, T_L	Force and Torque of the Load
F_{si}, T_{si}	Force and Torque of the i th Spherical Joint
ω_i	Angular Velocity of the i th Quadrotor
ω_{ci}	Angular Velocity of the i th cable
ω_L	Angular Velocity of the Load
C_a^b	Transformation Matrix from frame a to frame b
F_{qi}, T_{qi}	Force and Torque of the i th Quadrotor Propeller
ω_{qi}	Angular velocity of the i th Quadrotor Propeller
k_n	Constant that relates thrust generated by the propeller to its angular velocity
k_m	Constant that relates thrust generated by the propeller to its Torque
U_1, U_2, U_3, U_4	Quadrotor control inputs
K_t	Aerodynamic drag coefficient matrix for translational motion
d	Quadrotor arm length
p, q, r	Body angular velocities of the quadrotor.
ϕ	Quadrotor Roll Angle
θ	Quadrotor Pitch Angle
ψ	Quadrotor Heading angle
ϕ, θ, ψ	Quadrotor Euler Angles
ϕ_L, θ_L, ψ_L	Load Rock, Swing and Heading Angles
$s(), c(), t()$	sine, cosine and tangent function respectively

CHAPTER 1

INTRODUCTION

1.1 Aim of the Thesis

The aim of this thesis is to develop an algorithm for the autonomous formation flight of quadrotors carrying a slung load (also known as suspended load or sling load). The presence of the slung load in the system significantly alters the flying characteristics of the quadrotor, introduces additional degrees of freedom to the entire system and also complicates the dynamical equations of motion of the system, thereby presenting a challenge in the controller design. A full nonlinear system for the quadrotor-slung load system will be modelled and a control system is designed to fly the quadrotors in formation in spite of the presence of the slung load.

1.2 Literature Survey

A quadrotor is a rotary-wing UAV with hovering and vertical take-off and landing (VTOL) capabilities. Its dynamics is much simpler than that of a helicopter thereby enjoying the interest of researchers over many years. Quadrotors are used for various surveillance missions such as forest fire detection, livestock monitoring, and wildfire mapping; search and rescue missions and relief missions. They could also be used to easily take aerial images and videos by reporters and videographers as a result of their maneuverability and hovering capabilities. Quadrotors are able to easily transport foods, medicines and materials needed by disaster victims and are therefore being more and more invaluable in search and rescue missions. They are fast becoming standard equipment for search and rescue teams [1, 2].

A flight in which two or more aircrafts fly by maintaining the relative distance among them is called a formation flight. There are a lot of advantages of such flights [3,4]:

- Reduction in induced drag of fixed wing aircrafts in a V-formation flight results in a better fuel consumption rate thereby leading to an increased range.
- Aerial refuelling of the aircrafts in formation.
- Concentration of attack power by warplanes.
- In surveillance and reconnaissance missions, images with higher resolution can be obtained by overlapping the sensor data of the aircrafts in formation. Also, larger areas could be monitored more quickly.
- Formation flights in surveillance missions enables the synthesis of antennas with dimensions far larger than using a single aircraft thereby leading to an increased sensitivity of the antennas and consequently leading to better information gathering.
- Larger loads can be carried by the aircrafts in formation. This is the focus of this thesis.

Depending on the purpose as well as the numbers of aircrafts in a formation flight, numerous formation flight geometries exist. For a formation flight of more than two aircrafts, we have formation flight geometries such as the V-formation geometry, the finger-four formation geometry, wall formation geometry, ladder formation geometry, missing man formation geometry and so on. We will be utilizing a V-formation flight geometry for our three quadrotor slung load model. For a formation flight involving two aircrafts, formation flight geometries such as the echelon left geometry, echelon right geometry, line abreast geometry, trail formation geometry exist [5]. In all the above two-aircraft formation geometries listed, the leader and follower aircrafts are level with each other during the flight, but they could also be stepped, in which the leader and follower fly at different altitudes from each other. When the leader flies above the follower, it is called a stepped up formation geometry, and a stepped down formation geometry when the leader is below the follower aircraft [5]. We will be utilizing a line abreast formation flight for our two quadrotor slung load model.

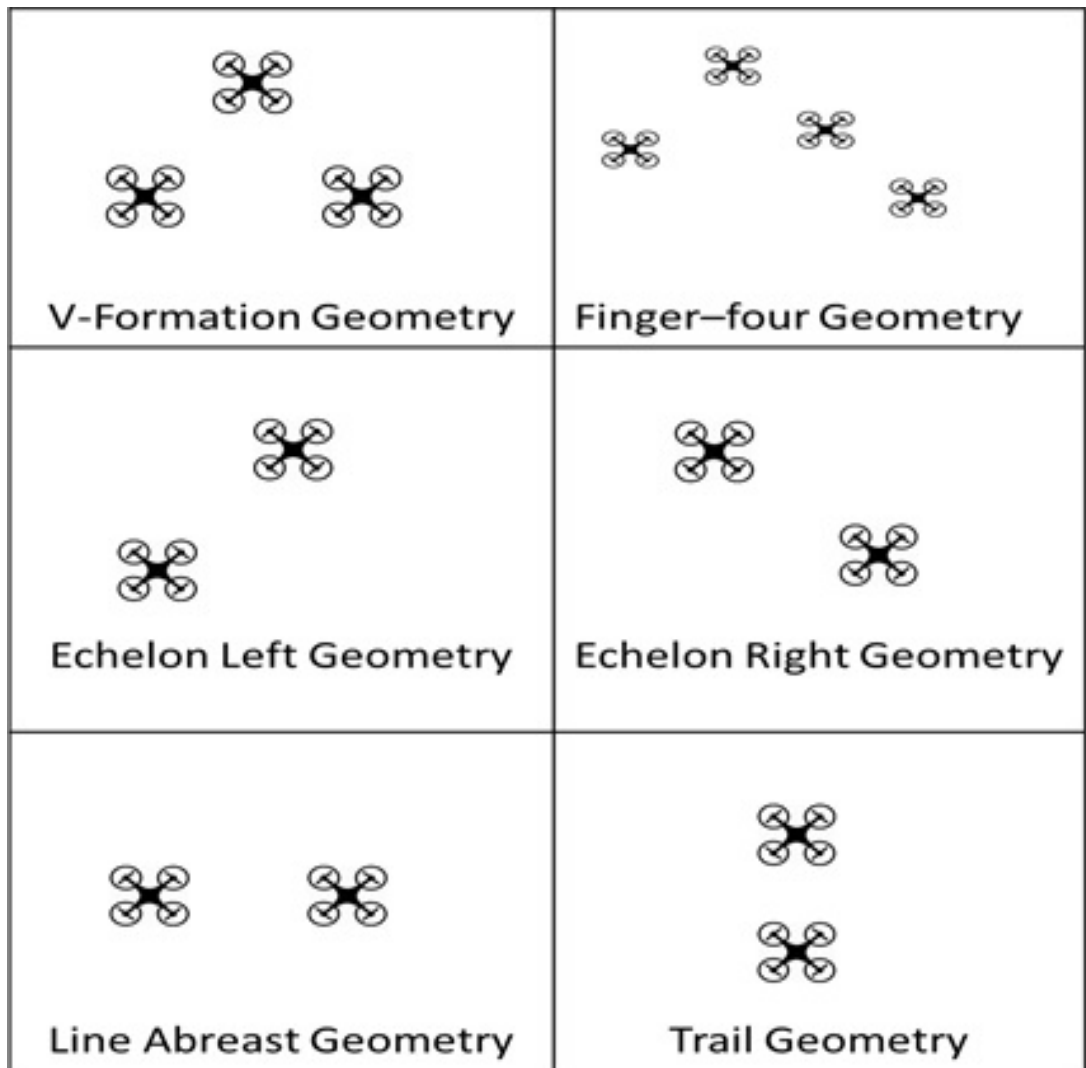


Figure 1.1: Various Formation Geometries

According to current legislation, a flight permit as well as pilot and aircraft certification is required for UAVs of over 4kg [6]. As a result, there is a predominance of quadrotors under 4 kg. As stated earlier, quadrotors are becoming invaluable in transporting foods, medicines and various supplies in search and rescue missions and thus, to carry heavier payloads, larger quadrotors will be needed. However, to circumvent this restriction on UAV flights over 4kg, various UAVs can be flown in formation to carry heavier loads. This load is usually carried by attaching it via a rope to the UAVs. Such a load, rope, UAV system is known as a slung load system. In our thesis, we will propose an algorithm for the autonomous formation flight of a two quadrotor slung load system and a three quadrotor slung load system as we believe that the quadrotor

slung load system will be a widespread approach in future search and rescue missions. There are a number of approaches to formation flight currently existing in literature. They include [7–11]:

- Leader-follower approach
- Virtual Leader approach
- Virtual Structure approach
- Virtual Reference Point approach
- Behavioral Approach
- Formation Graph Approach

The leader-follower approach is the most wide spread approach because of its ease of implementation. It is the also the approach used by manned formation flights. In the leader-follower approach, some of the aircrafts in the formation are designated as leader and the rest of the aircrafts are treated as followers. The leaders maintain a prescribed trajectory while the followers track a fixed relative distance from the neighboring aircraft. Thus, the formation behavior is prescribed by specifying the relative distances that the followers must maintain. The followers have the formation-hold autopilot implemented on them. The downside of this approach is that a rear aircraft usually exhibits a poorer response than its reference due to error propagation and it is not robust to leader's failure [7, 8]

The Virtual Leader approach was introduced to counter the problems of the Leader-Follower approach. In this approach, to create robustness to leader's failure, all the aircrafts in the formation receive the trajectory of a virtual leader. This trajectory is usually an ideal point in the formation that the corresponding aircraft must track. The downside of this approach is that the individual members of the formation have no idea about their relative distances to one another and subsequently, collision avoidance might be impossible [7]. In the virtual structure approach, the concept of leaders and followers is nonexistent. The constituent aircrafts of the formation are treated as if they were particles of a rigid body. In other words, the entire formation is treated

like a single rigid body structure, hence the name virtual structure [9, 12]. Due to the fact that the entire formation moves as a single rigid body and the individual members of the formation always maintain a fixed geometric relationship with one another, it is impossible to use this approach for formations that vary with time. Details about the other approaches can be found in [10, 11] and [13].

After choosing a formation approach, a control scheme is then selected. There are various nonlinear schemes used since the formation kinematics is nonlinear. Potential field method [14], constraint forces method [13], higher order sliding modes technique [15], adaptive output feedback method [16] are all examples of control schemes used in literature. In our previous work on formation flight, Lyapunov control approach as well as State-Dependent Ricatti Equations (SDRE) control approach were used and comparisons were made between them [17]. In this thesis, we will continue with the use of the Lyapunov control approach to formation flight on a leader-follower model designed in our previous masters' thesis work.

Flying a quadrotor with a slung load has not been extensively investigated in the literature [18]. The slung load dynamics significantly alters the flying characteristics of the quadrotor, presenting a challenge in controlling the UAV. The additional degrees of freedom of the load dynamics also significantly complicate the equations of motion of the quadrotor-slung load system. In this thesis, the approach presented by Stoneking for multi-body spacecrafts is employed to obtain the equations of motion for the modelling of our quadrotor slung load system. The building block equations are derived by applying Newton's and Euler's equations of motion to an "element" consisting of the number of bodies and number of joints in the system. Straightforward linear algebra operations are employed to eliminate extraneous constraint equations, resulting in a minimum-dimension system of equations to solve. This method thus combines a straightforward, easily-extendable, easily-mechanized formulation with an efficient computer implementation [19]. Using the Stoneking approach to modelling a multibody spacecraft, our quadrotor slung load system is modelled and a formation guidance controller is implemented on the system. After the selection of the formation guidance scheme, we must then select a control approach to ensure that our quadrotors track the reference signals coming from the formation guidance controller. There are a number of published works in literature about the control of

quadrotors. Some of these control approaches include sliding mode control [20,21], backstepping technique [22], PID controllers as well as linear quadratic control techniques [23], adaptive control [24] and fuzzy logic control [25].

In this thesis, two quadrotor control approaches are investigated. The first approach uses the Linear Quadratic Tracking (LQT) controller and the second approach uses a two-loop architecture in which a LQT controller in the outer loop tracks the translational velocities of the quadrotor and outputs a desired thrust vector direction which is then inputted into a Lyapunov function based quaternion nonlinear attitude controller in the inner loop. In the first control approach, Euler angle parametrization is utilized, while in the second quadrotor control approach, quaternion parameterization is employed. There are a number of advantages of using quaternions for attitude propagation such as the avoidance of singularity in the attitude propagation equations and the evaluation of trigonometric functions is also not required. Using quaternion parameterization is commonly used in the attitude control of Earth observation satellites when large slew angle maneuvers are needed [26]. The utilization of quaternions for quadrotor attitude control is becoming quite popular in literature. There have been a number of approaches proposed [27–29] and [30]. In [29], Tayebi uses a Lyapunov function that contained body angular velocities and quaternions. The attitude command signals in terms of roll, pitch and yaw commands were calculated from a position control algorithm and then converted to a quaternion command for the attitude control system. In [28], Reyes et.al, also use quaternions for attitude parameterization. A linear gain scheduled controller is then employed. In [27], Euler angles are used for attitude control and a sliding mode estimator and controller is used for the translational motion in a body fixed frame coordinate. In [30], the necessary thrust vector for the position control over a prescribed trajectory is first calculated, and then converted to an attitude trajectory by solving some nonlinear algebraic equations. Attitude control is then carried out using this trajectory via a linear controller. To use this linear controller, a new variable, which is the natural logarithm of the quaternions was used.

1.3 Contribution of the Thesis

The following are the contributions of this thesis:

1. A full dynamical nonlinear model of a one quadrotor, two quadrotor and three quadrotor slung load system is modelled.
2. A previously developed formation guidance algorithm for fixed wing UAVs is extended to two and three quadrotor slung load systems.
3. A new approach for the nonlinear control of quadrotors employing quaternion based nonlinear attitude control to generate desired thrust vector is presented.
4. An application of this new nonlinear control approach of quadrotors to a two quadrotor slung load system.
5. Modelling and simulation of a two quadrotor slung load system with flexible beams.

1.4 Content of the Thesis

In chapter 1, the definition and uses of quadrotors are discussed. Advantages, definition and the various types of formation flight geometries as well as the various approaches to tackle the autonomous formation flight of UAVs and the control algorithms used are also discussed. Various control approaches of quadrotors and the various approaches employed for the attitude of quadrotors using quaternion/Euler parametrizations are discussed.

In chapter 2, the nonlinear equations of motion of a single quadrotor slung load system is derived. The nonlinear model of the quadrotor used as well as its linearization for the implementation of the LQT controller to be implemented is discussed. The design of the LQT controller is also given. The performance of this controller on the nonlinear slung load model is presented.

In chapter 3, the nonlinear equations of motion of a two quadrotor slung load is derived. A Lyapunov based nonlinear formation guidance controller is then designed

and implemented on the two quadrotor slung load system. The performance of our control algorithm for the autonomous formation flight of our two quadrotor slung load system, which features the formation guidance controller on the outer loop and a LQT controller on the inner loop is presented.

In chapter 4, the nonlinear equations of motion of a three quadrotor slung load is derived. The control algorithm presented in chapter 3 is extended to the three quadrotor slung load system and its performance is presented.

In chapter 5, a nonlinear quaternion based attitude controller is presented. This controller is then implemented on the two quadrotor slung load system previously designed. The performance of this controller is also presented.

In chapter 6, a robustness analysis for the full nonlinear control scheme developed in chapter 5 is done. A stability and performance robustness test is done to see the limits of the control scheme.

chapter 7, the nonlinear control scheme designed in chapter 5 is modified to include the slung load reaction forces and torques as opposed to treating them as disturbances to the system as with the previous control designs. Simulations are given and comparisons with the previously designed controller are made

In chapter 8, using MSC ADAMS, which is a multibody dynamics simulation software, the two quadrotor slung load system is remodelled with flexible beams as opposed to the rigid beams used in the previous derivation. Our autonomous control algorithm is then tested against this model. A performance robustness test is also done by varying the stiffness of the flexible beams.

Finally, in chapter 9, conclusions are made from the performances of all the control algorithms developed. Also, recommendations for future works are given.

CHAPTER 2

ONE QUADROTOR SLUNG LOAD SYSTEM

In this chapter, the mathematical model of a single quadrotor slung load system is derived. The additional degrees of freedom of the load and cable dynamics significantly complicate the equations of motion of the quadrotor-slung load system. The approach previously proposed for multi-body spacecrafts is employed to model our quadrotor slung load system [19]. The building block equations are derived by applying Newton-Euler equations of motion to an "element" consisting of three bodies and two joints. In this case, the three bodies are the quadrotor, the load and the cable. The two joints are spherical joints through which the cable connects the quadrotor to the load. Straightforward linear algebra operations are employed to eliminate extraneous constraint equations, resulting in a minimum-dimension system of equations to solve. This method thus combines a straightforward, easily-extendable, easily-mechanized formulation with an efficient computer implementation.

2.1 Equation of Motion for the Quadrotor Slung load System

We assume that the cable connecting the quadrotor and load is stiff and with relatively negligible mass. It is attached to the quadrotor and load via spherical joints. The joint torques are assumed to be zero. Using the approach of Stoneking [19], the equations of motion are derived. The rotational equation for the quadrotor in the quadrotor fixed frame can be written as:

$$J_1 \dot{\omega}_1 = T_1 + T_{S_1} - \omega_1^\times J_1 \omega_1 + r_1^\times C_N^1 F_{S_1} \quad (21)$$

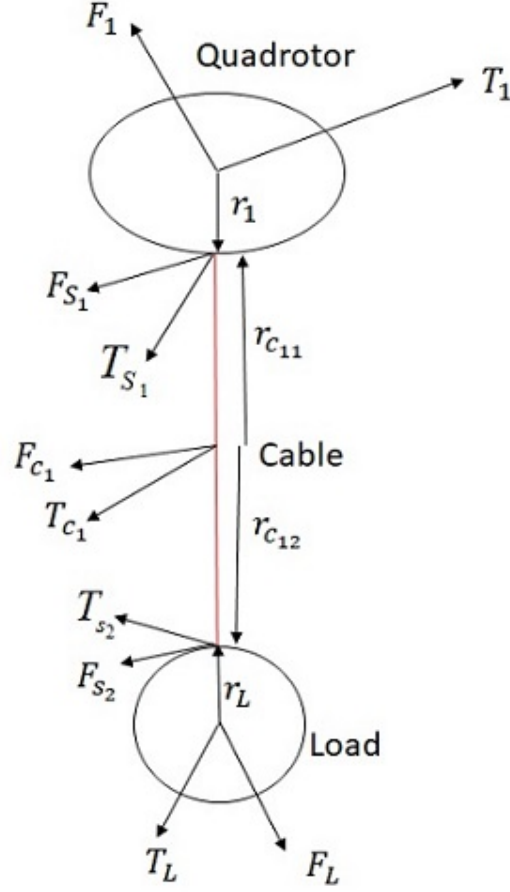


Figure 2.1: One Quadrotor Slung Load System

Similarly, the rotational equations of motion of the load in the load fixed frame as well as the cable in the cable fixed frame are:

$$\begin{aligned}
 J_{c_1} \dot{\omega}_{c_1} &= T_{c_1} - C_1^{c_1} T_{S_1} - r_{c_{11}}^\times C_N^{c_1} F_{S_1} + T_{s_2} + r_{c_{12}}^\times C_N^{c_1} F_{S_2} - \omega_{c_1}^\times J_{c_1} \omega_{c_1} \\
 J_L \dot{\omega}_L &= T_L - C_{c_1}^L T_{s_2} - r_L^\times C_N^L F_{S_2} - \omega_L^\times J_L \omega_L
 \end{aligned} \tag{22}$$

The translational equations for the Quadrotor, load and cable are written in the inertial frame:

$$\begin{aligned}
 m_1 \dot{v}_1 &= F_1 + F_{S_1} \\
 m_{c_1} \dot{v}_{c_1} &= F_{c_1} + F_{s_2} - F_{S_1} \\
 m_L \dot{v}_L &= F_L - F_{S_2}
 \end{aligned} \tag{23}$$

Table 2.1: Definition of Symbols used in the Derivation of the Equations of Motion

J_1, J_{c1}, J_L	Quadrotor, Cable and Load Inertias
F_1, T_1	Quadrotor Force and Torque
F_{c1}, T_{c1}	Cable Force and Torque
F_L, T_L	Load Force and Torque
F_{s1}, T_{s1}	Force and Torque at the first Spherical Joint connecting the cable to the Quadrotor
F_{s2}, T_{s2}	Force and Torque at the Second Spherical Joint connecting the cable to the Load
$\omega_1, \omega_{c1}, \omega_L$	Angular Velocity of Quadrotor, Cable and Load
r_1	Distance from quadrotor c.g to location of the spherical joint connecting the cable to the Quadrotor
r_L	Distance from Load c.g to location of the spherical joint connecting the cable to the Load
r_{c11}	Distance from cable c.g to location of the spherical joint connecting the cable to the Quadrotor
r_{c12}	Distance from cable c.g to location of the spherical joint connecting the cable to the Load
C_N^1	Transformation Matrix from inertial frame to quadrotor frame
C_N^{c1}	Transformation Matrix from inertial frame to cable frame
C_1^{c1}	Transformation Matrix from quadrotor frame to cable frame
C_{c1}^L	Transformation Matrix from cable frame to Load frame
C_N^L	Transformation Matrix from inertial frame to Load frame
ω_1^\times	Matrix to carry out cross product. ($\omega_1^\times r_1 = \omega_1 \times r_1$)
$\omega_1^{\times \times}$	Matrix to carry out cross product. ($\omega_1^{\times \times} r_1 = \omega_1 \times (\omega_1 \times r_1)$)

The constraint equations are obtained by equating the joint accelerations:

$$\begin{aligned}
 v_{S1} &= v_1 + \omega_1^\times r_1 = v_{c1} + \omega_{c1}^\times r_{c11} \\
 \dot{v}_1 + C_1^N \dot{\omega}_1^\times r_1 + C_1^N \omega_1^{\times \times} r_1 &= \dot{v}_{c1} + C_{c1}^N \dot{\omega}_{c1}^\times r_{c11} + C_{c1}^N \omega_{c1}^{\times \times} r_{c11} \\
 \Rightarrow \dot{v}_{c1} - \dot{v}_1 &= C_1^N \dot{\omega}_1^\times r_1 + C_1^N \omega_1^{\times \times} r_1 - C_{c1}^N \dot{\omega}_{c1}^\times r_{c11} - C_{c1}^N \omega_{c1}^{\times \times} r_{c11} \\
 v_{S2} &= v_{c1} + \omega_{c1}^\times r_{c12} = v_L + \omega_L^\times r_L \\
 \dot{v}_{c1} + C_{c1}^N \dot{\omega}_{c1}^\times r_{c12} + C_{c1}^N \omega_{c1}^{\times \times} r_{c12} &= \dot{v}_L + C_L^N \dot{\omega}_L^\times r_L + C_L^N \omega_L^{\times \times} r_L \\
 \Rightarrow \dot{v}_L - \dot{v}_{c1} &= C_{c1}^N \dot{\omega}_{c1}^\times r_{c12} + C_{c1}^N \omega_{c1}^{\times \times} r_{c12} - C_L^N \dot{\omega}_L^\times r_L - C_L^N \omega_L^{\times \times} r_L
 \end{aligned} \tag{24}$$

In vector-matrix form, all the above equations may be written as:

$$\begin{bmatrix} A & 0 & R \\ 0 & M & U \\ R^T & U^T & 0 \end{bmatrix} \begin{Bmatrix} \dot{x} \\ \dot{y} \\ f \end{Bmatrix} = \begin{Bmatrix} \tau \\ v \\ \vartheta \end{Bmatrix} \quad (25)$$

where

$$A = \begin{bmatrix} J_1 & 0 & 0 & 0 \\ 0 & J_{c_1} & 0 & 0 \\ 0 & 0 & J_L & 0 \\ 0 & 0 & 0 & m_1 I \end{bmatrix}, \quad R = \begin{bmatrix} -r_1^\times C_N^1 & 0 \\ r_{c_1}^\times C_N^{c_1} & -r_{c_1}^\times C_N^{c_1} \\ 0 & r_L^\times C_N^L \\ -I & 0 \end{bmatrix} \quad (26)$$

$$M = \begin{bmatrix} m_{c_1} I & 0 \\ 0 & m_L I \end{bmatrix}, \quad U = \begin{bmatrix} I & -I \\ 0 & I \end{bmatrix} \quad (27)$$

$$\tau = \begin{Bmatrix} T_1 - \omega_1^\times J_1 \omega_1 + T_{S_1} \\ T_{c_1} - \omega_{c_1}^\times J_{c_1} \omega_{c_1} - C_1^{c_1} T_{S_1} + T_{S_2} \\ T_L - \omega_L^\times J_L \omega_L - C_{c_1}^L T_{S_2} + T_{S_3} \\ F_1 \end{Bmatrix}, \quad (28)$$

$$v = \begin{Bmatrix} F_{c_1} \\ F_L \end{Bmatrix}, \quad \vartheta = \begin{Bmatrix} C_1^N \omega_1^{\times \times} r_1 - C_{c_1}^N \omega_{c_1}^{\times \times} r_{c_1} \\ C_{c_1}^N \omega_{c_1}^{\times \times} r_{c_1} - C_L^N \omega_L^{\times \times} r_L \end{Bmatrix}$$

$$\dot{x} = \begin{Bmatrix} \dot{\omega}_1 \\ \dot{\omega}_{c_1} \\ \dot{\omega}_L \\ \dot{v}_1 \end{Bmatrix}, \quad \dot{y} = \begin{Bmatrix} \dot{v}_{c_1} \\ \dot{v}_L \end{Bmatrix}, \quad f = \begin{Bmatrix} F_{s_1} \\ F_{s_2} \end{Bmatrix} \quad (29)$$

\dot{x} , \dot{y} and f can be decoupled in eqn. 25 by introducing unknown coefficient matrices α and β and performing row operations:

$$(A + \beta R^T) \dot{x} + (\alpha M + \beta U^T) \dot{y} + (R + \alpha U) f = \tau + \alpha v + \beta \vartheta \quad (210)$$

choose $\alpha = -RU^{-1}$, $\beta = RU^{-1}MU^{-T}$, then,

$$(A + \beta R^T) \dot{x} = \tau + \alpha v + \beta \vartheta \quad (211)$$

Once the above eqn. 211 is solved for \dot{x} , \dot{y} and f can then be easily computed from eqn. 25.

2.2 Quadrotor Modelling

A quadrotor is a rotary-wing UAV with hovering and vertical take-off and landing (VTOL) capabilities. As the name implies, a quadrotor has four motors. Each motor is connected to a fixed-pitch propeller. These propellers produce thrust forces independently if we assume that the coupling effects among them is negligible. The quadrotor is pitched or rolled by the differential thrusts of the propellers. It can also be yawed by the differential torques of the propellers. These differential thrusts and torques can be achieved by appropriately changing the angular velocities of the individual motors [31].

2.2.1 Control of Quadrotor

As stated earlier, a quadrotor can be controlled by creating differential thrusts and torques among the rotors. A typical quadrotor has a pair of rotors rotating in a clockwise direction, while the other pair rotates in a counterclockwise direction. Figure 2.2 shows the force and torque directions of the quadrotor model used in this thesis. The force and torque of the individual propellers can be related to its angular velocity through the following formulas [31]:

$$F_{qi} = k_n \omega_{qi}^2 \quad (212)$$

$$T_{qi} = k_m F_{qi} \quad (213)$$

In eqn. 212, k_n is a constant that relates the thrust generated by the propeller to its angular velocity. For the quadrotor used in this thesis, $k_n = 3.43 \times 10^{-7} N/rpm^2$. Similarly, In eqn. 213, k_m is a constant that relates the thrust to the torque generated by the propeller; $k_m = 0.016m$.

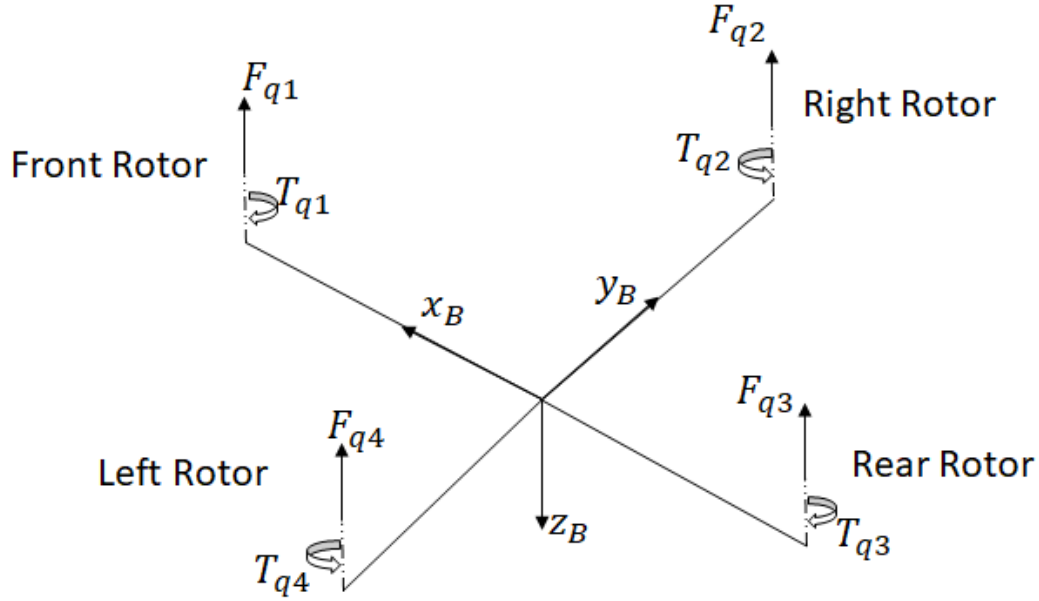


Figure 2.2: Quadrotor Rotor Configuration

To control the quadrotor, four control inputs can then be defined using the relations in equations 212 and 213. Let:

$$U_1 = F_{q1} + F_{q2} + F_{q3} + F_{q4} \quad (214)$$

$$U_2 = F_{q4} - F_{q2} \quad (215)$$

$$U_3 = F_{q1} - F_{q3} \quad (216)$$

$$U_4 = T_{q1} + T_{q3} - T_{q2} - T_{q4} \quad (217)$$

From eqn. 214 and fig. 2.2, the control input U_1 is the total force generated by the four propellers. This control input is used to change the altitude of the quadrotor, in other words, move the quadrotor in the z_B direction. Also, by changing the orientation of U_1 through rolling or pitching the quadrotor, we can move the quadrotor in the y_B direction or x_B direction respectively. From eqn. 215 and fig. 2.2, the control input U_2 is the differential thrust between the left and right rotor. U_2 is used to roll the quadrotor. From eqn. 216, we see that U_3 is the differential thrust between the front

and rear rotor. U_3 is used to pitch the quadrotor. U_4 from eqn. 217 is the net torque of the four rotors. U_4 is used to change the heading of the quadrotor.

As stated in section 2.2, quadrotors use fixed-pitch propellers. Thus, these control inputs can only be realized by appropriately adjusting the angular velocities of the rotors. We must therefore be able to relate these control inputs to the propeller angular velocities. By combining equations 212 through to 217, the following relation is obtained:

$$\begin{Bmatrix} U_1 \\ U_2 \\ U_3 \\ U_4 \end{Bmatrix} = \begin{bmatrix} k_n & k_n & k_n & k_n \\ 0 & -k_n & 0 & k_n \\ k_n & 0 & -k_n & 0 \\ k_n k_m & -k_n k_m & k_n k_m & -k_n k_m \end{bmatrix} \begin{Bmatrix} \omega_{q1}^2 \\ \omega_{q2}^2 \\ \omega_{q3}^2 \\ \omega_{q4}^2 \end{Bmatrix} \quad (218)$$

In addition, actuator dynamics for each rotor is modelled as:

$$\frac{20}{s + 20} \quad (219)$$

2.2.2 Dynamical Model of the Quadrotor

The nonlinear dynamical equations of motion of the quadrotor can be written using the Newton-Euler equations for translational and rotational motion. Based on the derivation from [31], the translational equations of motion is first derived in the quadrotor fixed frame and then converted into the earth fixed frame(Inertial Frame). The rotational equations are derived in the quadrotor fixed frame. The translational and rotational equations of motion for the quadrotor can be written in the quadrotor reference frame as [31]:

$$\sum F_{\text{net}} = m\dot{v}_B + \omega^\times m v_B \quad (220)$$

$$\sum M_{\text{net}} = J\dot{\omega} + \omega^\times J\omega \quad (221)$$

$\sum F_{\text{net}}$ and $\sum M_{\text{net}}$ are the net force and moment acting on the quadrotor expressed in the quadrotor fixed reference frame. The forces acting on the quadrotor are the

gravity, propulsive and aerodynamic forces. Therefore,

$$\sum F_{\text{net}} = F_{\text{gravity},B} + F_{\text{prop},B} + F_{\text{aero},B} = C_N^1 m \begin{bmatrix} 0 \\ 0 \\ g \end{bmatrix} - \begin{bmatrix} 0 \\ 0 \\ U_1 \end{bmatrix} - K_t v_B \quad (222)$$

likewise, the net moment acting on the quadrotor can be written as:

$$\sum M_{\text{net}} = M_{\text{prop},B} = \begin{bmatrix} U_2 d \\ U_3 d \\ U_4 \end{bmatrix} \quad (223)$$

where d is the quadrotor arm length, K_t is the aerodynamic drag coefficient diagonal matrix and U_1, U_2, U_3, U_4 are the quadrotor control inputs defined in section 2.2.1. Combining equations 220 through to 223 and carrying out the necessary simplifications as derived in [31], the translational velocity of the quadrotor written in the inertial reference frame and the rotational equation of motion in the quadrotor fixed reference frame can be written as:

$$\begin{bmatrix} \dot{v}_x \\ \dot{v}_y \\ \dot{v}_z \end{bmatrix} = \begin{bmatrix} 0 \\ 0 \\ g \end{bmatrix} - C_1^N \begin{bmatrix} 0 \\ 0 \\ U_1/m \end{bmatrix} - (K_t/m) \begin{bmatrix} v_x \\ v_y \\ v_z \end{bmatrix} \quad (224)$$

$$\begin{bmatrix} \dot{p} \\ \dot{q} \\ \dot{r} \end{bmatrix} = \begin{bmatrix} (I_y - I_z)qr/I_x \\ (I_z - I_x)pr/I_y \\ (I_x - I_y)pq/I_z \end{bmatrix} + \begin{bmatrix} U_2 d/I_x \\ U_3 d/I_y \\ U_4/I_z \end{bmatrix} \quad (225)$$

The rate of change of euler angles of the quadrotor can be written as follows [32]:

$$\begin{bmatrix} \dot{\phi} \\ \dot{\theta} \\ \dot{\psi} \end{bmatrix} = \begin{bmatrix} 1 & \sin(\phi) \tan(\theta) & \cos(\phi) \tan(\theta) \\ 0 & \cos(\phi) & -\sin(\phi) \\ 0 & \sin(\phi)/\cos(\theta) & \cos(\phi)/\cos(\theta) \end{bmatrix} \begin{bmatrix} p \\ q \\ r \end{bmatrix} \quad (226)$$

Equations 224, 225 and 226 give the nonlinear dynamical equations of motion of a quadrotor.

2.3 LQT Controller Design

For the single quadrotor slung load system modelled in this thesis, two LQT controllers were designed. One controller was designed to track the inertial reference velocities in the x and z direction and the other controller was designed to track both the heading of the quadrotor and the inertial velocity in the y direction. The dynamics of the load and rigid cable were not included in the design of the controllers. However, our controllers were tested against the nonlinear slung load model designed in section 2.1. In other words, the cable and load dynamics are treated as disturbances to the control system.

Given the following linear completely controllable and observable system: [33]

$$\begin{aligned}\dot{\mathbf{x}}(t) &= \mathbf{A}(t)\mathbf{x}(t) + \mathbf{B}(t)\mathbf{u}(t) \\ \mathbf{y}(t) &= \mathbf{C}(t)\mathbf{x}(t)\end{aligned}\tag{227}$$

Find the controller that minimizes the following performance index:

$$\lim_{t_f \rightarrow \infty} J = \lim_{t_f \rightarrow \infty} \frac{1}{2} \int_{t_0}^{t_f} [\mathbf{e}^t(t)\mathbf{Q}(t)\mathbf{e}(t) + \mathbf{u}^t(t)\mathbf{R}(t)\mathbf{u}(t)]dt\tag{228}$$

where the reference input $\mathbf{z}(t)$ and the error $\mathbf{e}(t) = \mathbf{z}(t) - \mathbf{y}(t)$ yield the following algebraic Ricatti and auxiliary equation to be solved:

$$-\mathbf{P}\mathbf{A} - \mathbf{A}^t\mathbf{P} + \mathbf{P}\mathbf{B}\mathbf{R}^{-1}\mathbf{B}^t\mathbf{P} - \mathbf{C}^t\mathbf{Q}\mathbf{C} = \mathbf{0}\tag{229}$$

$$\mathbf{g}(t) = [\mathbf{P}\mathbf{E} - \mathbf{A}^t]^{-1}\mathbf{W}\mathbf{z}(t)\tag{230}$$

where

$$\mathbf{E} = \mathbf{B}\mathbf{R}^{-1}\mathbf{B}^t\tag{231}$$

$$\mathbf{W} = \mathbf{C}^t\mathbf{Q}\tag{232}$$

then the optimal control law becomes:

$$\mathbf{u}(t) = -\mathbf{R}^{-1}\mathbf{B}^t[\mathbf{P}\mathbf{x}(t) - \mathbf{g}(t)]\tag{233}$$

or

$$\mathbf{u}(t) = \mathbf{K}\mathbf{x}(t) + \mathbf{K}_z\mathbf{z}(t)\tag{234}$$

where

$$\begin{aligned}\mathbf{K} &= -\mathbf{R}^{-1}\mathbf{B}^t\mathbf{P} \\ \mathbf{K}_Z &= \mathbf{R}^{-1}\mathbf{B}^t[\mathbf{P}\mathbf{E} - \mathbf{A}^t]^{-1}\mathbf{W}\end{aligned}\tag{235}$$

2.3.1 Linearization of the Nonlinear Quadrotor Model

To design our LQT controllers using the algorithm presented in section 2.3, the nonlinear quadrotor model derived in section 2.2.2 needs to be linearized.

Expanding equations 224 through to 226, we have:

$$\dot{v}_x = -(c(\phi)s(\theta)c(\psi))\frac{U_1}{m} - (s(\phi)s(\psi))\frac{U_1}{m} - \frac{k_x}{m}v_x = f_1\tag{236}$$

$$\dot{v}_y = -(c(\phi)s(\theta)s(\psi))\frac{U_1}{m} + (s(\phi)s(\psi))\frac{U_1}{m} - \frac{k_y}{m}v_y = f_5\tag{237}$$

$$\dot{v}_z = g - (c(\phi)c(\theta))\frac{U_1}{m} - \frac{k_z}{m}v_z = f_2\tag{238}$$

$$\dot{p} = \frac{I_y - I_z}{I_x}qr + \frac{d}{I_x}U_2 = f_6\tag{239}$$

$$\dot{q} = \frac{I_z - I_x}{I_y}pr + \frac{d}{I_y}U_3 = f_3\tag{240}$$

$$\dot{r} = \frac{I_x - I_y}{I_z}pq + \frac{1}{I_z}U_4 = f_7\tag{241}$$

$$\dot{\phi} = p + (s(\phi)t(\theta))q + (c(\phi)t(\theta))r = f_8\tag{242}$$

$$\dot{\theta} = c(\phi)q - s(\phi)r = f_4\tag{243}$$

$$\dot{\psi} = \frac{s(\phi)}{c(\theta)}q + \frac{c(\phi)}{c(\theta)}r = f_9\tag{244}$$

The above equations were linearized at the following equilibrium points:

$v_{x_e} = v_{y_e} = v_{z_e} = 0$; $p_e = q_e = r_e = 0$; $\phi_e = \theta_e = \psi_e = 0$; $U_{2_e}, U_{3_e}, U_{4_e} = 0$ and $U_{1_e} = mg$

By evaluating the matrices below at the given the equilibrium points, the linearized equations can be obtained in state-space form [34]:

$$[A] = \begin{bmatrix} \frac{\partial f_1}{\partial v_x} & \frac{\partial f_1}{\partial v_z} & \frac{\partial f_1}{\partial q} & \frac{\partial f_1}{\partial \theta} & \frac{\partial f_1}{\partial v_y} & \frac{\partial f_1}{\partial p} & \frac{\partial f_1}{\partial r} & \frac{\partial f_1}{\partial \phi} & \frac{\partial f_1}{\partial \psi} \\ \frac{\partial f_2}{\partial v_x} & \frac{\partial f_2}{\partial v_z} & \frac{\partial f_2}{\partial q} & \frac{\partial f_2}{\partial \theta} & \frac{\partial f_2}{\partial v_y} & \frac{\partial f_2}{\partial p} & \frac{\partial f_2}{\partial r} & \frac{\partial f_2}{\partial \phi} & \frac{\partial f_2}{\partial \psi} \\ \frac{\partial f_3}{\partial v_x} & \frac{\partial f_3}{\partial v_z} & \frac{\partial f_3}{\partial q} & \frac{\partial f_3}{\partial \theta} & \frac{\partial f_3}{\partial v_y} & \frac{\partial f_3}{\partial p} & \frac{\partial f_3}{\partial r} & \frac{\partial f_3}{\partial \phi} & \frac{\partial f_3}{\partial \psi} \\ \frac{\partial f_4}{\partial v_x} & \frac{\partial f_4}{\partial v_z} & \frac{\partial f_4}{\partial q} & \frac{\partial f_4}{\partial \theta} & \frac{\partial f_4}{\partial v_y} & \frac{\partial f_4}{\partial p} & \frac{\partial f_4}{\partial r} & \frac{\partial f_4}{\partial \phi} & \frac{\partial f_4}{\partial \psi} \\ \frac{\partial f_5}{\partial v_x} & \frac{\partial f_5}{\partial v_z} & \frac{\partial f_5}{\partial q} & \frac{\partial f_5}{\partial \theta} & \frac{\partial f_5}{\partial v_y} & \frac{\partial f_5}{\partial p} & \frac{\partial f_5}{\partial r} & \frac{\partial f_5}{\partial \phi} & \frac{\partial f_5}{\partial \psi} \\ \frac{\partial f_6}{\partial v_x} & \frac{\partial f_6}{\partial v_z} & \frac{\partial f_6}{\partial q} & \frac{\partial f_6}{\partial \theta} & \frac{\partial f_6}{\partial v_y} & \frac{\partial f_6}{\partial p} & \frac{\partial f_6}{\partial r} & \frac{\partial f_6}{\partial \phi} & \frac{\partial f_6}{\partial \psi} \\ \frac{\partial f_7}{\partial v_x} & \frac{\partial f_7}{\partial v_z} & \frac{\partial f_7}{\partial q} & \frac{\partial f_7}{\partial \theta} & \frac{\partial f_7}{\partial v_y} & \frac{\partial f_7}{\partial p} & \frac{\partial f_7}{\partial r} & \frac{\partial f_7}{\partial \phi} & \frac{\partial f_7}{\partial \psi} \\ \frac{\partial f_8}{\partial v_x} & \frac{\partial f_8}{\partial v_z} & \frac{\partial f_8}{\partial q} & \frac{\partial f_8}{\partial \theta} & \frac{\partial f_8}{\partial v_y} & \frac{\partial f_8}{\partial p} & \frac{\partial f_8}{\partial r} & \frac{\partial f_8}{\partial \phi} & \frac{\partial f_8}{\partial \psi} \\ \frac{\partial f_9}{\partial v_x} & \frac{\partial f_9}{\partial v_z} & \frac{\partial f_9}{\partial q} & \frac{\partial f_9}{\partial \theta} & \frac{\partial f_9}{\partial v_y} & \frac{\partial f_9}{\partial p} & \frac{\partial f_9}{\partial r} & \frac{\partial f_9}{\partial \phi} & \frac{\partial f_9}{\partial \psi} \end{bmatrix} \quad (245)$$

$$[B] = \begin{bmatrix} \frac{\partial f_1}{\partial U_1} & \frac{\partial f_1}{\partial U_2} & \frac{\partial f_1}{\partial U_3} & \frac{\partial f_1}{\partial U_4} \\ \frac{\partial f_2}{\partial U_1} & \frac{\partial f_2}{\partial U_2} & \frac{\partial f_2}{\partial U_3} & \frac{\partial f_2}{\partial U_4} \\ \frac{\partial f_3}{\partial U_1} & \frac{\partial f_3}{\partial U_2} & \frac{\partial f_3}{\partial U_3} & \frac{\partial f_3}{\partial U_4} \\ \frac{\partial f_4}{\partial U_1} & \frac{\partial f_4}{\partial U_2} & \frac{\partial f_4}{\partial U_3} & \frac{\partial f_4}{\partial U_4} \\ \frac{\partial f_5}{\partial U_1} & \frac{\partial f_5}{\partial U_2} & \frac{\partial f_5}{\partial U_3} & \frac{\partial f_5}{\partial U_4} \\ \frac{\partial f_6}{\partial U_1} & \frac{\partial f_6}{\partial U_2} & \frac{\partial f_6}{\partial U_3} & \frac{\partial f_6}{\partial U_4} \\ \frac{\partial f_7}{\partial U_1} & \frac{\partial f_7}{\partial U_2} & \frac{\partial f_7}{\partial U_3} & \frac{\partial f_7}{\partial U_4} \\ \frac{\partial f_8}{\partial U_1} & \frac{\partial f_8}{\partial U_2} & \frac{\partial f_8}{\partial U_3} & \frac{\partial f_8}{\partial U_4} \\ \frac{\partial f_9}{\partial U_1} & \frac{\partial f_9}{\partial U_2} & \frac{\partial f_9}{\partial U_3} & \frac{\partial f_9}{\partial U_4} \end{bmatrix} \quad (246)$$

Evaluating the above matrices $[A]$, $[B]$ and separating the longitudinal and lateral states, we obtained the following system matrices:

$$A_{long} = \begin{bmatrix} \frac{-k_x}{m} & 0 & 0 & -g \\ 0 & \frac{-k_z}{m} & 0 & 0 \\ 0 & 0 & 0 & 0 \\ 0 & 0 & 1 & 0 \end{bmatrix}, B_{long} = \begin{bmatrix} 0 & 0 \\ \frac{-1}{m} & 0 \\ 0 & \frac{d}{I_y} \\ 0 & 0 \end{bmatrix}, x_{long} = \begin{bmatrix} v_x \\ v_z \\ q \\ \theta \end{bmatrix}, \mathbf{u}_{long} = \begin{bmatrix} U_1 \\ U_3 \end{bmatrix} \quad (247)$$

where A_{long} and B_{long} are the longitudinal system matrices, x_{long} contain the longitu-

dinal states and u_{long} contain the longitudinal control inputs.

$$A_{late} = \begin{bmatrix} \frac{-k_y}{m} & 0 & 0 & g & 0 \\ 0 & 0 & 0 & 0 & 0 \\ 0 & 0 & 0 & 0 & 0 \\ 0 & 1 & 0 & 0 & 0 \\ 0 & 0 & 1 & 0 & 0 \end{bmatrix}, B_{late} = \begin{bmatrix} 0 & 0 \\ \frac{d}{I_x} & 0 \\ 0 & \frac{1}{I_z} \\ 0 & 0 \\ 0 & 0 \end{bmatrix}, x_{late} = \begin{bmatrix} v_y \\ p \\ r \\ \phi \\ \psi \end{bmatrix}, u_{late} = \begin{bmatrix} U_2 \\ U_4 \end{bmatrix} \quad (248)$$

where A_{late} and B_{late} are the lateral system matrices, x_{late} contain the lateral states and u_{late} contain the lateral control inputs.

Table 2.2: Properties of the Quadrotor, Load and Stiff Cable

Quadrotor Mass, m	0.65 kg
Load Mass, m_L	0.2 kg
Cable mass, m_{c1}	0.01 kg
Cable Length, $r_{c11} + r_{c12}$	1 m
Load Radius, r_L	0.5 m
Quadrotor Arm length, d	0.23 m
Quadrotor Inertia Matrix, J_1	$\begin{bmatrix} 7.5 \times 10^{-3} & 0 & 0 \\ 0 & 7.5 \times 10^{-3} & 0 \\ 0 & 0 & 1.3 \times 10^{-2} \end{bmatrix}$
Load Inertia Matrix, J_L	$\begin{bmatrix} 2.0 \times 10^{-2} & 0 & 0 \\ 0 & 2.0 \times 10^{-2} & 0 \\ 0 & 0 & 2.0 \times 10^{-2} \end{bmatrix}$
Cable Inertia Matrix, J_{c1}	$\begin{bmatrix} 8.3 \times 10^{-4} & 0 & 0 \\ 0 & 8.3 \times 10^{-4} & 0 \\ 0 & 0 & 1.0 \times 10^{-7} \end{bmatrix}$
Drag Coefficient Matrix, K_t	$\begin{bmatrix} 0.1 & 0 & 0 \\ 0 & 0.1 & 0 \\ 0 & 0 & 0.1 \end{bmatrix} N/(m/s)$

2.3.2 Velocity_x and Velocity_z LQT Controller Design

As stated earlier in section 2.3, one controller was designed to track the quadrotor inertial velocities in the x and z direction. To design this controller, the linearized longitudinal system matrices obtained in eqn. 247 was used. The controller gains were obtained using the algorithm detailed in section 2.3. Using the values from table 2.2, the longitudinal system matrices are:

$$A_{long} = \begin{bmatrix} -0.15 & 0 & 0 & -9.81 \\ 0 & -0.15 & 0 & 0 \\ 0 & 0 & 0 & 0 \\ 0 & 0 & 1 & 0 \end{bmatrix}, B_{long} = \begin{bmatrix} 0 & 0 \\ -1.54 & 0 \\ 0 & 30.67 \\ 0 & 0 \end{bmatrix} \quad (249)$$

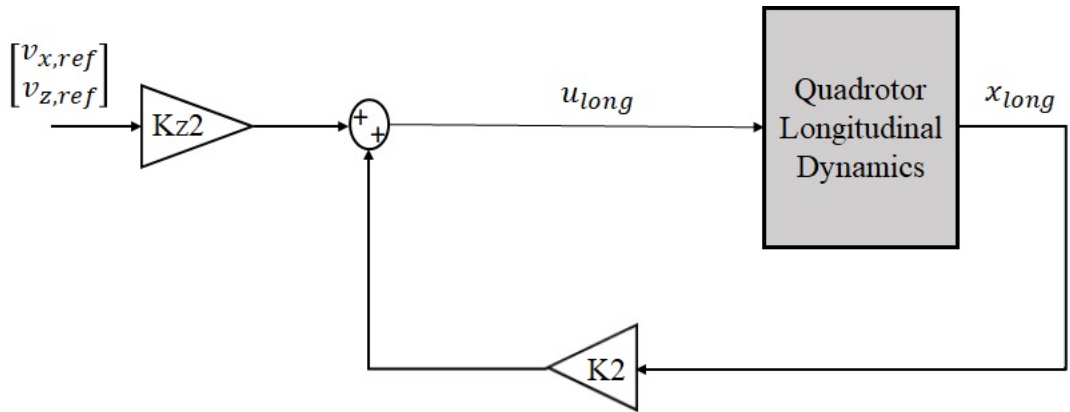


Figure 2.3: Velocity_x, Velocity_z control system schematic

Table 2.3: LQT Gains for the Velocity_x and Velocity_z Controller

K2				Kz2	
0	49.90	0	0	0	-50
0.96	0	-0.43	-2.86	-1	0

The real part of all the eigenvalues in table 2.4 are all negative. Thus, we have an asymptotically stable system. This controller will then be tested against the nonlinear one quadrotor slung load model.

Table 2.4: Eigenvalues of the Velocity_x and Velocity_z Controller

Eigenvalues
-6.70
-3.35+5.80i
-3.35+5.80i
-76.92

2.3.3 Velocity_y and Heading LQT Controller Design

As stated earlier in section 2.3 as well, a second LQT controller is also designed to track the inertial velocity in the y direction as well as the heading of the quadrotor. To design this controller, the linearized lateral system matrices obtained in eqn. 248 was used. The controller gains were obtained using the algorithm detailed in section 2.3. Using the values from table 2.2, the lateral system matrices are:

$$A_{late} \begin{bmatrix} -0.15 & 0 & 0 & 9.81 & 0 \\ 0 & 0 & 0 & 0 & 0 \\ 0 & 0 & 0 & 0 & 0 \\ 0 & 1 & 0 & 0 & 0 \\ 0 & 0 & 1 & 0 & 0 \end{bmatrix}, B_{late} = \begin{bmatrix} 0 & 0 \\ 30.67 & 0 \\ 0 & 76.92 \\ 0 & 0 \\ 0 & 0 \end{bmatrix} \quad (250)$$

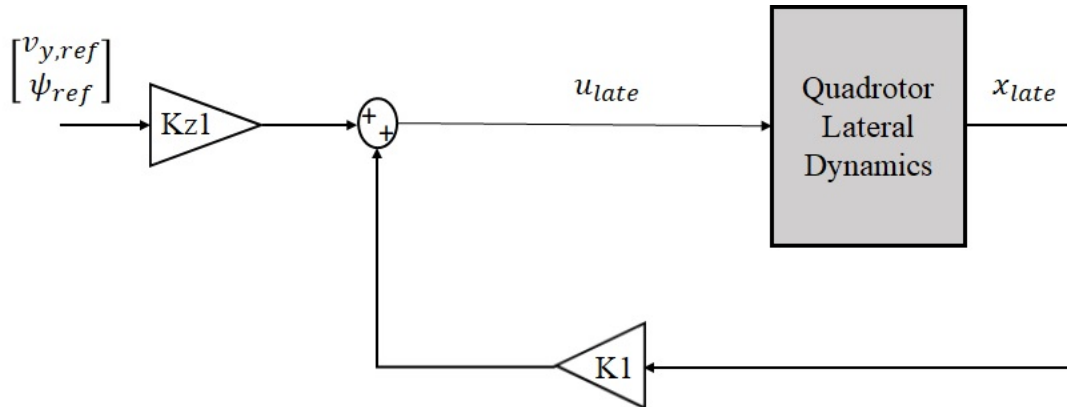


Figure 2.4: Velocity_y and Heading control system schematic

The real part of all the eigenvalues in table 2.6 are all negative. Thus, we have an

Table 2.5: LQT Gains for the Velocity_x and Heading Controller

K1					Kz1	
-0.96	-0.43	0	-2.86	0	1	0
0	0	-0.16	0	-1	0	1

Table 2.6: Eigenvalues of the Velocity_y and Heading Controller

Eigenvalues
-6.70
-3.35+5.80i
-3.35+5.80i
-6.20+6.20i
-6.20-6.20i

asymptotically stable system. This controller will also be tested against the nonlinear one quadrotor slung load model. We will test to see their performances in spite of the disturbance from the slung load.

2.4 One Quadrotor Slung Load System Results and Discussion

Using the equations of motion derived in section 2.1, a nonlinear model of the single quadrotor slung load system is developed on the MATLAB/SIMULINK platform. The two linear controllers developed in section 2.3.2 and section 2.3.3, that is, the Velocity_x and Velocity_z LQT controller as well as the Velocity_y and Heading LQT controller are then tested against the nonlinear model. To test our one quadrotor slung load system, velocity commands are sent to the quadrotor. We then check to see if our quadrotor can track these commands in spite of the dynamics of the slung load.

From fig. 2.5, the quadrotor is able to track the reference velocities quite closely. The disturbance from the slung load can also be observed from these plots in terms of the oscillatory responses. Figure 2.6 shows the quadrotor and load positions in three

dimensions. The trajectory can be broken into three phases, with the first phase involves a climb, followed by a period a straight level flight and finally the introduction of a side velocity, that is velocity in y direction. Figure 2.7 shows the load rock, swing and heading angles. The load rock angle is the left to right swinging motion of the slung load. The load swing angle is the forward to back swinging motion of the slung load. From fig. 2.7, we see that from 40 secs onwards, after the introduction of the side velocity v_y , the load starts swinging from left to right 12 to -5 degrees between finally settling down around 0 degrees as the simulation progresses. Also from the same figure, we see oscillations in the load swing angle. That is, the load swings forward and backwards between +50 and -50 degrees as the quadrotor moves forward, but later settles to around 0 degrees later on as the simulation progressed. Finally, fig. 2.8 shows the propeller speeds of the four rotors of the quadrotor. We see no saturation in the speeds and therefore these speeds are realizable by the electric motors of the quadrotor. From all these results, we can conclude that the quadrotor is able to track the desired reference velocities in spite of the disturbances from the slung load. However, this is done at cost of swinging and rocking motion of the load.

To reduce the swinging and rocking motion of the load, additional constraints would have to be added to the system. This can be achieved by introducing another quadrotor and cable into the system to limit the motion of the load. Thus, the modelling of a two quadrotor slung load system will be discussed in the next chapter.

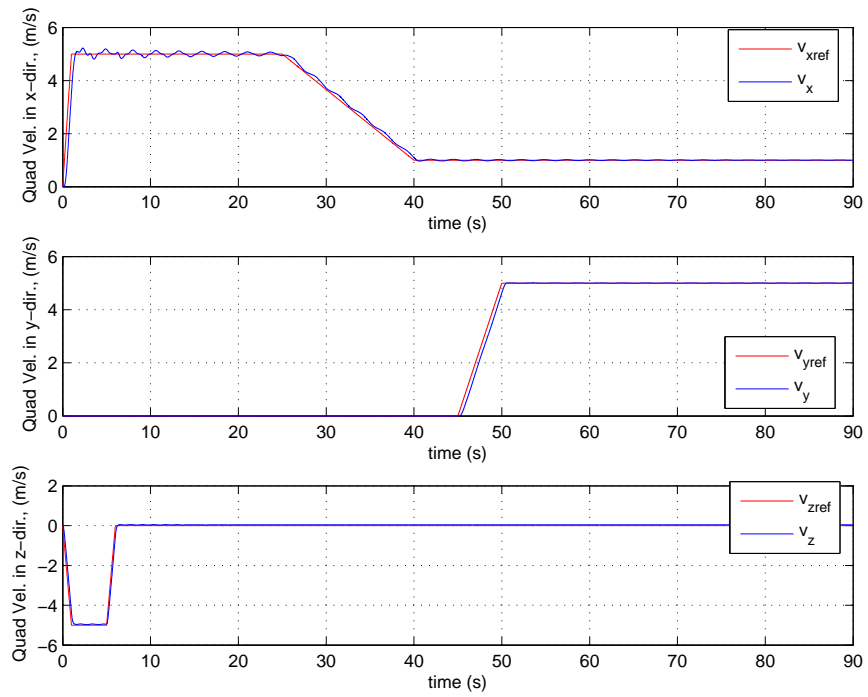


Figure 2.5: Quadrotor Velocity in x, y and z directions respectively (One Quadrotor)

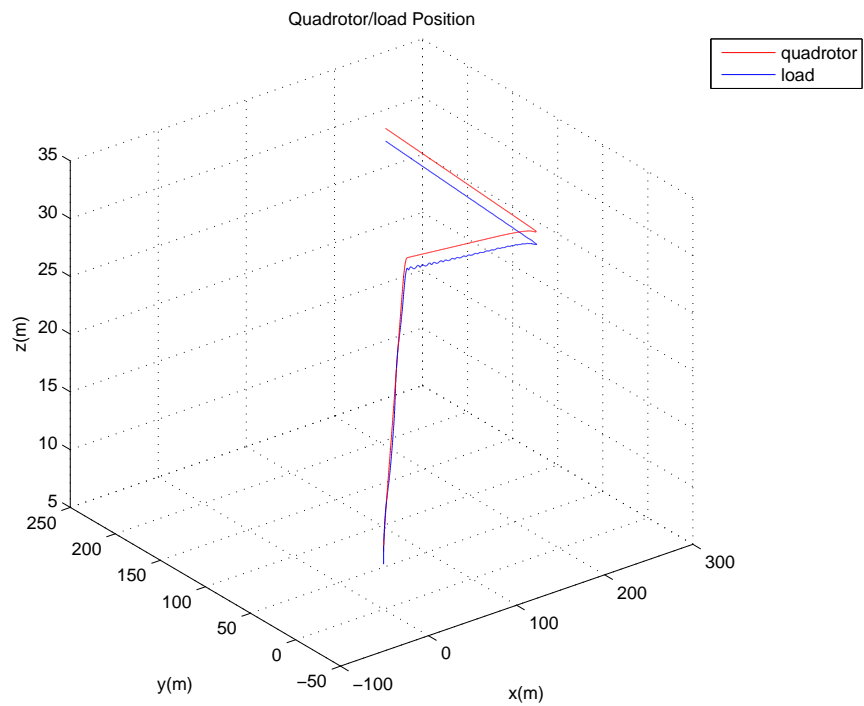


Figure 2.6: Quadrotor and Load Position (One Quadrotor)

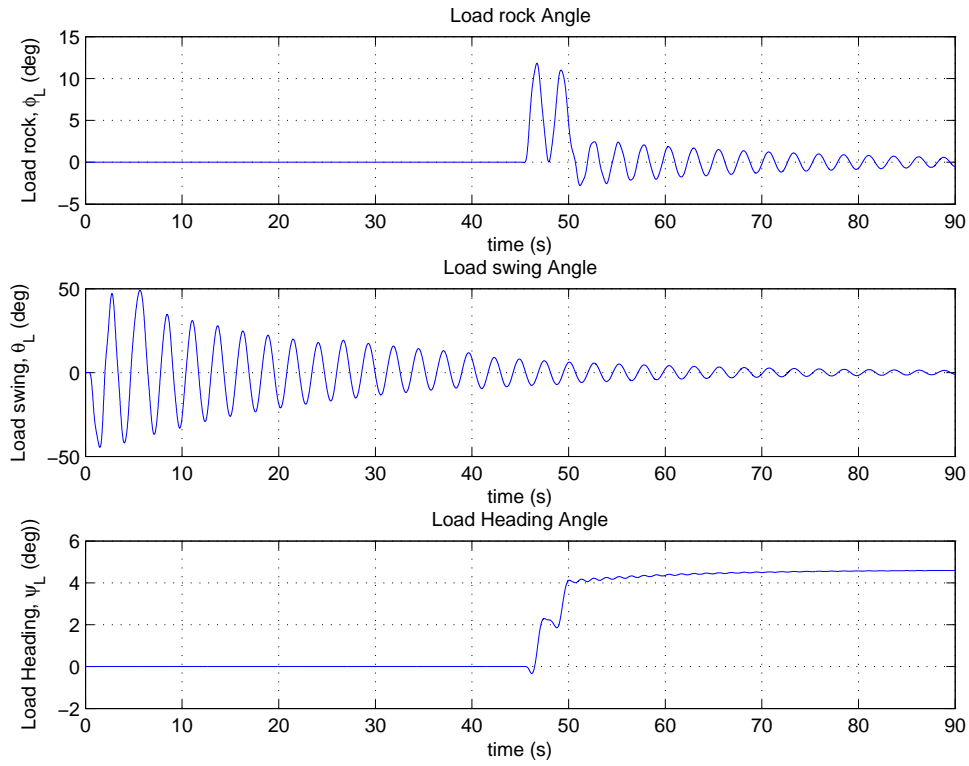


Figure 2.7: Swing, Rock and Heading Angles of the Load (One Quadrotor)

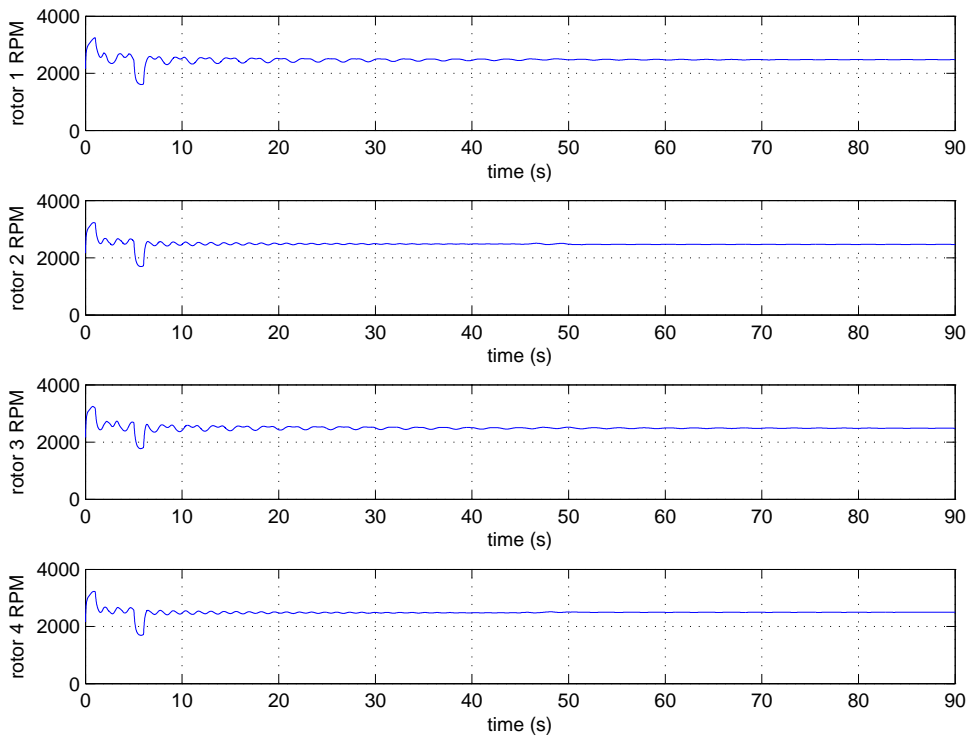


Figure 2.8: Propeller Speeds of the Quadrotor (One Quadrotor)

CHAPTER 3

TWO QUADROTOR SLUNG LOAD SYSTEM

In this chapter, the equations of motion for a two-quadrotor slung load system is derived. Using these equations of motion, a nonlinear two quadrotor slung load model is designed. A Lyapunov based formation guidance controller is then designed and implemented on the two quadrotors to make them fly in a fixed formation geometry. LQT controllers are implemented on the quadrotors to track the reference signals from the formation guidance controller. The simulation results are presented and discussed as well.

From the results presented in section 2.4 for the single quadrotor case, we see that the quadrotor is able to track the desired reference velocity signals, albeit with some swinging and rocking motion of the load. To reduce these load swing and rock angles, the load needs to be further constrained. By introducing a second quadrotor and cable into the system as well as constraining the quadrotors to fly in a formation, we expect to significantly reduce to swinging and rocking motion of the load.

3.1 Equation of Motion for the Two Quadrotor Slung Load System

In this section, the derivation of the equations of motion for the two quadrotor slung load system is presented. The same approach used in deriving the equations for the single quadrotor case is also employed here. In this model, we have five bodies and four spherical joints. The five bodies are the two quadrotors, the two cables and the load. The first spherical joint connects the first cable at one end to the first quadrotor, and at the other end of the cable, the second spherical joint connects it to the load. The third spherical joint connects the second cable at one end to the second quadrotor,

and at the other end of the cable, the fourth spherical joint connects it to the load. In deriving the equations of motion, we assume that the cables are stiff and that the joint torques are zero.

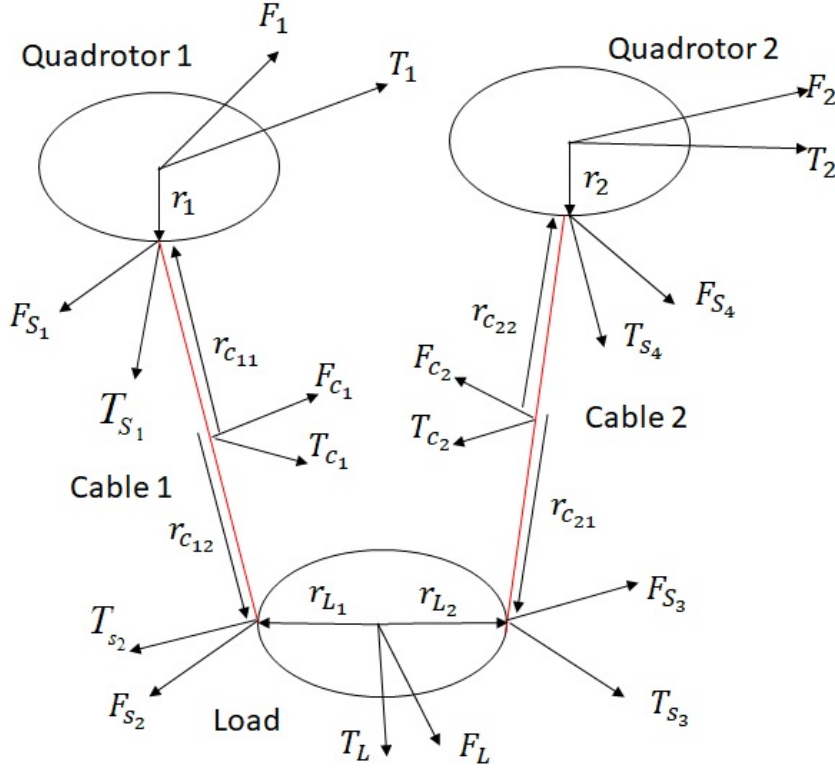


Figure 3.1: Two Quadrotor Slung Load System

The rotational equations for the two quadrotor in their own respective quadrotor fixed reference frame can be written as:

$$\begin{aligned} J_1 \dot{\omega}_1 &= T_1 + T_{S_1} - \omega_1^\times J_1 \omega_1 + r_1^\times C_N^1 F_{S_1} \\ J_2 \dot{\omega}_2 &= T_2 - C_{c_2}^2 T_{S_4} - r_2^\times C_N^2 F_{S_4} - \omega_2^\times J_2 \omega_2 \end{aligned} \quad (31)$$

Similarly, the rotational equations of motion of the load and cables in their own respective load and cable fixed frame of reference can be written as:

$$\begin{aligned} J_{c_1} \dot{\omega}_{c_1} &= T_{c_1} - C_1^{c_1} T_{S_1} - r_{c_{11}}^\times C_N^{c_1} F_{S_1} + T_{s_2} + r_{c_{12}}^\times C_N^{c_1} F_{S_2} - \omega_{c_1}^\times J_{c_1} \omega_{c_1} \\ J_L \dot{\omega}_L &= T_L - C_{c_1}^L T_{s_2} - r_{L_1}^\times C_N^L F_{S_2} + T_{s_3} + r_{L_2}^\times C_N^L F_{S_3} - \omega_L^\times J_L \omega_L \\ J_{c_2} \dot{\omega}_{c_2} &= T_{c_2} - C_L^{c_2} T_{S_3} - r_{c_{21}}^\times C_N^{c_2} F_{S_3} + T_{s_4} + r_{c_{22}}^\times C_N^{c_2} F_{S_4} - \omega_{c_2}^\times J_{c_2} \omega_{c_2} \end{aligned} \quad (32)$$

The translational equations written in the inertial frame of reference are:

$$\begin{aligned}
m_1 \dot{v}_1 &= F_1 + F_{S_1} \\
m_{c_1} \dot{v}_{c_1} &= F_{c_1} + F_{s_2} - F_{S_1} \\
m_L \dot{v}_L &= F_L + F_{S_3} - F_{S_2} \\
m_{c_2} \dot{v}_{c_2} &= F_{c_2} + F_{S_4} - F_{S_3} \\
m_2 \dot{v}_2 &= F_2 - F_{S_4}
\end{aligned} \tag{33}$$

The constraint equations can then be obtained by equating the joint accelerations:

$$\begin{aligned}
v_{S_1} &= v_1 + \omega_1^\times r_1 = v_{c_1} + \omega_{c_1}^\times r_{c11} \\
\dot{v}_1 + C_1^N \dot{\omega}_1^\times r_1 + C_1^N \omega_1^{\times \times} r_1 &= \dot{v}_{c_1} + C_{c_1}^N \dot{\omega}_{c_1}^\times r_{c11} + C_{c_1}^N \omega_{c_1}^{\times \times} r_{c11} \\
\Rightarrow \dot{v}_{c_1} - \dot{v}_1 &= C_1^N \dot{\omega}_1^\times r_1 + C_1^N \omega_1^{\times \times} r_1 - C_{c_1}^N \dot{\omega}_{c_1}^\times r_{c11} - C_{c_1}^N \omega_{c_1}^{\times \times} r_{c11} \\
v_{S_2} &= v_{c_1} + \omega_{c_1}^\times r_{c12} = v_L + \omega_L^\times r_{L1} \\
\dot{v}_{c_1} + C_{c_1}^N \dot{\omega}_{c_1}^\times r_{c12} + C_{c_1}^N \omega_{c_1}^{\times \times} r_{c12} &= \dot{v}_L + C_L^N \dot{\omega}_L^\times r_{L1} + C_L^N \omega_L^{\times \times} r_{L1} \\
\Rightarrow \dot{v}_L - \dot{v}_{c_1} &= C_{c_1}^N \dot{\omega}_{c_1}^\times r_{c12} + C_{c_1}^N \omega_{c_1}^{\times \times} r_{c12} - C_L^N \dot{\omega}_L^\times r_{L1} - C_L^N \omega_L^{\times \times} r_{L1} \\
v_{S_3} &= v_L + \omega_L^\times r_{L2} = v_{c_2} + \omega_{c_2}^\times r_{c21} \\
\dot{v}_L + C_L^N \dot{\omega}_L^\times r_{L2} + C_L^N \omega_L^{\times \times} r_{L2} &= \dot{v}_{c_2} + C_{c_2}^N \dot{\omega}_{c_2}^\times r_{c21} + C_{c_2}^N \omega_{c_2}^{\times \times} r_{c21} \\
\Rightarrow \dot{v}_{c_2} - \dot{v}_L &= C_L^N \dot{\omega}_L^\times r_{L2} + C_L^N \omega_L^{\times \times} r_{L2} - C_{c_2}^N \dot{\omega}_{c_2}^\times r_{c21} - C_{c_2}^N \omega_{c_2}^{\times \times} r_{c21} \\
v_{S_4} &= v_{c_2} + \omega_{c_2}^\times r_{c22} = v_2 + \omega_2^\times r_2 \\
\dot{v}_{c_2} + C_{c_2}^N \dot{\omega}_{c_2}^\times r_{c22} + C_{c_2}^N \omega_{c_2}^{\times \times} r_{c22} &= \dot{v}_2 + C_2^N \dot{\omega}_2^\times r_2 + C_2^N \omega_2^{\times \times} r_2 \\
\Rightarrow \dot{v}_2 - \dot{v}_{c_2} &= C_{c_2}^N \dot{\omega}_{c_2}^\times r_{c22} + C_{c_2}^N \omega_{c_2}^{\times \times} r_{c22} - C_2^N \dot{\omega}_2^\times r_2 - C_2^N \omega_2^{\times \times} r_2
\end{aligned} \tag{34}$$

In vector-matrix form, all the above equations may be written as:

$$\begin{bmatrix} A & 0 & R \\ 0 & M & U \\ R^T & U^T & 0 \end{bmatrix} \begin{Bmatrix} \dot{x} \\ \dot{y} \\ f \end{Bmatrix} = \begin{Bmatrix} \tau \\ v \\ \vartheta \end{Bmatrix} \tag{35}$$

where

$$A = \begin{bmatrix} J_1 & 0 & 0 & 0 & 0 & 0 \\ 0 & J_{c_1} & 0 & 0 & 0 & 0 \\ 0 & 0 & J_L & 0 & 0 & 0 \\ 0 & 0 & 0 & J_{c_2} & 0 & 0 \\ 0 & 0 & 0 & 0 & J_2 & 0 \\ 0 & 0 & 0 & 0 & 0 & m_1 I \end{bmatrix}, R = \begin{bmatrix} -r_1^\times C_N^1 & 0 & 0 & 0 \\ r_{c_{11}}^\times C_N^{c_1} & -r_{c_{12}}^\times C_N^{c_1} & 0 & 0 \\ 0 & r_{L_1}^\times C_N^L & -r_{L_2}^\times C_N^L & 0 \\ 0 & 0 & r_{c_{21}}^\times C_N^{c_2} & r_{c_{22}}^\times C_N^{c_2} \\ 0 & 0 & 0 & r_2^\times C_N^2 \\ -I & 0 & 0 & 0 \end{bmatrix} \quad (36)$$

$$M = \begin{bmatrix} m_{c_1} I & 0 & 0 & 0 \\ 0 & m_L I & 0 & 0 \\ 0 & 0 & m_{c_2} I & 0 \\ 0 & 0 & 0 & m_2 I \end{bmatrix}, U = \begin{bmatrix} I & -I & 0 & 0 \\ 0 & I & -I & 0 \\ 0 & 0 & I & -I \\ 0 & 0 & 0 & I \end{bmatrix} \quad (37)$$

$$\tau = \begin{pmatrix} T_1 - \omega_1^\times J_1 \omega_1 + T_{S_1} \\ T_{c_1} - \omega_{c_1}^\times J_{c_1} \omega_{c_1} - C_1^{c_1} T_{S_1} + T_{s_2} \\ T_L - \omega_L^\times J_L \omega_L - C_{c_1}^L T_{s_2} + T_{s_3} \\ T_{c_2} - \omega_{c_2}^\times J_{c_2} \omega_{c_2} - C_L^{c_2} T_{s_3} + T_{s_4} \\ T_2 - \omega_2^\times J_2 \omega_2 - C_{c_2}^2 T_{s_4} \\ F_1 \end{pmatrix}, \quad (38)$$

$$v = \begin{pmatrix} F_{c_1} \\ F_L \\ F_{c_2} \\ F_2 \end{pmatrix}, \quad \vartheta = \begin{pmatrix} C_1^N \omega_1^{\times \times} r_1 - C_{c_1}^N \omega_{c_1}^{\times \times} r_{c_{11}} \\ C_{c_1}^N \omega_{c_1}^{\times \times} r_{c_{12}} - C_L^N \omega_L^{\times \times} r_{L_1} \\ C_L^N \omega_L^{\times \times} r_{L_2} - C_{c_2}^N \omega_{c_2}^{\times \times} r_{c_{21}} \\ C_{c_2}^N \omega_{c_2}^{\times \times} r_{c_{22}} - C_2^N \omega_2^{\times \times} r_2 \end{pmatrix}$$

$$\dot{x} = \begin{pmatrix} \dot{\omega}_1 \\ \dot{\omega}_{c_1} \\ \dot{\omega}_L \\ \dot{\omega}_{c_2} \\ \dot{\omega}_2 \\ \dot{v}_1 \end{pmatrix}, \quad \dot{y} = \begin{pmatrix} \dot{v}_{c_1} \\ \dot{v}_L \\ \dot{v}_{c_2} \\ \dot{v}_2 \end{pmatrix}, \quad f = \begin{pmatrix} F_{S_1} \\ F_{S_2} \\ F_{S_3} \\ F_{S_4} \end{pmatrix} \quad (39)$$

\dot{x} , \dot{y} and f can be decoupled in eqn. 35 by introducing unknown coefficient matrices α and β and performing row operations:

$$(A + \beta R^T) \dot{x} + (\alpha M + \beta U^T) \dot{y} + (R + \alpha U) f = \tau + \alpha v + \beta \vartheta \quad (310)$$

choose $\alpha = -RU^{-1}$, $\beta = RU^{-1}MU^{-T}$, then,

$$(A + \beta R^T) \dot{x} = \tau + \alpha v + \beta \vartheta \quad (311)$$

Once the above eqn. 311 is solved for \dot{x} , \dot{y} and f can then be easily computed from eqn. 35. Refer to table 2.1 for the definition of the terms used in the derivation of the above equations.

For the two quadrotor slung load system, the load rock, swing and heading angles, $(\phi_L, \theta_L, \psi_L)$, are defined as shown in the figures below:

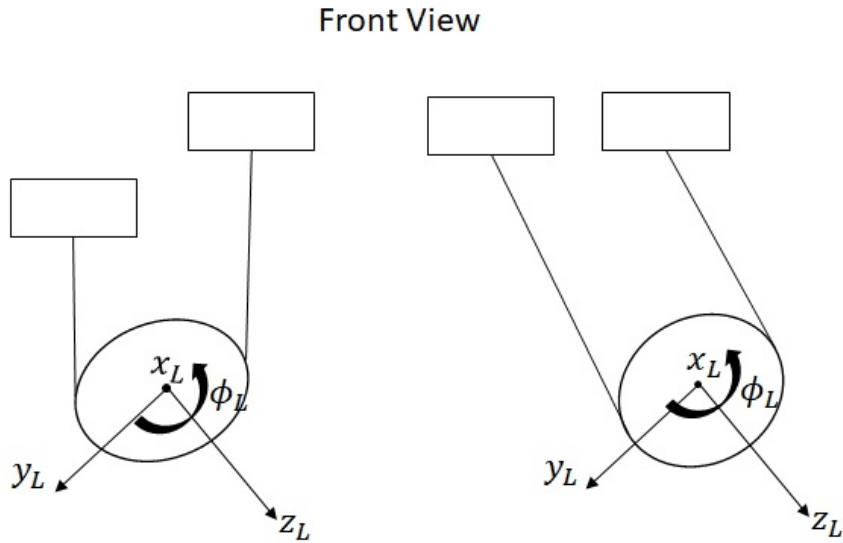


Figure 3.2: Two Quadrotor Slung Load System Rock Angle

Figure 3.2 shows the load rock angle. It is the angle deflection of the load as it swings from side to side, or as result of a difference in the relative z-positions of the leader and follower quadrotor. Figure 3.3 shows the load swing and heading angles. The load swing is the angle deflection of the load as it swings forwards and backwards. The change in heading angle occurs as a result of a difference in the relative x-positions of the leader and follower quadrotor.

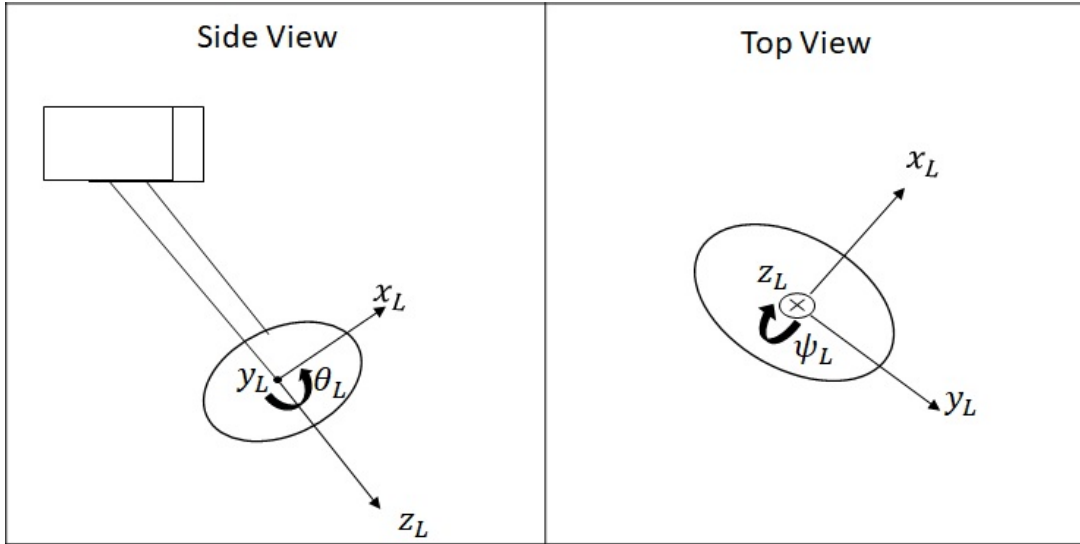


Figure 3.3: Two Quadrotor Slung Load system Swing Angle (Left) and Heading Angle (Right)

3.2 Formation-Hold Control System Approach

The leader follower approach is used to tackle the formation flight problem in this thesis. As stated in section 1.2, in the leader follower approach, some of the aircrafts in the formation are designated as leader and the rest of the aircrafts are treated as followers. The leaders maintain a prescribed trajectory while the followers track a fixed relative distance from the neighboring aircraft. Thus, the formation behavior is prescribed by specifying the relative distances that the followers must maintain. Since we have only two aircrafts, one of the quadrotors will be designated as the leader and will receive the reference velocity commands. The other quadrotor will be the follower. The follower quadrotor will try to maintain its relative distance to the leader in spite of the motion of the leader through the help of the formation guidance controller.

The formation hold control system designed in this thesis employs a two-loop architecture. This control system is implemented on the follower quadrotor. The outer loop contains a Lyapunov function based formation guidance system which takes in the leader and follower quadrotor positions, the desired relative position the follower quadrotor must maintain as well as the leader quadrotor velocities and outputs the

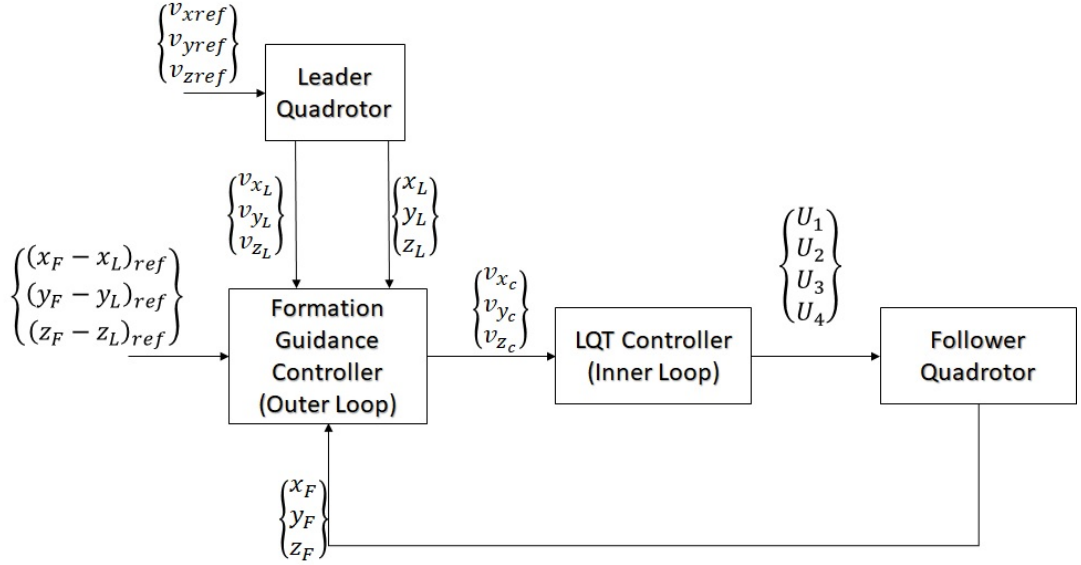


Figure 3.4: Formation-Hold Control System Schematic

velocities that the follower quadrotor must track to maintain the formation geometry. The inner loop contains LQT controllers to track the velocities coming from the outer loop formation guidance controller. The details for the outer loop Lyapunov function based formation guidance controller will be discussed in the next section. The details for the LQT controller design has already been discussed in section 2.3, the exact LQT controllers designed in that section will be employed in our two-loop formation-hold control system.

3.2.1 Lyapunov function based Formation Guidance Controller

The Lyapunov stability theorem states that: Let $x = 0$ be an equilibrium point of a nonlinear system $\dot{x} = f(x)$. Let $V : D \rightarrow R$ be a continuously differentiable function in the neighborhood D of $x = 0$, such that $V(0) = 0$ and $V(x) > 0$ in $D - \{0\}$. If $\dot{V}(x) \leq 0$, then $x = 0$ is stable. Moreover, if $\dot{V}(x) < 0$ in $D - \{0\}$, then $x = 0$ is asymptotically stable [35].

The Lyapunov stability theorem approach may be used to design stabilizing controllers for nonlinear systems [35]. Our formation guidance controller is thus designed using the Lyapunov stability theorem. We used this approach to design a controller that guides our follower quadrotor to match the heading of the leader quadrotor,

as well as maintain a desired relative distance with the leader quadrotor.

Consider the following Lyapunov function [36]:

$$V = \frac{1}{2} \left\{ \Delta x \quad \Delta y \quad \Delta z \quad \Delta \psi \right\} Q \begin{Bmatrix} \Delta x \\ \Delta y \\ \Delta z \\ \Delta \psi \end{Bmatrix} \quad (312)$$

where,

$$\begin{aligned} \Delta x &= x_L + a - x_F \\ \Delta y &= y_L + b - y_F \\ \Delta z &= z_L + c - z_F \\ \Delta \psi &= \psi_L - \psi_F \end{aligned} \quad (313)$$

(x_L, y_L, z_L) and (x_F, y_F, z_F) are the positions of the leader and the follower quadrotors with respect to the inertial frame. (a, b, c) is the desired relative position of the follower with respect to the leader quadrotor. Q is a positive definite matrix. ψ_L, ψ_F are the leader and follower headings. The derivative of the Lyapunov function gives:

$$\dot{V} = (\Delta x \quad \Delta y \quad \Delta z \quad \Delta \psi) Q \begin{Bmatrix} \Delta \dot{x} \\ \Delta \dot{y} \\ \Delta \dot{z} \\ \Delta \dot{\psi} \end{Bmatrix} \quad (314)$$

To ensure that eqn. 314 is negative definite, we make it equal to:

$$-(\Delta x \quad \Delta y \quad \Delta z \quad \Delta \psi) R \begin{Bmatrix} \Delta x \\ \Delta y \\ \Delta z \\ \Delta \psi \end{Bmatrix} \quad (315)$$

where R is a positive definite matrix. Thus we have:

$$\dot{V} = (\Delta x \quad \Delta y \quad \Delta z \quad \Delta \psi) Q \begin{Bmatrix} \Delta \dot{x} \\ \Delta \dot{y} \\ \Delta \dot{z} \\ \Delta \dot{\psi} \end{Bmatrix} = -(\Delta x \quad \Delta y \quad \Delta z \quad \Delta \psi) R \begin{Bmatrix} \Delta x \\ \Delta y \\ \Delta z \\ \Delta \psi \end{Bmatrix} \quad (316)$$

simplifying eqn. 316 and multiplying both sides of the equation by Q^{-1} gives:

$$\begin{Bmatrix} \Delta \dot{x} \\ \Delta \dot{y} \\ \Delta \dot{z} \\ \Delta \dot{\psi} \end{Bmatrix} = -Q^{-1}R \begin{Bmatrix} \Delta x \\ \Delta y \\ \Delta z \\ \Delta \psi \end{Bmatrix} \quad (317)$$

Differentiating eqn. 313 and substituting the result into eqn. 317, the reference signal going from the Lyapunov based formation guidance controller to the follower quadrotor can be obtained:

$$\begin{Bmatrix} V_{x_F} \\ V_{y_F} \\ V_{z_F} \\ \dot{\psi}_F \end{Bmatrix}_{ref} = \begin{Bmatrix} V_{x_L} \\ V_{y_L} \\ V_{z_L} \\ \dot{\psi}_L \end{Bmatrix} + Q^{-1}R \begin{Bmatrix} \Delta x \\ \Delta y \\ \Delta z \\ \Delta \psi \end{Bmatrix} + \begin{Bmatrix} \dot{a} \\ \dot{b} \\ \dot{c} \\ 0 \end{Bmatrix} \quad (318)$$

Our formation guidance scheme works for both fixed and time varying formation geometries. It is also worth mentioning that although heading command is not necessary to track the formation geometry, it is included in the guidance algorithm to avoid twisting of the cables attached to the load. Thus, holding the heading in place while tracking the formation geometry helps to reduce the chances of cable entanglement. Holding the heading also introduces additional constraints to limit the swinging and rocking of the slung load.

3.3 Two Quadrotor Slung Load System Results and Discussion

The two quadrotor slung load system is simulated using the equations of motion derived in section 3.1 on the SIMULINK/MATLAB platform. Reference velocity signals are sent to the leader quadrotor. The leader quadrotor tracks these velocities using the LQT velocity and heading controllers developed in section 2.3.2 and section 2.3.3. The formation-hold control system which consists of a Lyapunov function based formation guidance controller on the outer loop and LQT velocity and heading controller on the inner loop is then implemented on the follower quadrotor. The desired reference relative distance the follower quadrotor must maintain with the leader

quadrotor is sent to the formation guidance controller. The velocities that the follower quadrotor must track to maintain the formation geometry is then sent into the inner loop controllers from the outer loop controller. Refer to table 2.2 for the quadrotor, cable and load properties. Our control system is then tested to see if our quadrotors can track the reference trajectory and fly in formation in spite of the dynamics of the slung load. We also test to see if the overall swing and rock angles of the load is reduced.

To test our overall control system, it is desired that initial separation distances of the leader and follower quadrotor be maintained in spite of the motion of the leader quadrotor. In other words, the leader and follower quadrotor should fly at the same altitude, maintain a distance of 1 *m* between each other in the *y*-direction and a relative distance of 0 *m* in the *x*-direction. Thus the reference relative distance sent to the formation guidance loop is: $(x_F - x_L, y_F - y_L, z_F - z_L) = (0, 1, 0)$.

From fig. 3.5, we see that the leader quadrotor is able to closely track the desired reference velocities in spite of the slung load. It also tracks it relatively smoothly. Figures 3.6 and 3.7 show the two quadrotor and load positions. We see from those figures that the follower quadrotor is able to keep up with the leader quadrotor.

Figure 3.8 shows the time history of the relative positions of the leader and follower quadrotor. The follower quadrotor is able to maintain the desired formation geometry in spite of the motion of the leader quadrotor. From the relative *x*-direction, we see an initial lag as the leader quadrotor begins its forward motion, the follower quadrotor quickly catches up to the leader quadrotor to maintain the desired relative distance in the *x*-direction. From the same figure, in the *y*-direction, the follower is able to maintain its relative position with the leader quadrotor. However, 45 secs to 50 secs, we see some lag as the leader quadrotor begins to track the side velocity v_y . The follower quadrotor is able to recover quickly however. Figure 3.9 shows the load rock, swing and heading angles. We see that these angles are greatly reduced as compared to the one quadrotor case. The two quadrotors are able to carry the load in a smooth fashion. We see a deflection in the load rock angle from -10 degrees to 10 degrees in the first 10 secs. This is as a result of the configuration of the two quadrotor slung load system. The load rotated around its *x*-axis as the leader quadrotor initially climbed,

but as the follower quadrotor moved to maintain the formation geometry, the load rock angle quickly returns to 0 degrees. We also see an initial heading change of the load as the leader quadrotor started its forward motion. This also quickly returns to 0 degrees as the follower quadrotor starts moving to maintain the formation geometry. Figures 3.10 and 3.11 shows the propeller speeds of the two quadrotors. There are no saturations in the speeds of the rotors.

We expect that these load rock and heading angles could still be reduced if we introduce even more constraints on the load by having a three quadrotor slung model. The results of the three quadrotor slung load model will be presented in the next chapter.

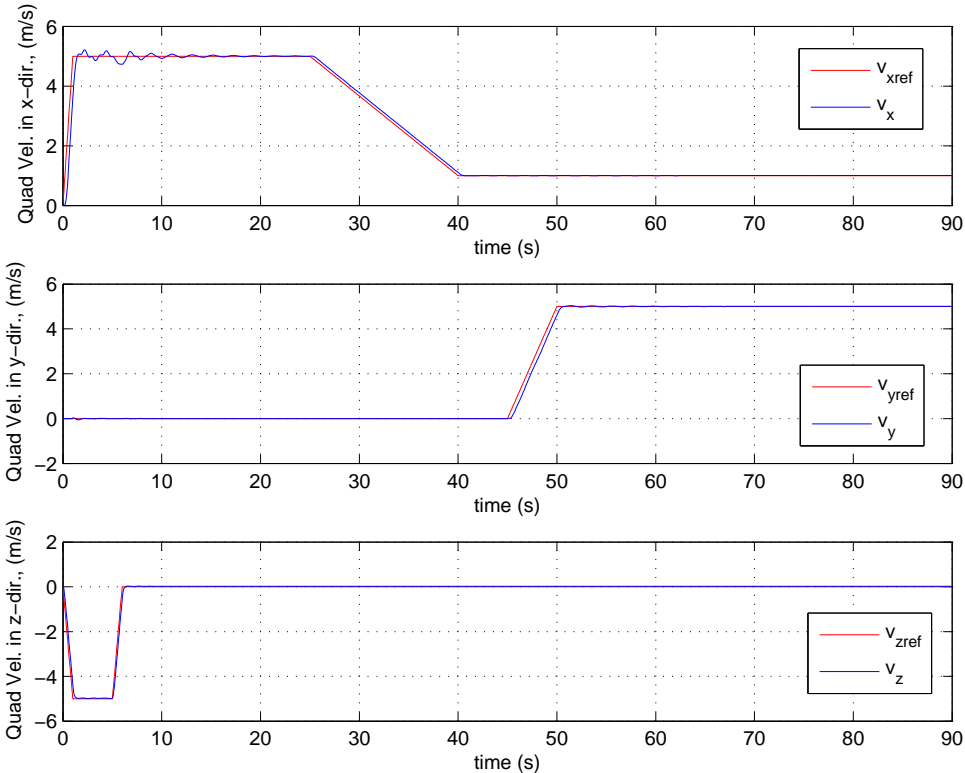


Figure 3.5: Leader Quadrotor Velocity in x, y and z directions respectively (Two Quadrotor)

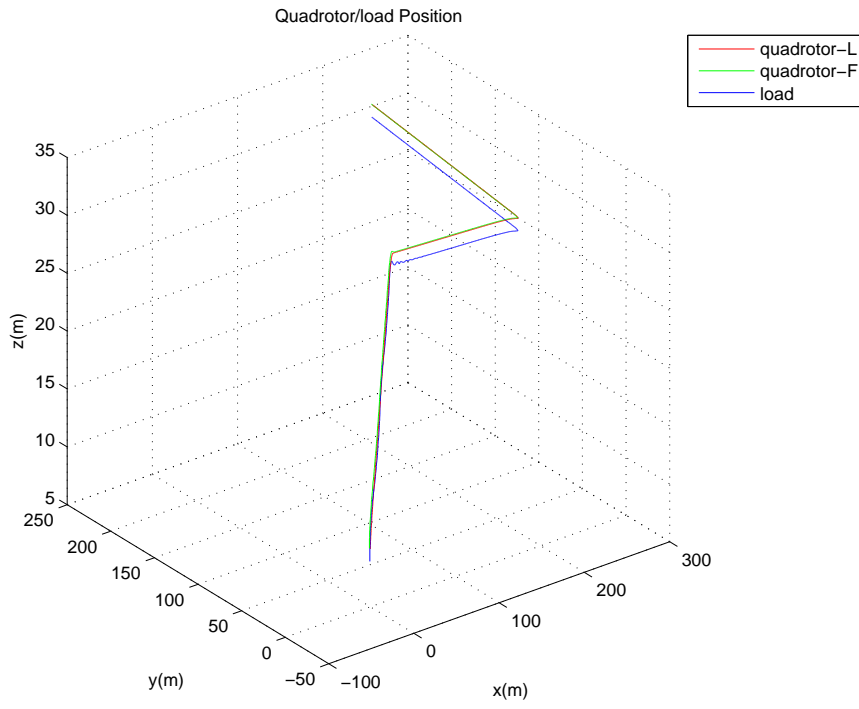


Figure 3.6: Leader and Follower Quadrotor position and Load Position (Two Quadrotor)

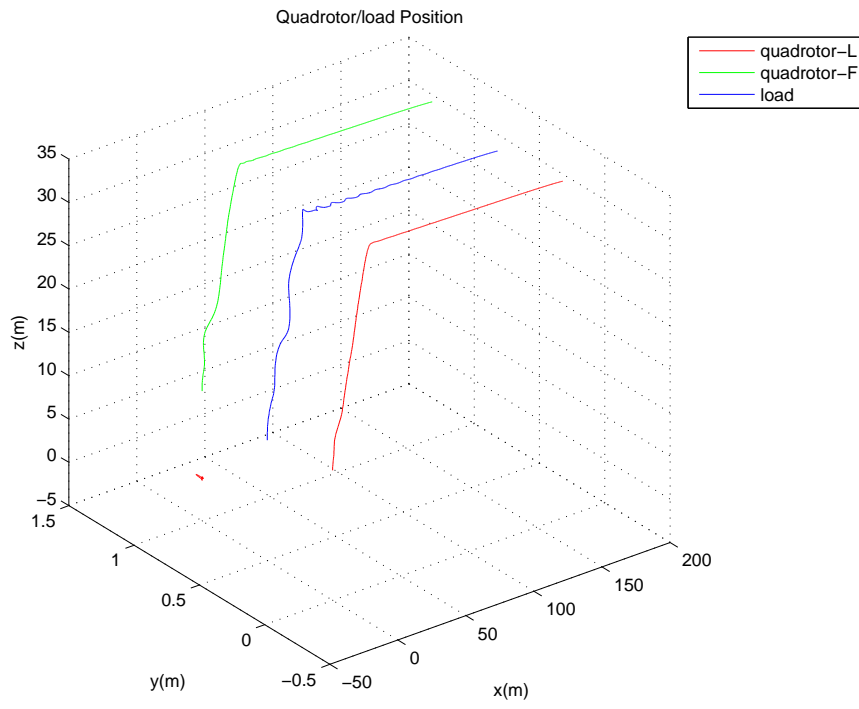


Figure 3.7: Leader and Follower Quadrotor position and Load Position (Two Quadrotor, 40 secs simulation)

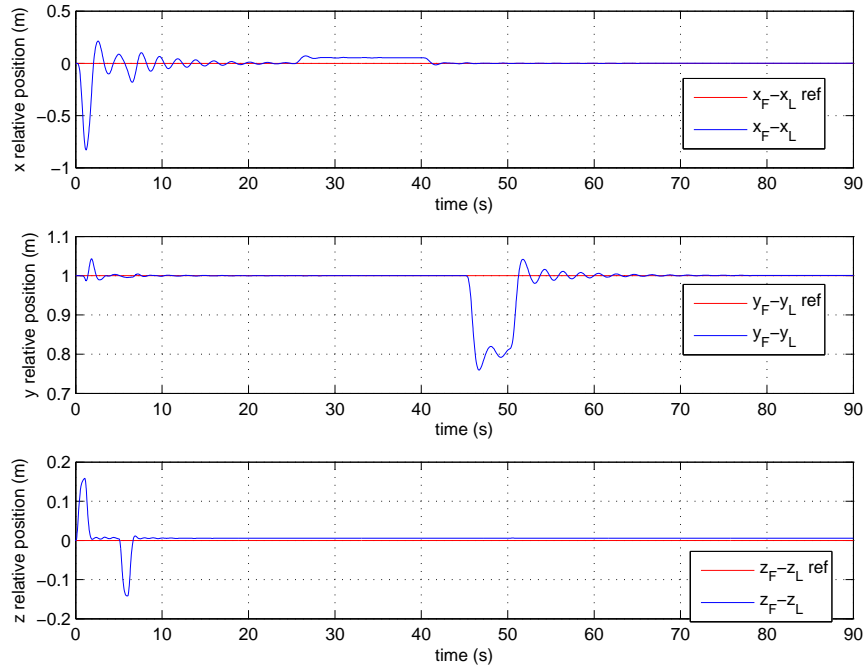


Figure 3.8: Leader and Follower Quadrotor relative positions (Two Quadrotor)

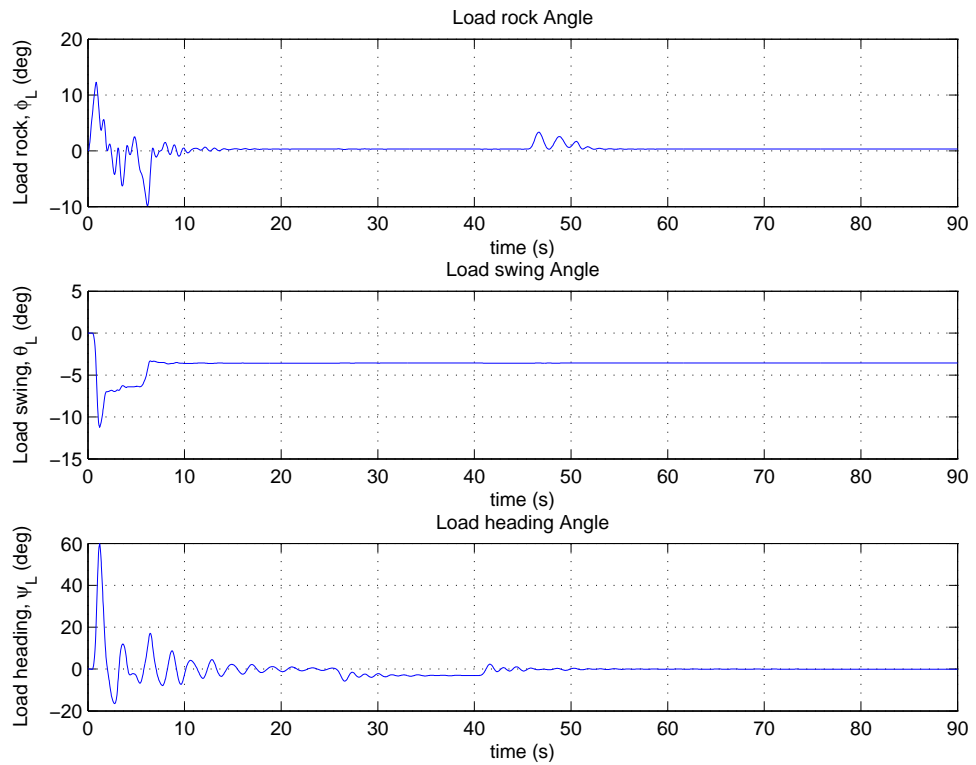


Figure 3.9: Swing, Rock and Heading Angles of the Load (Two Quadrotor)

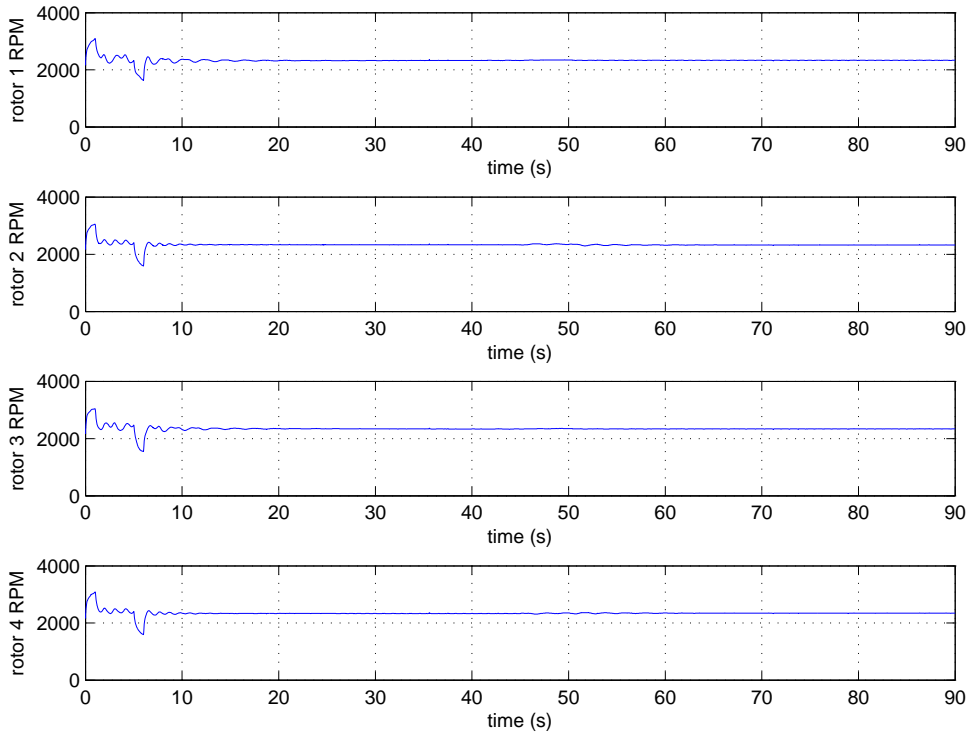


Figure 3.10: Propeller Speeds of the Leader Quadrotor (Two Quadrotor)

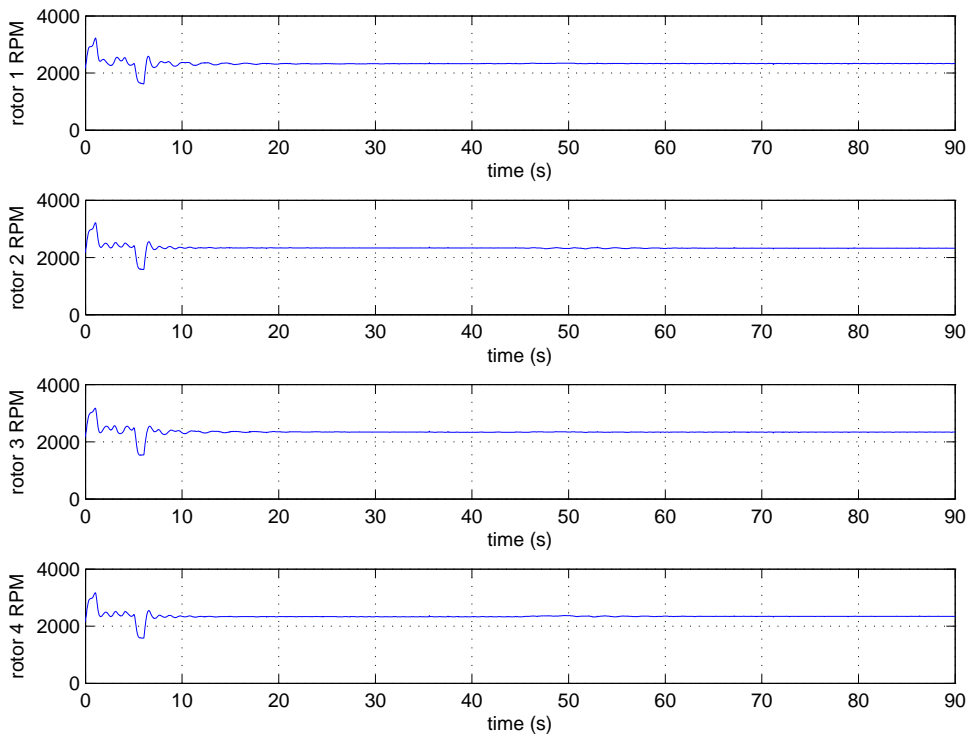


Figure 3.11: Propeller Speeds of the Follower Quadrotor (Two Quadrotor)

CHAPTER 4

THREE QUADROTOR SLUNG LOAD SYSTEM

In this chapter, the equations of motion of a three quadrotor slung load model is presented. These equations are then used to model this nonlinear system on the MATLAB/SIMULINK platform. The formation-hold control system designed in section 3.2.1 is implemented on two of the quadrotors designated as the follower quadrotors. The results of the simulation is the presented and discussed. Refer to table 2.1 for the definition of terms used in the derivation of the equations of motion, and to table 2.2 for the quadrotor, cable and load properties used in the simulation.

4.1 Equation of Motion for the Three Quadrotor Slung Load System

The same assumptions and approach used for the two quadrotor case in section 3.1 is also used in modelling the three quadrotor slung load case. The joint torques are assumed to be zero and the cables are assumed to be stiff rigid bars. Newton-Euler equations are written for 7 bodies, made of three quadrotors, a suspended load and three rigid cables. Constraint equations are written for the 6 spherical joints connecting the three rigid cables to each of the quadrotors and the load.

After deriving the rotational and translational equations of motion for each of the quadrotors, cables and load as well as establishing the joint constraint equations, the obtained equations can then be written in a vector-matrix form.

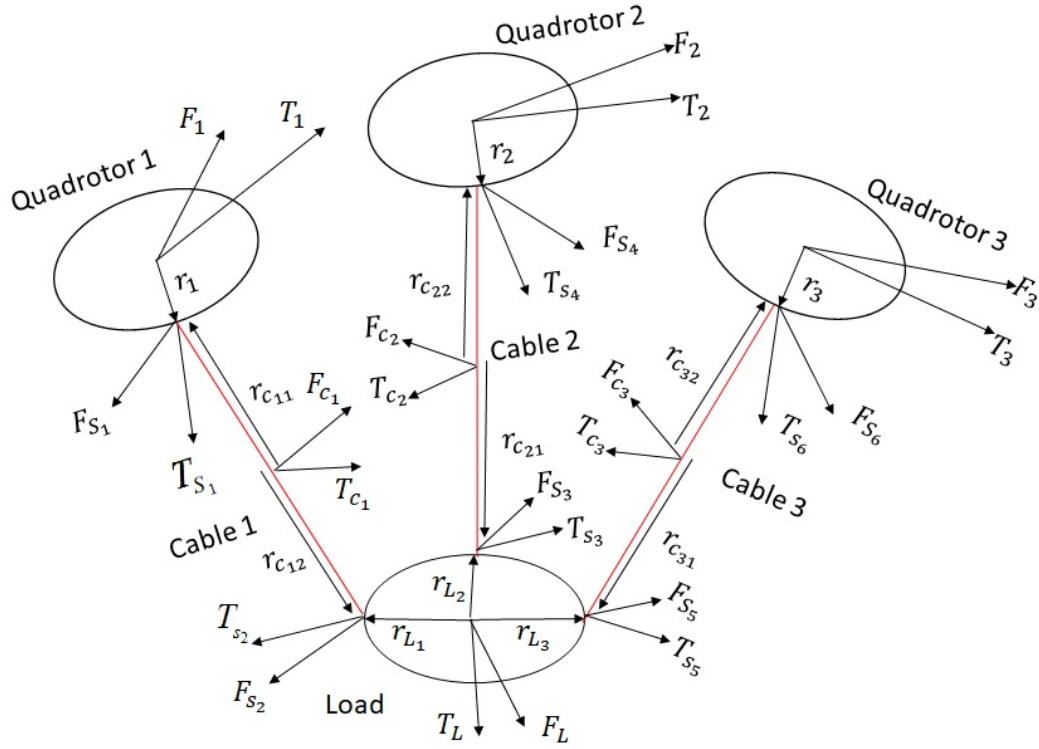


Figure 4.1: Three Quadrotor Slung Load System

In vector-matrix form, the equation may be written as:

$$\begin{bmatrix} A & 0 & R \\ 0 & M & U \\ R^T & U^T & 0 \end{bmatrix} \begin{Bmatrix} \dot{x} \\ \dot{y} \\ f \end{Bmatrix} = \begin{Bmatrix} \tau \\ v \\ \vartheta \end{Bmatrix} \quad (41)$$

where

$$A = \begin{bmatrix} J_1 & 0 & 0 & 0 & 0 & 0 & 0 & 0 \\ 0 & J_{c1} & 0 & 0 & 0 & 0 & 0 & 0 \\ 0 & 0 & J_L & 0 & 0 & 0 & 0 & 0 \\ 0 & 0 & 0 & J_{c2} & 0 & 0 & 0 & 0 \\ 0 & 0 & 0 & 0 & J_2 & 0 & 0 & 0 \\ 0 & 0 & 0 & 0 & 0 & J_{c3} & 0 & 0 \\ 0 & 0 & 0 & 0 & 0 & 0 & J_3 & 0 \\ 0 & 0 & 0 & 0 & 0 & 0 & 0 & m_1 I \end{bmatrix} \quad (42)$$

$$R = \begin{bmatrix} -r_1^\times C_N^1 & 0 & 0 & 0 & 0 & 0 \\ r_{c_{11}}^\times C_N^{c_1} & -r_{c_{12}}^\times C_N^{c_1} & 0 & 0 & 0 & 0 \\ 0 & r_{L_1}^\times C_N^L & -r_{L_2}^\times C_N^L & 0 & -r_{L_3}^\times C_N^L & 0 \\ 0 & 0 & r_{c_{21}}^\times C_N^{c_2} & -r_{c_{22}}^\times C_N^{c_2} & 0 & 0 \\ 0 & 0 & 0 & r_2^\times C_N^2 & 0 & 0 \\ 0 & 0 & 0 & 0 & r_{c_{31}}^\times C_N^{c_3} & r_{c_{32}}^\times C_N^{c_3} \\ 0 & 0 & 0 & 0 & 0 & r_3^\times C_N^3 \\ -I & 0 & 0 & 0 & 0 & 0 \end{bmatrix} \quad (43)$$

$$M = \begin{bmatrix} m_{c_1} I & 0 & 0 & 0 & 0 & 0 \\ 0 & m_L I & 0 & 0 & 0 & 0 \\ 0 & 0 & m_{c_2} I & 0 & 0 & 0 \\ 0 & 0 & 0 & m_2 I & 0 & 0 \\ 0 & 0 & 0 & 0 & m_{c_3} I & 0 \\ 0 & 0 & 0 & 0 & 0 & m_3 I \end{bmatrix} \quad (44)$$

$$U = \begin{bmatrix} I & -I & 0 & 0 & 0 & 0 \\ 0 & I & -I & 0 & -I & 0 \\ 0 & 0 & I & -I & 0 & 0 \\ 0 & 0 & 0 & I & 0 & 0 \\ 0 & 0 & 0 & 0 & I & -I \\ 0 & 0 & 0 & 0 & 0 & I \end{bmatrix}$$

$$\tau = \left\{ \begin{array}{c} T_1 - \omega_1^\times J_1 \omega_1 + T_{S_1} \\ T_{c_1} - \omega_{c_1}^\times J_{c_1} \omega_{c_1} - C_1^{c_1} T_{S_1} + T_{s_2} \\ T_L - \omega_L^\times J_L \omega_L - C_L^L T_{S_2} + T_{s_3} + T_{s_5} \\ T_{c_2} - \omega_{c_2}^\times J_{c_2} \omega_{c_2} - C_L^{c_2} T_{S_3} + T_{s_4} \\ T_2 - \omega_2^\times J_2 \omega_2 - C_{c_2}^2 T_{S_4} \\ T_{c_3} - \omega_{c_3}^\times J_{c_3} \omega_{c_3} - C_L^{c_3} T_{S_5} + T_{s_6} \\ T_3 - \omega_3^\times J_3 \omega_3 - C_{c_3}^3 T_{S_6} \\ F_1 \end{array} \right\}, \quad (45)$$

$$v = \left\{ \begin{array}{c} F_{c_1} \\ F_L \\ F_{c_2} \\ F_2 \\ F_{c_3} \\ F_3 \end{array} \right\}, \vartheta = \left\{ \begin{array}{c} C_1^N \omega_1^{\times \times} r_{c_11} - C_{c_1}^N \omega_{c_1}^{\times \times} r_{c_11} \\ C_{c_1}^N \omega_{c_1}^{\times \times} r_{c_12} - C_L^N \omega_L^{\times \times} r_{L1} \\ C_L^N \omega_L^{\times \times} r_{L2} - C_{c_2}^N \omega_{c_2}^{\times \times} r_{c_21} \\ C_{c_2}^N \omega_{c_2}^{\times \times} r_{c_22} - C_2^N \omega_2^{\times \times} r_2 \\ C_L^N \omega_L^{\times \times} r_{L3} - C_{c_3}^N \omega_{c_3}^{\times \times} r_{c_31} \\ C_{c_3}^N \omega_{c_3}^{\times \times} r_{c_32} - C_3^N \omega_3^{\times \times} r_3 \end{array} \right\}$$

$$\dot{x} = \left\{ \begin{array}{c} \dot{\omega}_1 \\ \dot{\omega}_{c_1} \\ \dot{\omega}_L \\ \dot{\omega}_{c_2} \\ \dot{\omega}_2 \\ \dot{\omega}_{c_3} \\ \dot{\omega}_3 \\ \dot{v}_1 \end{array} \right\}, \quad \dot{y} = \left\{ \begin{array}{c} \dot{v}_{c_1} \\ \dot{v}_L \\ \dot{v}_{c_2} \\ \dot{v}_2 \\ \dot{v}_{c_3} \\ \dot{v}_3 \end{array} \right\}, \quad f = \left\{ \begin{array}{c} F_{S_1} \\ F_{S_2} \\ F_{S_3} \\ F_{S_4} \\ F_{S_5} \\ F_{S_6} \end{array} \right\} \quad (46)$$

\dot{x} , \dot{y} and f can be decoupled in eqn. 41 by introducing unknown coefficient matrices α and β and performing row operations:

$$(A + \beta R^T) \dot{x} + (\alpha M + \beta U^T) \dot{y} + (R + \alpha U) f = \tau + \alpha v + \beta \vartheta \quad (47)$$

choose $\alpha = -RU^{-1}$, $\beta = RU^{-1}MU^{-T}$, then,

$$(A + \beta R^T) \dot{x} = \tau + \alpha v + \beta \vartheta \quad (48)$$

Once the above eqn. 48 is solved for \dot{x} , \dot{y} and f can then be easily computed from eqn. 41.

4.2 Three Quadrotor Slung Load System Result and Discussion

The three quadrotor slung system is modelled using the equations of motion derived in section 4.1 on the SIMULINK/MATLAB platform. One quadrotor is designated as the leader, while the other two quadrotors are the followers. The two followers have to maintain a fixed relative distance to the leader quadrotor. The formation-hold control system developed in section 3.2.1 is implemented on the two quadrotors. The leader control receives the desired reference velocities and the follower quadrotors have to maintain the formation geometry in spite of the motion of the leader quadrotor.

To test the model, the three quadrotors are initially aligned in a v-formation geometry, with the leader quadrotor 0.5 m ahead of the two followers, and the two followers 1 m apart. The two follower quadrotors are to also fly at the same altitude as the leader quadrotor.

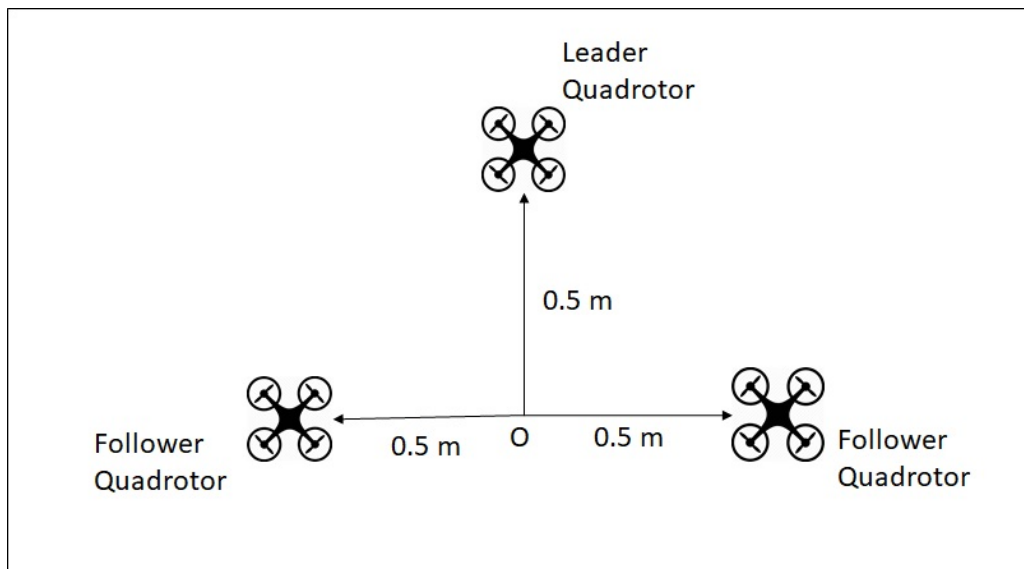


Figure 4.2: Three quadrotor formation geometry

Hence the desired formation geometry reference sent to the formation-hold control system is thus $(x_{F1} - x_L, y_{F1} - y_L, z_{F1} - z_L) = (-0.5, -0.5, 0)$ and $(x_{F2} - x_L, y_{F2} - y_L, z_{F2} - z_L) = (-0.5, 0.5, 0)$. The same velocity reference as the one and two quadrotor slung load case is also used here for the leader quadrotor. We then test to see if the formation geometry is maintained in spite of the motion of the leader quadrotor and the dynamics of the slung load. We also check the deflection of the

load angles.

Figure 4.3 shows that the leader quadrotor is able to smoothly track the reference velocities in spite of the slung load. Figures 4.4 and 4.5 show the time history of quadrotors and load positions. From these figures, we see that the formation geometry is being maintained and the follower quadrotors, that is, quadrotor-1 and quadrotor-3 are keeping up with the leader quadrotor. Figures 4.6 and 4.7 show the time history of the relative distances between the leader quadrotor and the follower quadrotors. We see a little bit of lag in the x-direction of their relative distances as the leader initially begins its forward motion but the follower quadrotors quickly recover. There is also a bit of lag in the y-direction of the relative distances in the 45 to 50 secs time frame as the leader quadrotor begins to track the side velocity, v_y . However, the follower quadrotors recover nicely. Figure 4.8 shows the time history of the load swing, rock and heading angles. The three quadrotor slung load system carries the load quite smoothly for the entire duration of the simulation. The minimal change in the heading angle, and the load rock and swing angles are close to zero for the entire simulation except for the initial jump in swing angle at the beginning of the simulation. Figures 4.9 to 4.11 show the propeller speeds of the three quadrotors. There are no saturations in the speeds of the rotors.

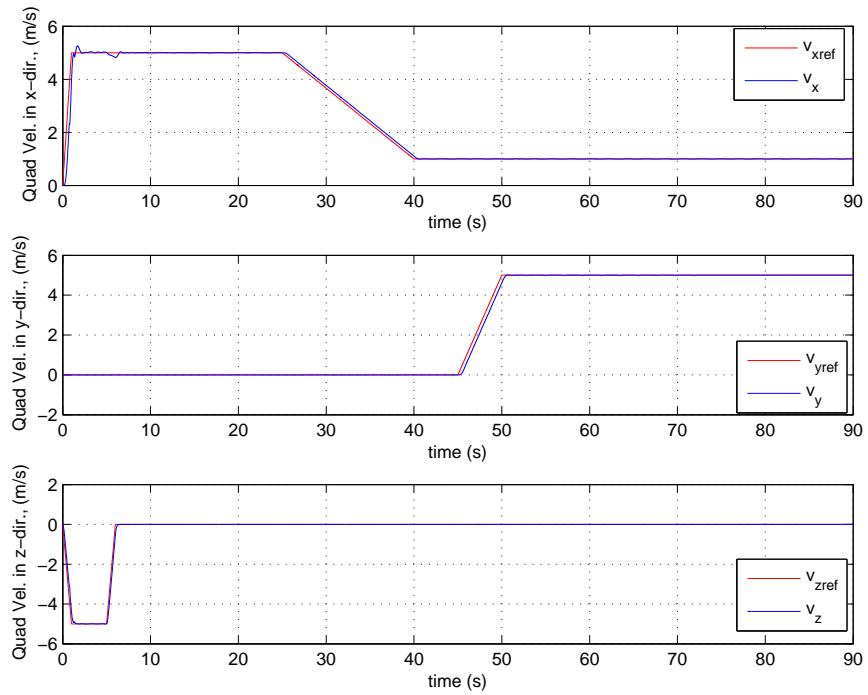


Figure 4.3: Leader Quadrotor Velocity in x, y and z directions respectively (Three Quadrotor)

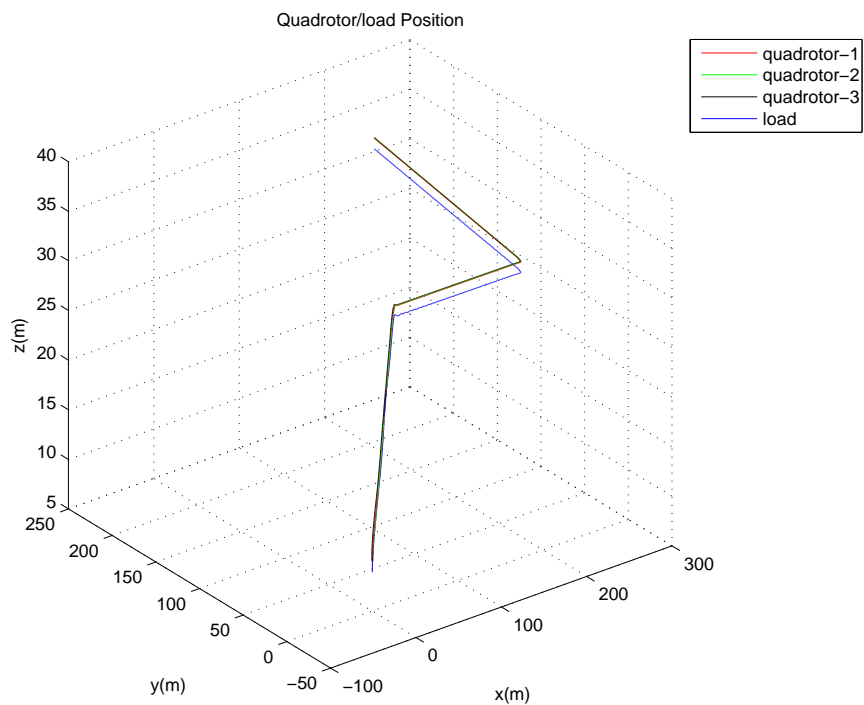


Figure 4.4: Leader and Follower Quadrotor position and Load Position (Three Quadrotor)

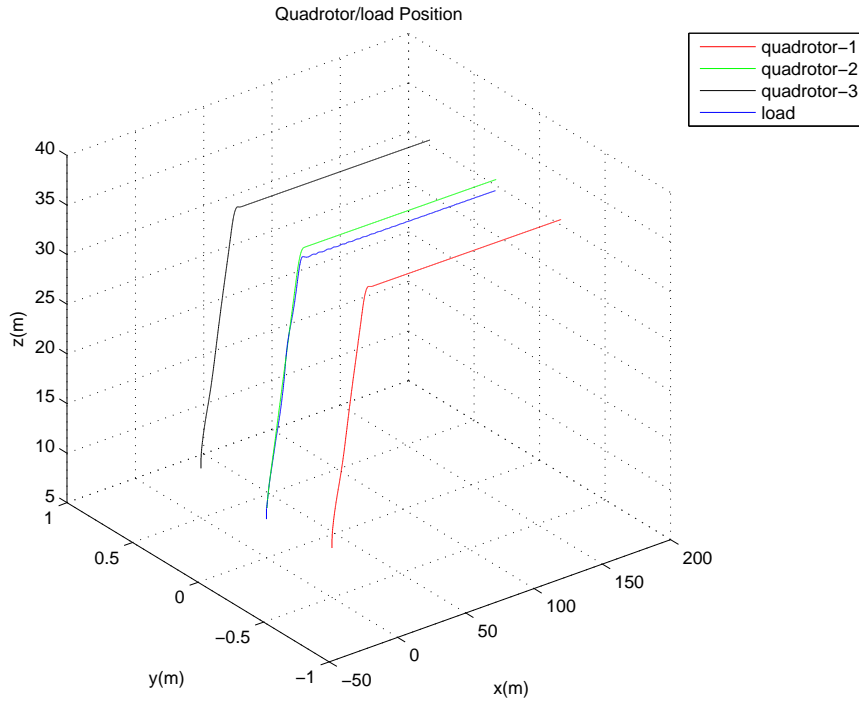


Figure 4.5: Leader and Follower Quadrotor position and Load Position (Three Quadrotor, 40 secs simulation)

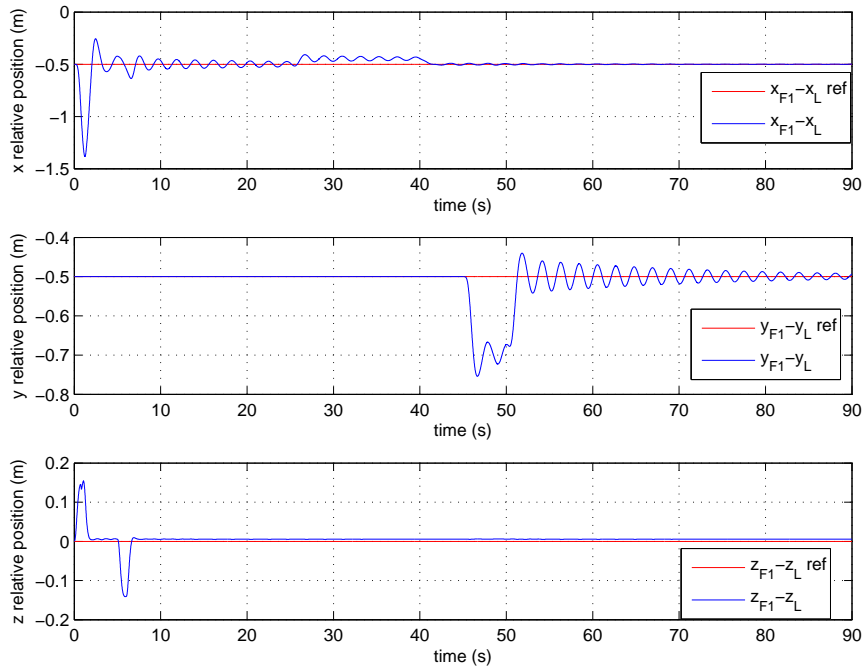


Figure 4.6: Leader and 1st Follower Quadrotor relative positions (Three Quadrotor)

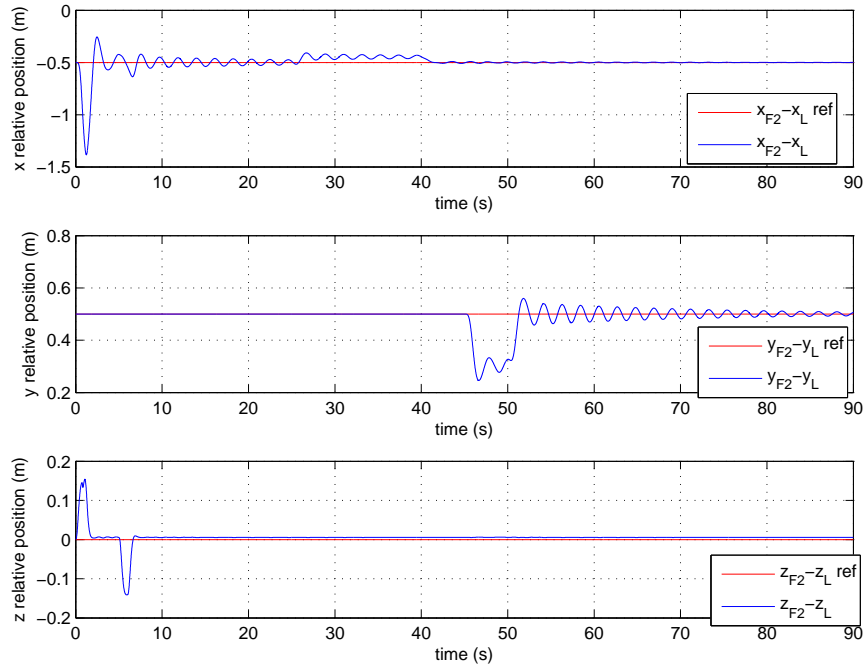


Figure 4.7: Leader and 2nd Follower Quadrotor relative positions (Three Quadrotor)

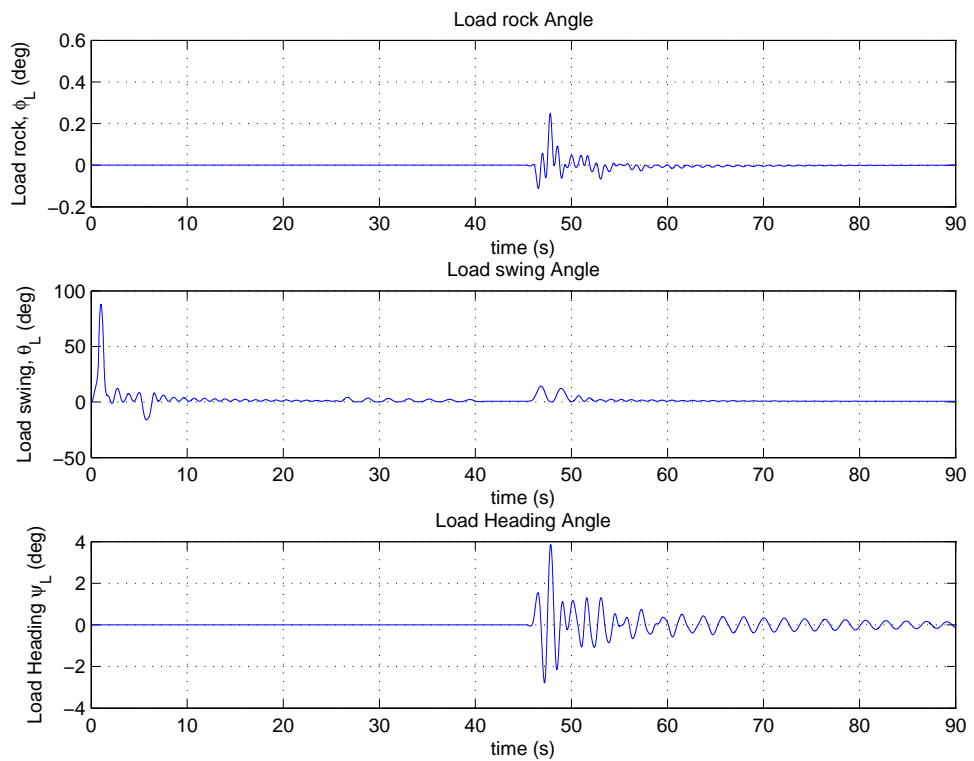


Figure 4.8: Swing, Rock and Heading Angles of the Load (Three Quadrotor)

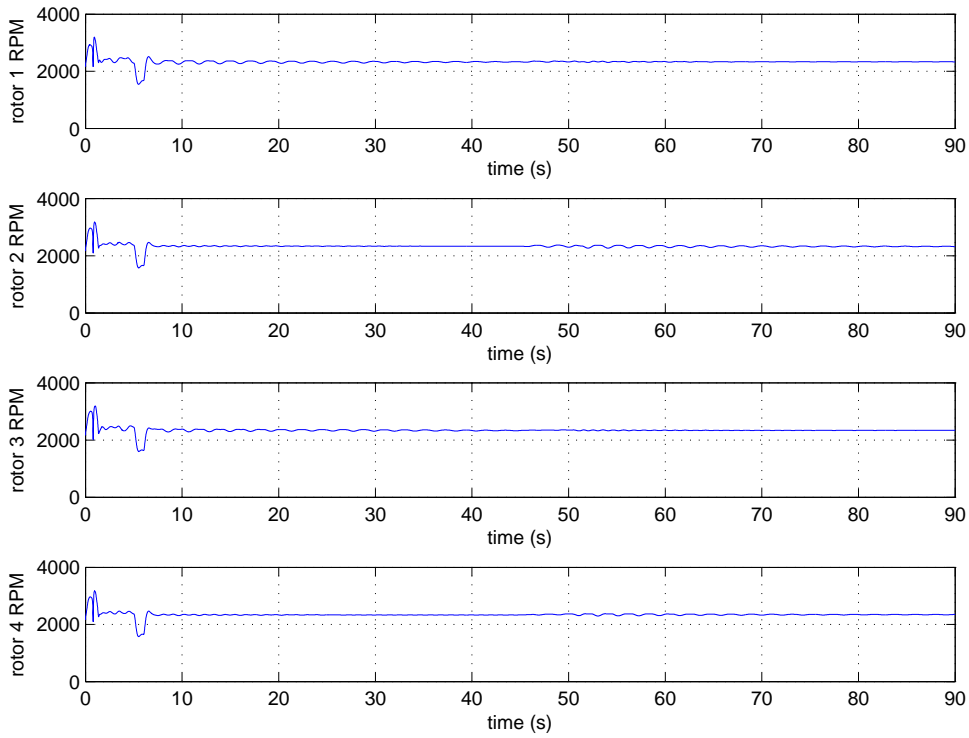


Figure 4.9: Propeller Speeds of the Leader Quadrotor (Three Quadrotor)

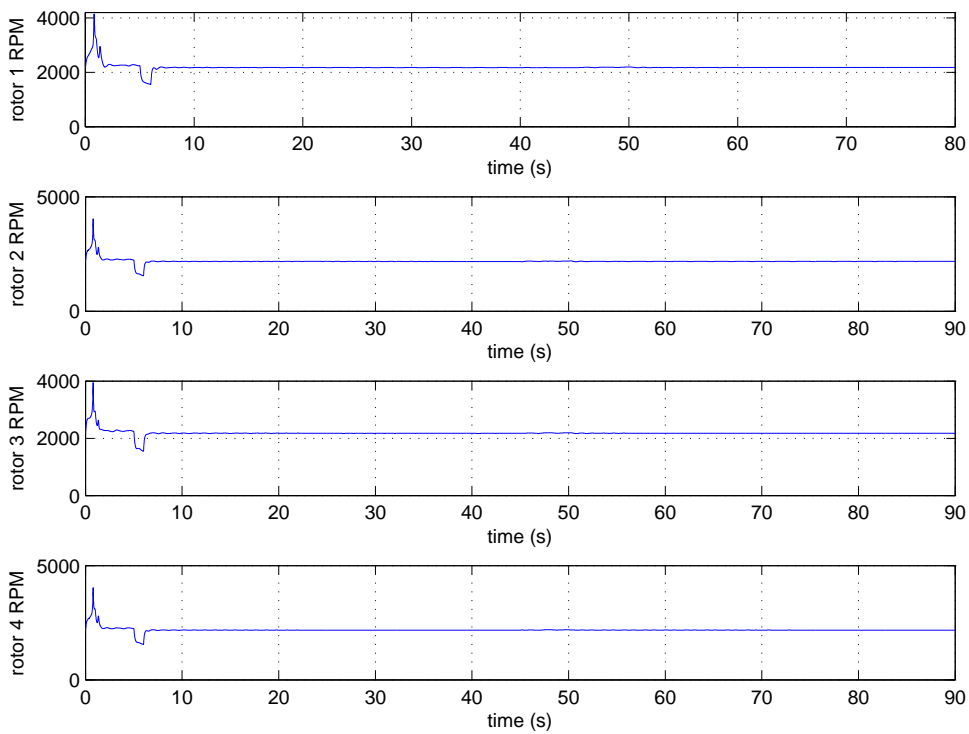


Figure 4.10: Propeller Speeds of the 1st Follower Quadrotor (Three Quadrotor)

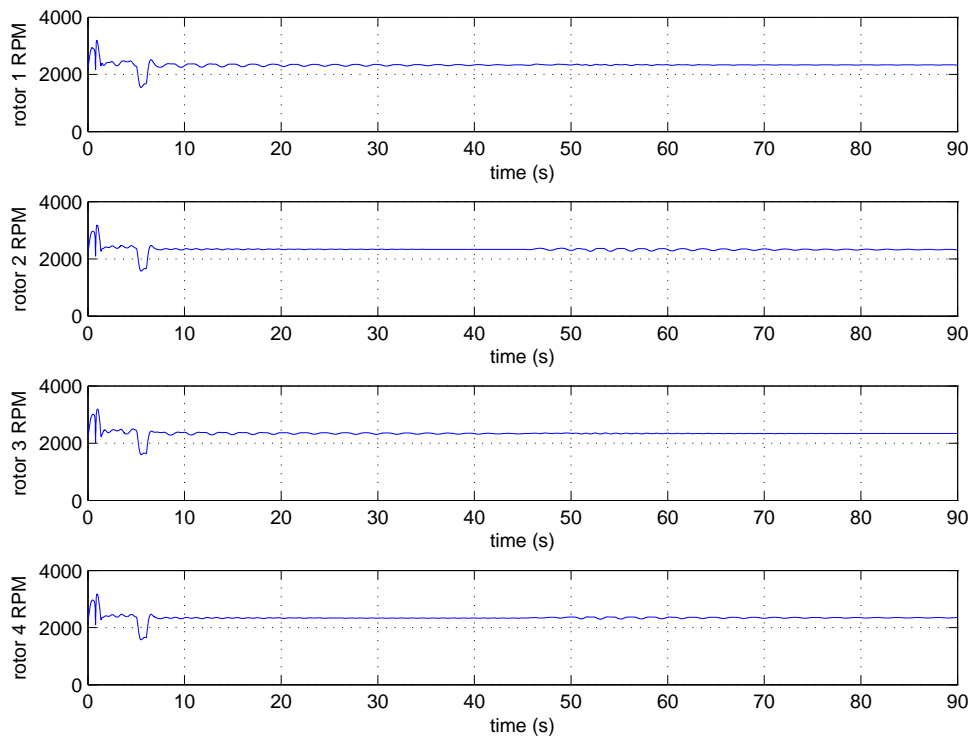


Figure 4.11: Propeller Speeds of the 2nd Follower Quadrotor (Three Quadrotor)

CHAPTER 5

TWO QUADROTOR SLUNG LOAD SYSTEM: QUATERNION BASED ATTITUDE CONTROL APPROACH

In the previous chapters, the control scheme implemented for the slung load systems involved a two-loop architecture, in which we had a Lyapunov function based formation guidance controller on the outer loop and two LQT controllers in the inner loop. In this chapter, we will be replacing the inner loop LQT controllers with a quaternion based nonlinear attitude controller. Thus our overall control approach will be more nonlinear than the approach presented in the previous chapters.

The overall control algorithm for the formation flight of the two quadrotor slung load system presented in this chapter employs a three-loop architecture. The outermost loop implements the Lyapunov function based formation guidance controller. This controller receives the desired relative distance of the quadrotors in the formation and outputs the control velocity to track this relative distance. Details of its design has already been given in section 3.2.1. The middle loop contains a LQT controller which tracks the velocity commands from the outermost loop by generating a control force command that our quadrotor must track to achieve the desired velocity command. This generated control force is then sent into the innermost loop of the control system. Through the pitching and rolling motion of the quadrotor, the innermost loop orients the total force acting on the quadrotor to match the control force command coming from the middle loop. The innermost loop controller is designed using to-go quaternion as well as a Lyapunov function and is thus nonlinear. In summary, the translational control of the quadrotor takes place in the middle loop and the attitude control of the quadrotor takes place in the innermost loop. The details for the design of the middle and innermost loops will be presented in the coming sections.

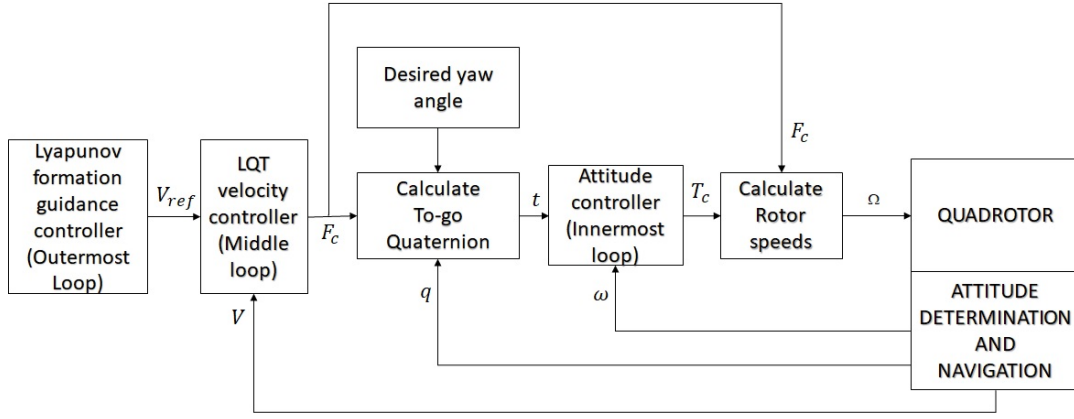


Figure 5.1: Two quadrotor slung load control system schematic: new approach

5.1 Problem Formulation and Implementation

5.1.1 Definition of the to-go quaternion

A quaternion is parameter that can be used represent the orientation or attitude of a body. It consists of a vectorial part \mathbf{q} and a scalar part q_4 . Thus, a quaternion, q can be written as $q = \mathbf{q} + q_4$. Given two attitudes of a body, q and d , where q is the current attitude of the body and d is the desired attitude of that body. A third quaternion, t , called the to-go quaternion can be defined to rotate the current quaternion, q of the body into the desired quaternion, d of that body. The desired quaternion, d , may be written using quaternion multiplication as [37]:

$$d = q \otimes t \quad (51)$$

multiplying both sides of eqn. 51 by the inverse quaternion, q^{-1} , the to-go quaternion can be obtained in terms of the current and desired attitude quaternion as:

$$t = q^{-1} \otimes d \quad (52)$$

Applying the quaternion multiplication rule, the to-go quaternion becomes:

$$\begin{aligned} t &= (-\mathbf{q} + q_4) \otimes (\mathbf{d} + d_4) \\ &= -\mathbf{q} \times \mathbf{d} - d_4 \mathbf{q} + q_4 \mathbf{d} + \mathbf{q} \cdot \mathbf{d} + d_4 q_4 \end{aligned} \quad (53)$$

where the cross product of the vectorial part of quaternion \mathbf{q} and \mathbf{d} is $\mathbf{q} \times \mathbf{d}$ and the dot product of the vectorial part of the quaternion \mathbf{q} and \mathbf{d} is $\mathbf{q} \cdot \mathbf{d}$.

The derivative of the to-go quaternion may be found as [37]:

$$\begin{aligned}\dot{\mathbf{t}} &= -\frac{1}{2}\omega^\times \mathbf{t} - \frac{1}{2}\omega t_4 \\ \dot{t}_4 &= \frac{1}{2}\omega^T \mathbf{t}\end{aligned}\tag{54}$$

where $\omega^\times \mathbf{t}$ is the cross product of the angular velocity of the body fixed frame with respect to the inertial frame and the vectorial part of the to-go quaternion.

5.1.2 Mechanization of the Attitude Control

As stated earlier, the attitude of the quadrotor is controlled by orienting the overall thrust vector of the quadrotor with the control force vector from the LQT velocity controller. To carry out this control, we must first realize that the quadrotor has all its propellers generating the thrust perpendicular to the quadrotor plane. Thus, in the body fixed coordinates of the quadrotor, the thrust vector direction is:

$$\gamma^B = -\mathbf{k}\tag{55}$$

In the navigation frame, the desired thrust vector direction, dictated by the LQT velocity control system is given as:

$$\lambda^N = \frac{F_{xC}^N \mathbf{I} + F_{yC}^N \mathbf{J} + F_{zC}^N \mathbf{K}}{F_{total}}\tag{56}$$

where

$$F_{total} = \sqrt{(F_{xC}^N)^2 + (F_{yC}^N)^2 + (F_{zC}^N)^2}\tag{57}$$

The desired thrust vector direction can then be transformed to the body fixed frame using quaternion multiplication or DCM from either quaternion or Euler angles:

$$\lambda^B = q^{-1} \otimes \lambda^N \otimes q = C_N^B \lambda^N\tag{58}$$

Since we must rotate the current thrust vector direction to the desired thrust vector direction, we need to obtain the rotation axis and angle. The rotation axis η^B around which the quadrotor is rotated as well as the rotation angle β can be found thus:

$$\gamma^B \times \lambda^B = -\mathbf{k} \times \lambda^B = \eta^B \sin(\beta)\tag{59}$$

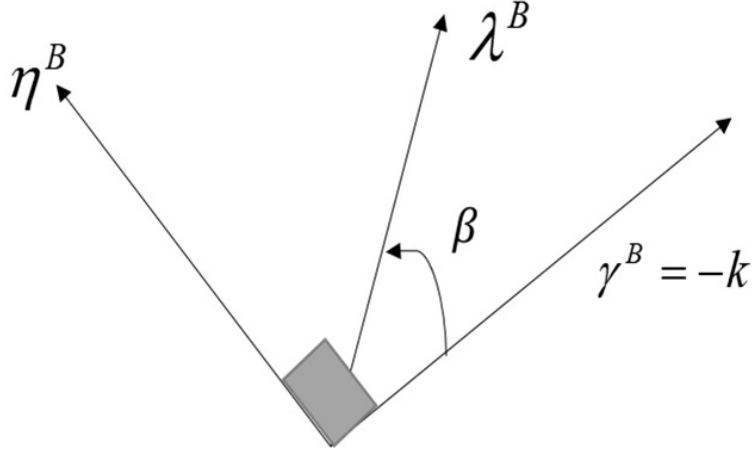


Figure 5.2: Current Thrust Vector, γ^B , Desired Thrust Vector, λ^B , Rotation Axis, η^B , Rotation Angle, β

and

$$\gamma^B \cdot \lambda^B = -\lambda_z^B = \cos(\beta) \quad (510)$$

Then the to-go quaternion can now be obtained as follows:

$$s_4 = \cos(\beta/2) = \sqrt{\frac{1 - \lambda_z^B}{2}} \quad (511)$$

$$\mathbf{s} = \eta^B \sin(\beta/2) = \frac{-\mathbf{k} \times \lambda^B}{2s_4} = \frac{\lambda_y^B \mathbf{i} - \lambda_x^B \mathbf{j}}{2s_4} \quad (512)$$

We must also include another quaternion to properly orient the quadrotor in the yaw direction. The desired thrust vector direction coming from the LQT controller will not properly orient our quadrotor in yaw as this is not needed to track the velocity commands. However, holding the heading also introduces additional constraints to limit the swinging and rocking of the slung load. This quaternion can be written as:

$$\begin{aligned} \mathbf{y} &= \mathbf{k} \sin(\Delta\psi/2) \\ y_4 &= \cos(\Delta\psi/2) \end{aligned} \quad (513)$$

where $\Delta\psi = \psi_{commanded} - \psi$

The total to-go quaternion can then be obtained by multiplying the quaternion associated with thrust vector direction with the quaternion associated with yaw rotation:

$$t = s \otimes y \quad (514)$$

5.1.3 LQT Velocity Controller Design (Middle Loop)

The LQT optimal control law is gotten by minimizing over a performance index through solving the algebraic Riccati equation. Details about this has already been presented before in section 2.3. As pertaining to our problem, our LQT velocity controller should receive velocity commands and output the required thrust vector direction to track the velocity commands. To do this, the newton equation for translation of the quadrotor written in the inertial frame is:

$$\begin{aligned}\dot{v}_x &= \frac{-k_x}{m}v_x + \frac{1}{m}F_x \\ \dot{v}_y &= \frac{-k_y}{m}v_y + \frac{1}{m}F_y \\ \dot{v}_z &= \frac{-k_z}{m}v_z + \frac{1}{m}F_z + g\end{aligned}\tag{515}$$

Equation 515 can then be written in state-space form as:

$$\begin{Bmatrix} \dot{v}_x \\ \dot{v}_y \\ \dot{v}_z \end{Bmatrix} = \begin{bmatrix} \frac{-k_x}{m} & 0 & 0 \\ 0 & \frac{-k_y}{m} & 0 \\ 0 & 0 & \frac{-k_z}{m} \end{bmatrix} \begin{Bmatrix} v_x \\ v_y \\ v_z \end{Bmatrix} + \begin{bmatrix} \frac{1}{m} & 0 & 0 \\ 0 & \frac{1}{m} & 0 \\ 0 & 0 & \frac{1}{m} \end{bmatrix} \begin{Bmatrix} F_x \\ F_y \\ F_z \end{Bmatrix} + \begin{Bmatrix} 0 \\ 0 \\ g \end{Bmatrix}\tag{516}$$

From eqn. 516, we see a constant input vector term $\begin{Bmatrix} 0 \\ 0 \\ g \end{Bmatrix}$. Due to this constant input vector term, a new gain in addition to the ones obtained in section 2.3 needs to be obtained. From reference [33], this gain term is:

$$\mathbf{K}_f = -\mathbf{R}^{-1}\mathbf{B}^t[\mathbf{P}\mathbf{E} - \mathbf{A}^t]^{-1}\mathbf{P}\tag{517}$$

thus the optimal control law is:

$$\mathbf{u}(t) = \mathbf{K}\mathbf{x}(t) + \mathbf{K}_Z\mathbf{z}(t) + \mathbf{K}_f\mathbf{f}(t)\tag{518}$$

where the gains \mathbf{K} and \mathbf{K}_Z have been obtained in section 2.3 in eqn. 235.

Using equations 516, 517 and 235, our LQT controller is then designed.

All the eigenvalues in table 5.2 are all negative. Thus, we have an asymptotically stable system.

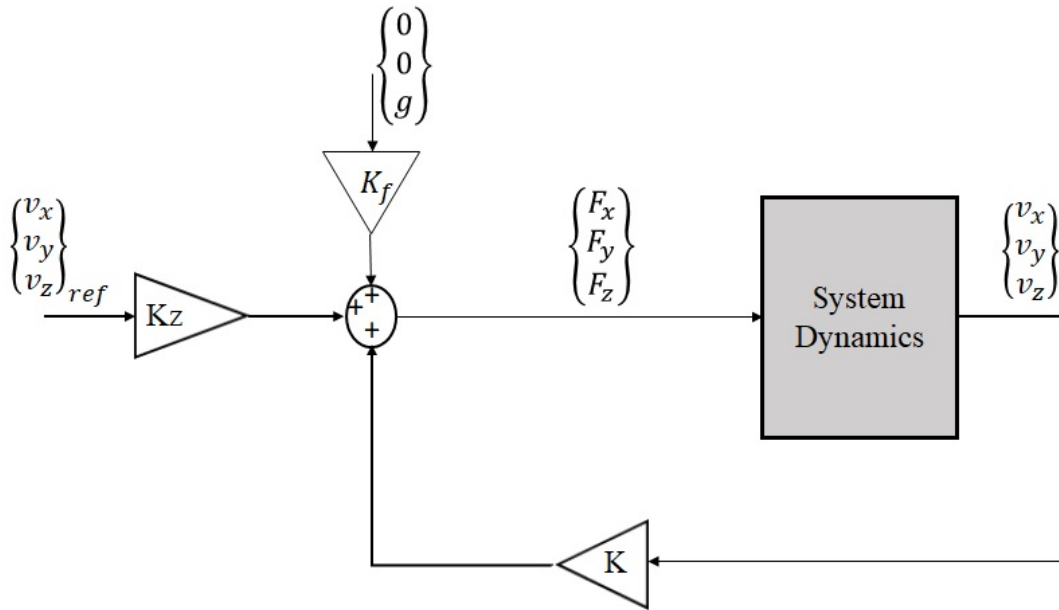


Figure 5.3: LQT Velocity Control System with Thrust vector output

Table 5.1: LQT Gains for the Velocity Controller with Thrust vector output

\mathbf{K}	$\begin{bmatrix} -1.32 & 0 & 0 \\ 0 & -1.32 & 0 \\ 0 & 0 & -19.90 \end{bmatrix}$
\mathbf{K}_z	$\begin{bmatrix} 1.41 & 0 & 0 \\ 0 & 1.41 & 0 \\ 0 & 0 & 19.99 \end{bmatrix}$
\mathbf{K}_f	$\begin{bmatrix} -0.60 & 0 & 0 \\ 0 & -0.60 & 0 \\ 0 & 0 & -0.65 \end{bmatrix}$

Table 5.2: Eigenvalues of the Velocity_x and Velocity_z Controller

Eigenvalues	Settling Time
-2.18	1.47 Sec
-30.77	0.10 Sec
-2.18	1.47 Sec

5.1.4 Quaternion based Attitude Controller Design (Innermost Loop)

The rotational equations of the quadrotor as obtained in eqn. 225 can be rewritten as:

$$\begin{bmatrix} \dot{p} \\ \dot{q} \\ \dot{r} \end{bmatrix} = \begin{bmatrix} (I_y - I_z)qr/I_x \\ (I_z - I_x)pr/I_y \\ (I_x - I_y)pq/I_z \end{bmatrix} + \begin{bmatrix} d/I_x & 0 & 0 \\ 0 & d/I_y & 0 \\ 0 & 0 & 1/I_z \end{bmatrix} \begin{bmatrix} U_2 \\ U_3 \\ U_4 \end{bmatrix} \quad (519)$$

The quadrotor attitude will be controlled by a Lyapunov function based nonlinear controller. As stated earlier, the attitude control of the quadrotor will be implemented by rotating the total thrust vector of the quadrotor to align with the desired thrust vector direction obtained from the middle loop LQT controller designed in section 5.1.3. The quadrotor will be rotated using the to-go quaternion obtained in eqn. 514.

$$\text{Let } S = \begin{bmatrix} (I_x - I_z)qr/I_x \\ (I_z - I_x)pr/I_y \\ (I_x - I_y)pq/I_z \end{bmatrix}, G = \begin{bmatrix} d/I_x & 0 & 0 \\ 0 & d/I_y & 0 \\ 0 & 0 & 1/I_z \end{bmatrix} \text{ and } U = \begin{bmatrix} U_2 \\ U_3 \\ U_4 \end{bmatrix}$$

Also, consider the following Lyapunov function [38]:

$$V = \frac{1}{2}\omega^T M^{-1} J \omega + 2(1 - t_4) \quad (520)$$

It is assumed that a positive definite M^{-1} exists and $M^{-1}J$ is also a positive definite symmetric matrix. Then the derivative of the Lyapunov function becomes:

$$\dot{V} = \omega^T M^{-1} J \dot{\omega} - \omega^T \mathbf{t} \quad (521)$$

To ensure that eqn. 521 is negative definite, we make it equal to:

$$-\omega^T M^{-1} N \omega \quad (522)$$

where $M^{-1}N$ is a positive definite matrix. Thus we have :

$$\dot{V} = \omega^T M^{-1} J \dot{\omega} - \omega^T \mathbf{t} = -\omega^T M^{-1} N \omega \quad (523)$$

simplifying the above equation and multiplying both sides by M , we obtain:

$$J \dot{\omega} - M \mathbf{t} = -N \omega \quad (524)$$

substituting eqn. 519 into eqn. 524, we have:

$$J(S + GU) - M \mathbf{t} = -N \omega \quad (525)$$

solving eqn. 525 for U , the control law for the attitude control of the quadrotor can then be obtained as:

$$U = G^{-1}[J^{-1}(M\mathbf{t} - N\omega) - S] \quad (526)$$

Using the control law obtained in eqn. 526 with $U = \begin{bmatrix} U_2 \\ U_3 \\ U_4 \end{bmatrix}$ and making $U_1 = F_{total} =$

$\sqrt{(F_{xC}^N)^2 + (F_{yC}^N)^2 + (F_{zC}^N)^2}$ where F_{total} is the magnitude of the thrust vector obtained from the LQT velocity controller in section 5.1.3, the rotor speeds to control the translational and rotational motion of the quadrotor can be obtained.

In the design of the overall control system, the three controllers in the three-loop architecture were tuned to the settling times in table 5.3

Table 5.3: Controller Settling Times

Lyapunov Formation Guidance controller (Outermost Loop)	LQT Velocity Controller (Middle Loop)	Quaternion based Attitude Controller (Innermost Loop)
2 Sec	1.47 Sec	0.38 Sec
2 Sec	0.10 Sec	
1 Sec	1.47 Sec	

5.2 Two Quadrotor Slung Load System Result and Discussion (New Approach)

The new control system designed in this chapter is tested against the nonlinear two quadrotor slung load model already designed in chapter 3. To test the control system, the same formation flight scenario employed in section 3.3 is used. The leader quadrotor is sent desired velocity commands, and a desired relative distance command is sent to the formation guidance controller to enable the follower quadrotor maintain that distance. It is desired that the initial formation geometry be maintained in spite of the leader quadrotor motion. The reference relative distance sent to the formation guidance controller is: $(x_F - x_L, y_F - y_L, z_F - z_L) = (0, 1, 0)$.

From fig. 5.4, we see that the leader quadrotor is able to closely follow the desired velocity commands in spite of the slung load. Figures 5.5 and 5.6 show the two quadrotor and load positions. The follower quadrotor is able to keep up with the leader quadrotor. Figure 5.7 shows the time history of the relative position of the follower quadrotor to the leader quadrotor. We see that the desired relative distance is being tracked albeit a really small steady state error. In the first 8 secs, we see the follower quadrotor oscillating between lagging behind and overtaking the leader quadrotor, the amplitude of the oscillation progressively reduces until the follower quadrotor settles at the desired relative distance with the leader quadrotor in the x-direction. Between 45 secs and 50 secs, we see some lag as the leader quadrotor begins to track the side velocity v_y . The follower quadrotor is able to recover quickly however. Figure 5.8 shows the load rock, swing and heading angles. The two quadrotors are able to carry the load in a smooth fashion. We see a deflection in the load rock angle from -10 degrees to 20 degrees in the first 10 secs. This is as a result of the configuration of the two quadrotor slung load system. The load rotated around its x-axis as the leader quadrotor initially climbed, but as the follower quadrotor moved to maintain the formation geometry, the load rock angle quickly returns to 0 degrees. We see an oscillation in the heading angle of the load between -50 degrees to 50 degrees in the first 10 seconds of the simulation. The amplitude of this oscillation also progressively reduces to zero as well. This heading angle oscillation is as a result of the follower quadrotor oscillating between lagging behind and overtaking the leader quadrotor in the first 10 seconds of the simulation. Figures 5.9 and 5.10 shows the propeller speeds of the two quadrotors. There are no saturations in the speeds of the rotors.

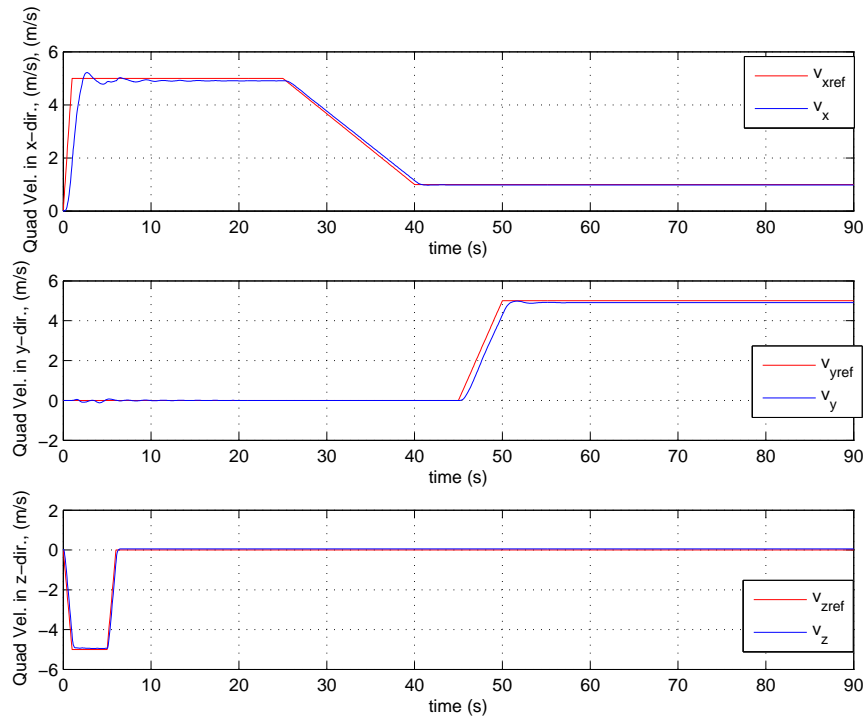


Figure 5.4: Leader Quadrotor Velocity in x, y and z directions respectively (Two Quadrotor, New Approach)

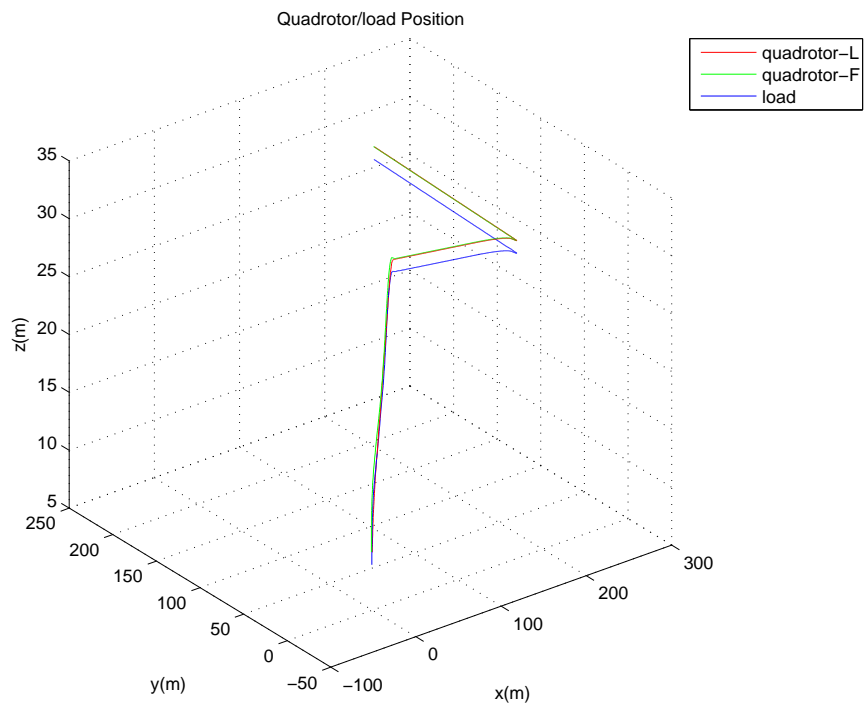


Figure 5.5: Leader and Follower Quadrotor position and Load Position (Two Quadrotor, New Approach)

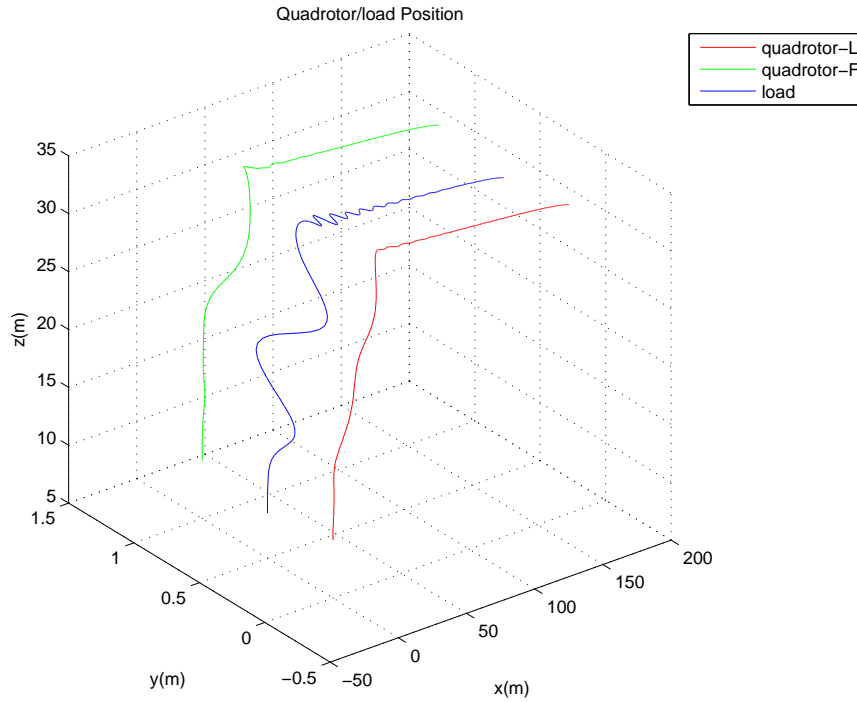


Figure 5.6: Leader and Follower Quadrotor position and Load Position (Two Quadrotor, New Approach, 40 secs Simulation)

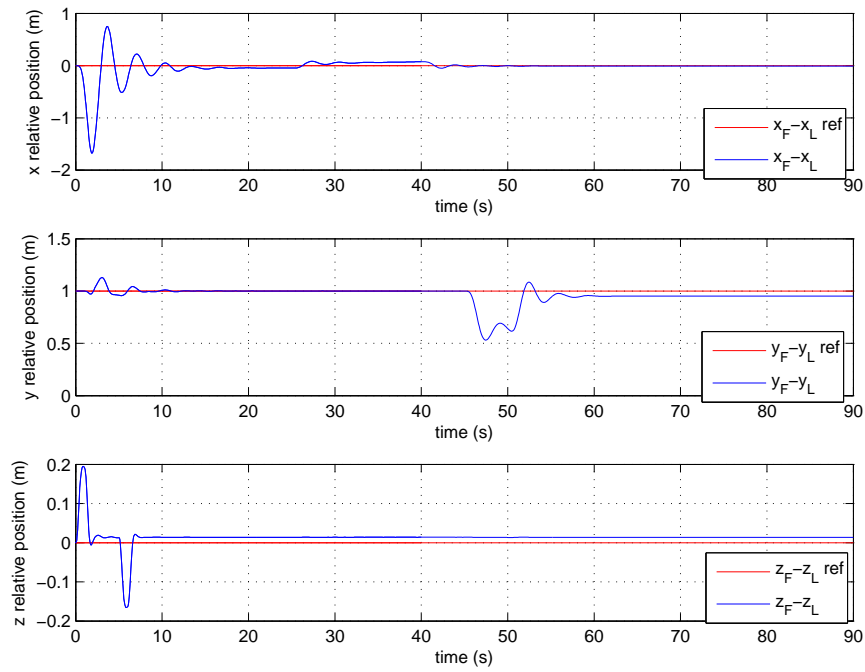


Figure 5.7: Leader and Follower Quadrotor relative positions (Two Quadrotor, New Approach)

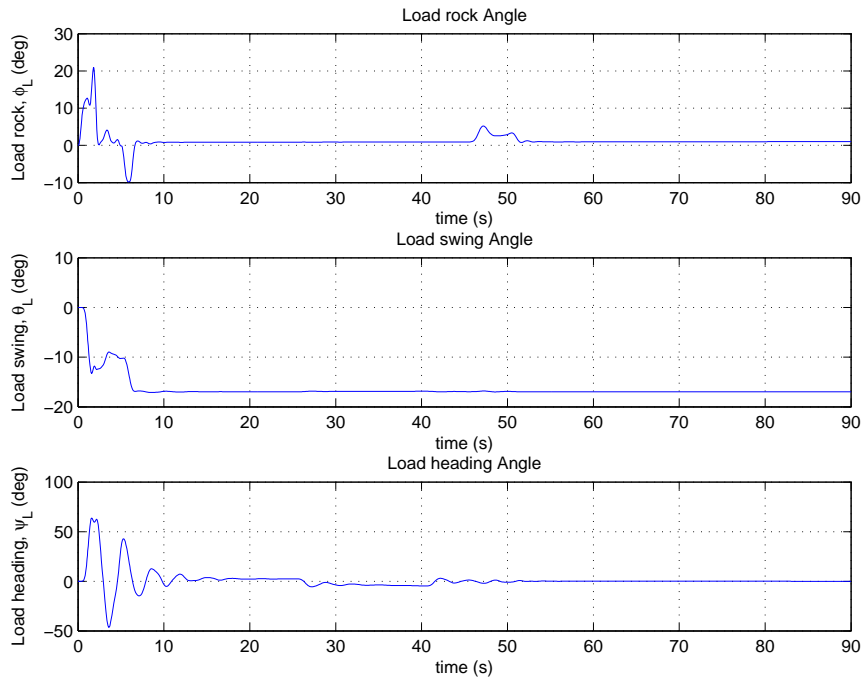


Figure 5.8: Swing, Rock and Heading Angles of the Load (Two Quadrotor, New Approach)

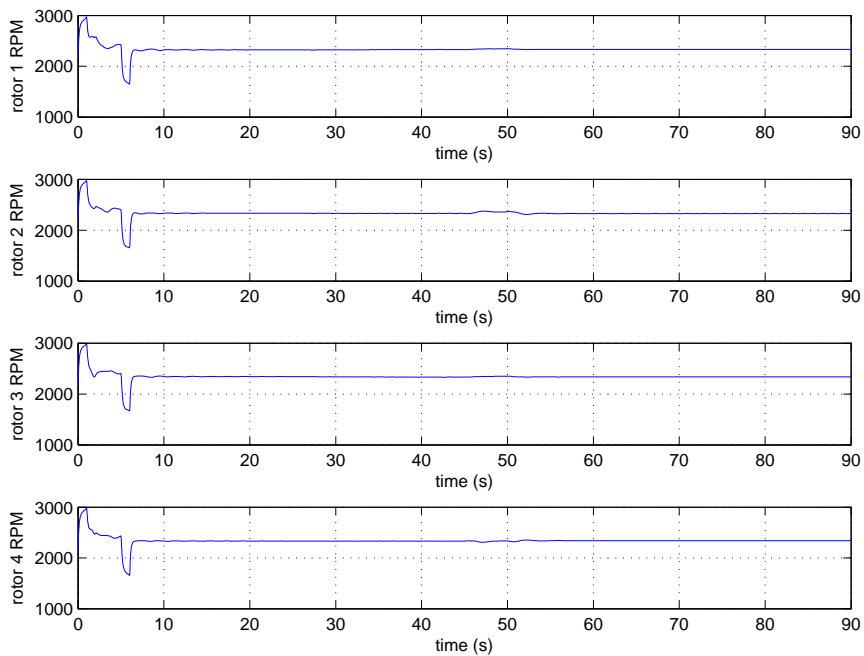


Figure 5.9: Propeller Speeds of the Leader Quadrotor (Two Quadrotor, New Approach)

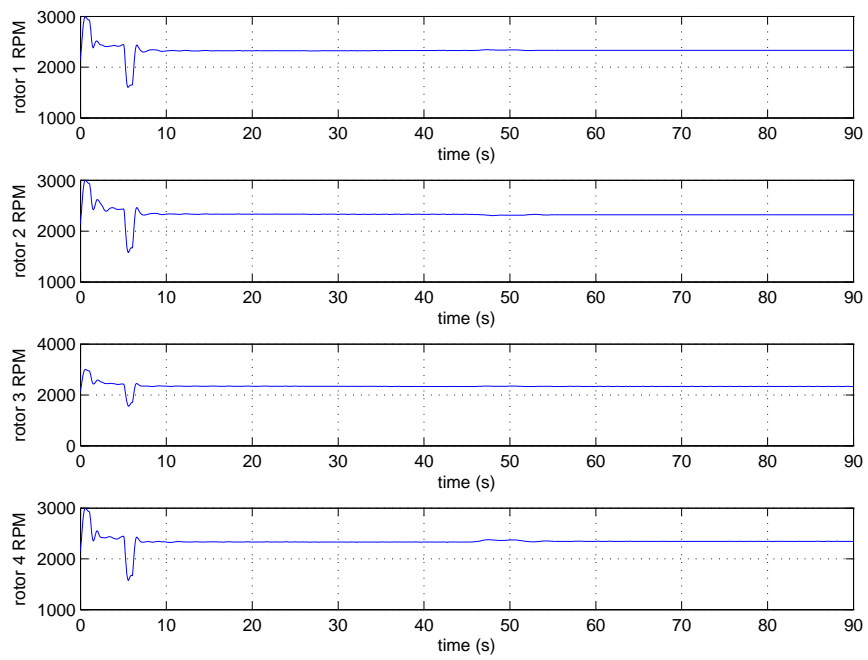


Figure 5.10: Propeller Speeds of the Follower Quadrotor (Two Quadrotor, New Approach)

5.3 Alternative Approach: Full Nonlinear Control Algorithm for a Two Quadrotor Slung Load System

In the previous section (section 5.1), a three loop control architecture is used on the follower quadrotor to fly the formation together with the slung load. It featured a nonlinear formation guidance loop in its outermost loop, a LQT controller in the middle loop where the desired thrust vector direction to properly orient the quadrotor is obtained, and finally, a nonlinear attitude controller in its innermost loop. Although, the control algorithm performs brilliantly, as seen in section 5.2, it is not fully nonlinear.

In this section, a full nonlinear control algorithm is presented. It features a two-loop architecture as opposed to the three-loop architecture presented in section 5.1.

5.3.1 Alternative Approach: Full Nonlinear Control Algorithm Problem Formulation and Implementation

In this section, new fully nonlinear controllers are developed. The Outer and middle loop are combined into a single loop. The inner loop algorithm is the same as presented in section 5.1. The new two loop structure is shown in fig. 5.11.

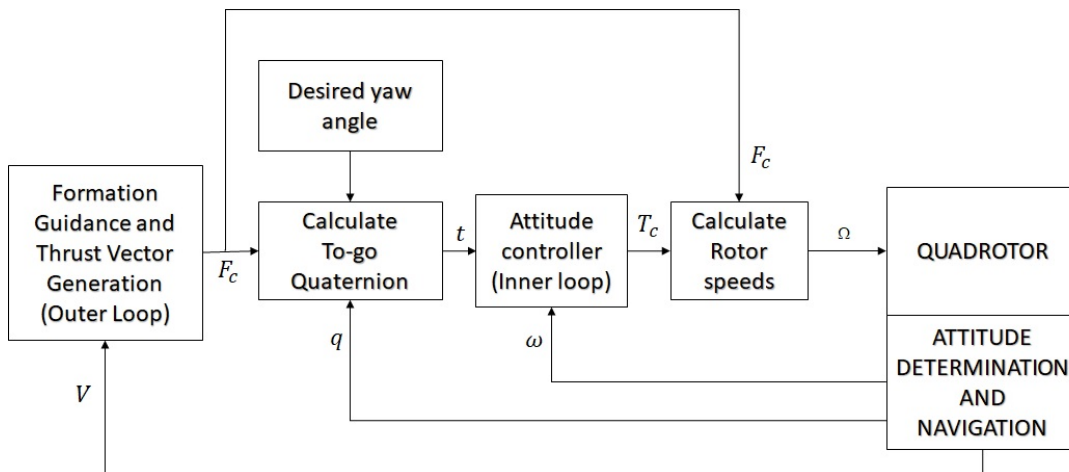


Figure 5.11: Follower quadrotor guidance and control using a two loop approach

5.3.2 Guidance and Control Loop

The outer loop is based on a Lyapunov function as follows:

$$L = \frac{1}{2}\Delta V^T m_F \Delta V + \frac{1}{2}\Delta r^T R \Delta r \quad (527)$$

where

$$\Delta r = \begin{Bmatrix} x_L + a - x_F \\ y_L + b - y_F \\ z_L + c - z_F \end{Bmatrix}, \Delta V = \begin{Bmatrix} v_{x_L} - v_{x_F} \\ v_{y_L} - v_{y_F} \\ v_{z_L} - v_{z_F} \end{Bmatrix} \quad (528)$$

(x_L, y_L, z_L) and (x_F, y_F, z_F) are the positions of the leader and the follower quadrotors with respect to the inertial frame. (a, b, c) is the desired relative position of the follower with respect to the leader quadrotor. $(v_{x_L}, v_{y_L}, v_{z_L})$ and $(v_{x_F}, v_{y_F}, v_{z_F})$ are the velocities of the leader and follower quadrotors with respect to the inertial frame. R is a positive definite matrix and m_F is the mass of the follower quadrotor. Assuming a fixed formation geometry, i.e, $(\dot{a}, \dot{b}, \dot{c}) = 0$, the derivative of the Lyapunov function gives:

$$\dot{L} = \Delta V^T m_F \Delta \dot{V} + \Delta V^T R \Delta r \quad (529)$$

To ensure that eqn. 529 is negative definite, it is equated to a negative definite function:

$$-\Delta V^T S \Delta V \quad (530)$$

where S is a positive definite matrix. Thus we have:

$$\dot{L} = \Delta V^T m_F \Delta \dot{V} + \Delta V^T R \Delta r = -\Delta V^T S \Delta V \quad (531)$$

Simplifying eqn. 531 and solving for the follower acceleration, we have:

$$m_F \dot{v}_F = m_F \dot{v}_L + R \Delta r + S \Delta V \quad (532)$$

Using the Newton's equation for translation, $m_F \dot{v}_F$ is written in the inertial frame as:

$$m_F \dot{v}_F = - \begin{bmatrix} \tilde{k}_x & 0 & 0 \\ 0 & \tilde{k}_y & 0 \\ 0 & 0 & \tilde{k}_z \end{bmatrix} \begin{Bmatrix} v_{x_F}^2 \\ v_{y_F}^2 \\ v_{z_F}^2 \end{Bmatrix} + \begin{Bmatrix} F_x \\ F_y \\ F_z \end{Bmatrix} + \begin{Bmatrix} 0 \\ 0 \\ m_F g \end{Bmatrix} \quad (533)$$

Substituting eqn. 533 into eqn. 532 and solving for the thrust vector direction, we obtain:

$$\begin{Bmatrix} F_x \\ F_y \\ F_z \end{Bmatrix} = \begin{bmatrix} \tilde{k}_x & 0 & 0 \\ 0 & \tilde{k}_y & 0 \\ 0 & 0 & \tilde{k}_z \end{bmatrix} \begin{Bmatrix} v_{x_F}^2 \\ v_{y_F}^2 \\ v_{z_F}^2 \end{Bmatrix} - \begin{Bmatrix} 0 \\ 0 \\ m_F g \end{Bmatrix} + m_F \dot{v}_L + R\Delta r + S\Delta V \quad (534)$$

The control law obtained in eqn. 534 above, helps the follower quadrotor maintain the prescribed formation geometry. It is also the thrust vector that will be sent to the inner controller. This inner loop is the same as presented in section 5.1.4.

The two controllers are tuned to the settling times in table 5.4. Similar settling times with the three loop controllers designed in section 5.1 is used to enable comparison between the three loop and two loop control algorithms designed.

Table 5.4: Controller Settling Times (Full Nonlinear)

Lyapunov Formation Guidance/Thrust Vector controller (Outer Loop)	Quaternion based Attitude Controller (Inner Loop)
2 Sec	0.38 Sec
2 Sec	0.38 Sec
1 Sec	0.38 Sec

5.3.3 Result and Discussion

To test the performance of the new two loop guidance control system, two flight scenarios are employed. The first scenario is the same formation flight scenario employed for the three loop case in section 5.2 and in the second scenario, a circular flight trajectory is employed. The desired velocity commands are sent to the leader quadrotor, and a desired relative distance command is sent to the follower quadrotor. The leader and follower quadrotor are carrying a slung load as before. It is desired that the initial formation geometry be maintained in spite of the leader quadrotor motion. The reference relative distance sent to the formation guidance controller is:

$(x_F - x_L, y_F - y_L, z_F - z_L) = (0, 1, 0)$. The simulation results for the first flight scenario are presented in figures 5.12 - 5.18.

Figure 5.12 presents the leader quadrotor response to the velocity commands. From the figure, it may be observed that the leader quadrotor closely follows the desired velocity commands in spite of the slung load. Figure 5.13 and 5.14 show the time history of the formation. The follower quadrotor is able to keep up with the leader quadrotor for the duration of the flight. Figure 5.15 shows the time history of the relative position of the follower quadrotor to the leader quadrotor. From the figure, it may be observed that the desired relative distance is closely tracked. Comparing figures 5.7 and 5.15, it may be concluded that the full nonlinear two loop controller outperforms the controller designed in section 5.1. Thus, the two loop controller is more responsive in tracking the formation geometry in spite of the leader quadrotor manoeuvre. Figures 5.16 shows the load rock, swing and heading angles. The two quadrotors are able to carry the load in a smooth fashion. We see a deflection in the load rock angle from approximately 4 degrees to 10 degrees in the first 10 secs and then settles to about 5 degrees for the remaining duration of the flight. The load rock angle is more oscillatory in the first 10 secs than the load rock angle of the controller designed in section 5.1 (fig. 5.8), however, its amplitude is much smaller. The swing angle of the load oscillates between -4 degrees and 4 degrees in the first 10 secs of simulation and then settles at 2 degrees. The heading angle oscillates between -20 degs and 30 degs in the first 10 secs. Comparing this with the results of the controller in section 5.1 (fig. 5.8), it is initially more oscillatory but with a smaller amplitude. Figures 5.17 and 5.18 show the propeller speeds of the two quadrotors. There are no saturations in the speeds of the rotors. In addition, the propeller speed history of the follower quadrotor is similar to those presented in fig. 5.10. Overall, it may be concluded that the two loop nonlinear architecture gives better results.

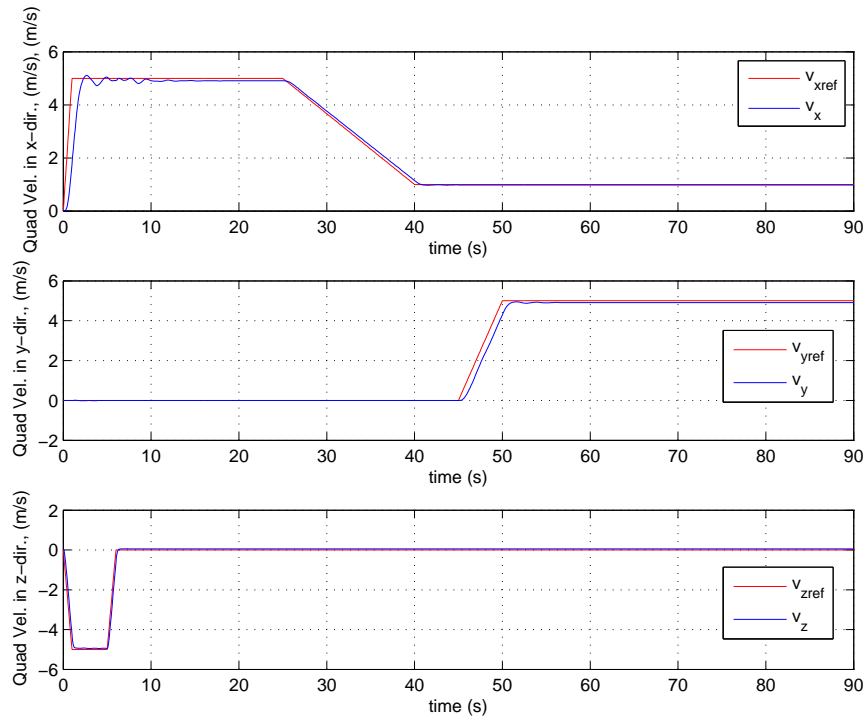


Figure 5.12: Leader Quadrotor Velocity in x, y and z directions respectively (Two Quadrotor, Alternative Approach)

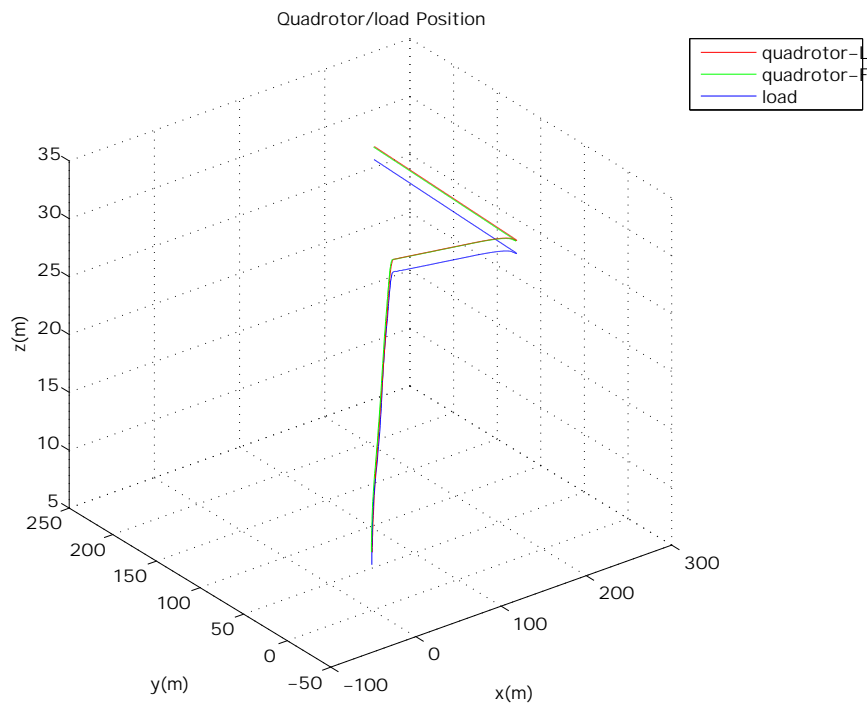


Figure 5.13: Leader and Follower Quadrotor position and Load Position (Two Quadrotor, Alternative Approach)

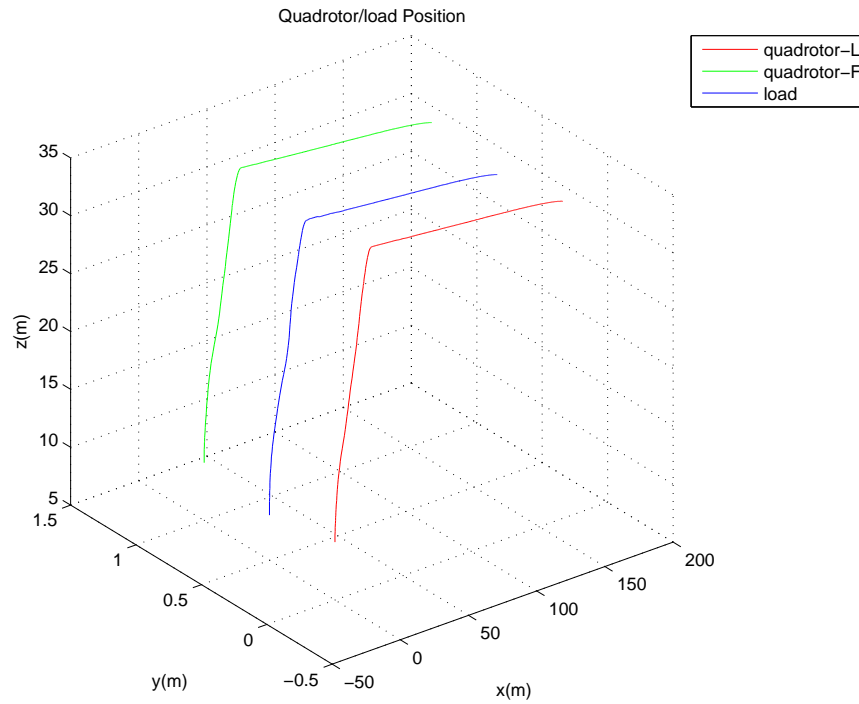


Figure 5.14: Leader and Follower Quadrotor position and Load Position (Two Quadrotor, Alternative Approach, 40 secs simulation)

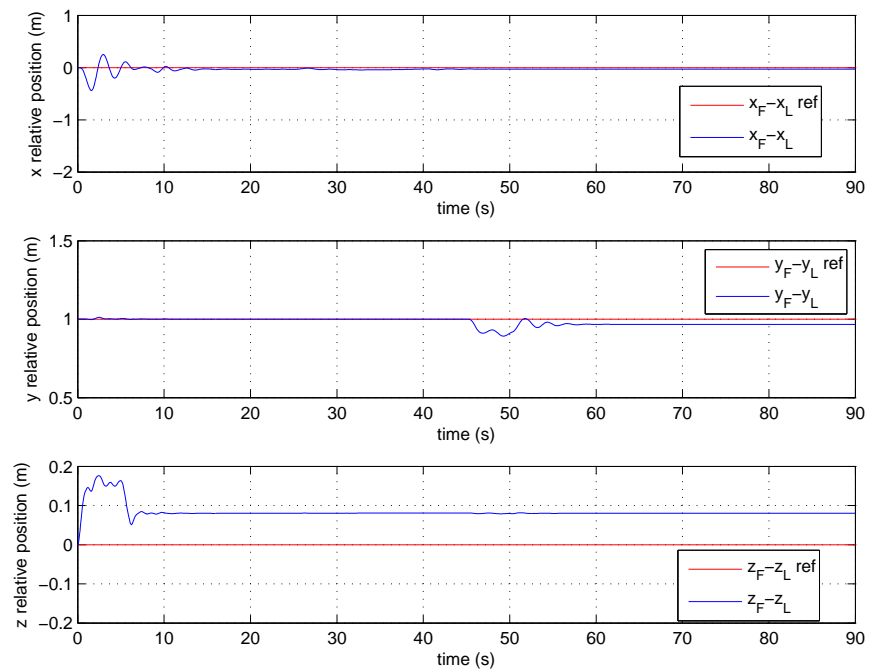


Figure 5.15: Leader and Follower Quadrotor relative positions (Two Quadrotor, Alternative Approach)

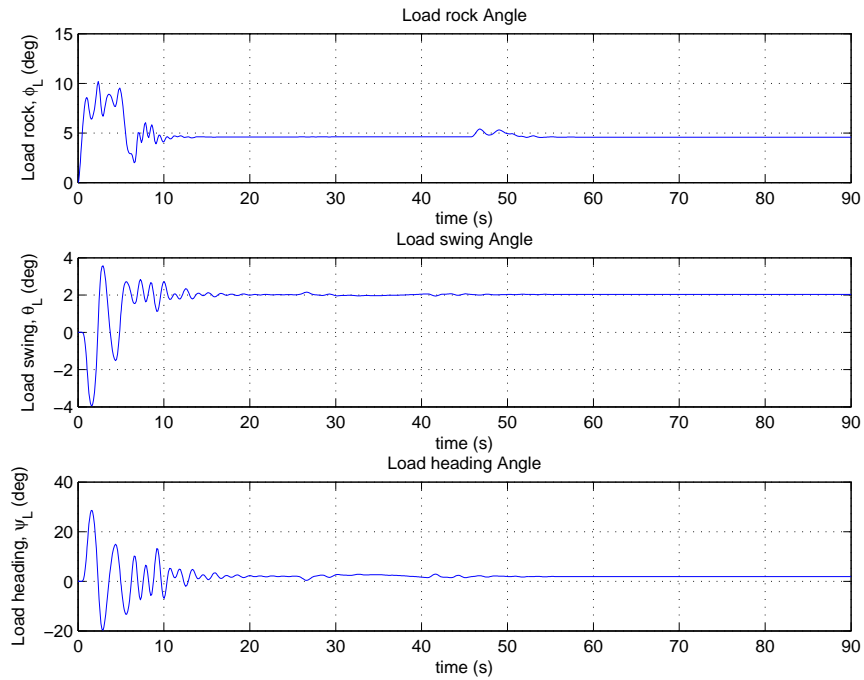


Figure 5.16: Swing, Rock and Heading Angles of the Load (Two Quadrotor, Alternative Approach)

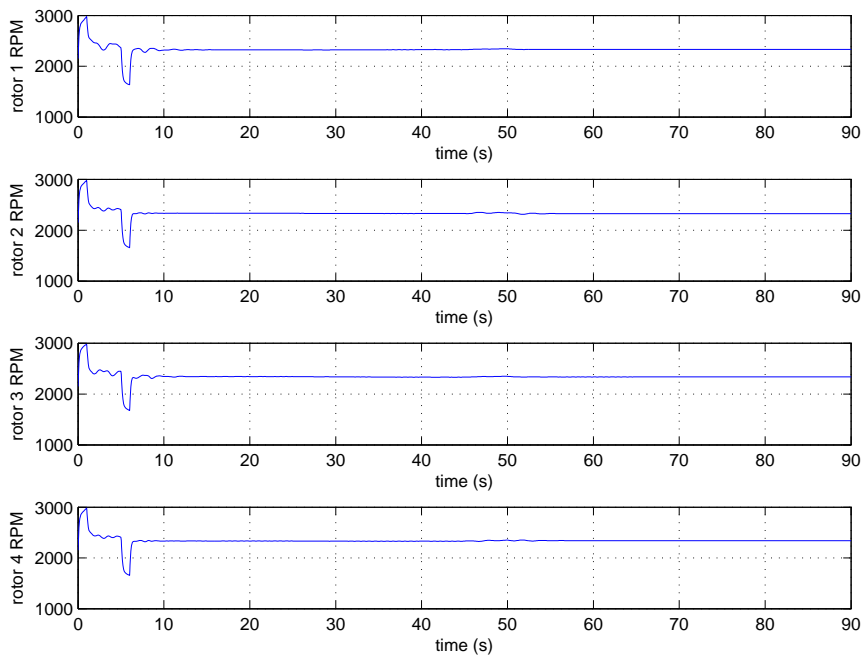


Figure 5.17: Propeller Speeds of the Leader Quadrotor (Two Quadrotor, Alternative Approach)

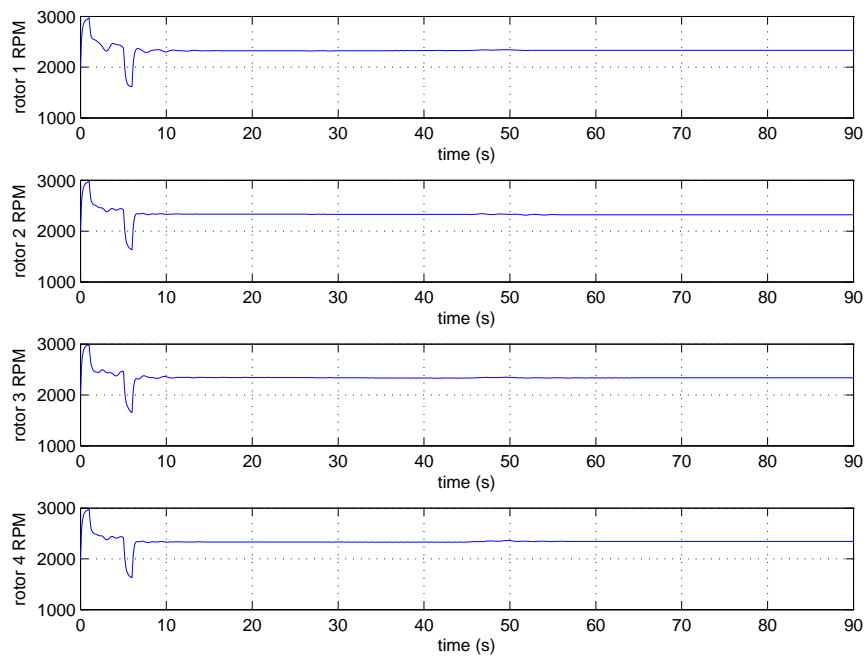


Figure 5.18: Propeller Speeds of the Follower Quadrotor (Two Quadrotor, Alternative Approach)

The simulation results of the circular flight trajectory for the second flight scenario of the leader quadrotor are presented below. The follower quadrotor is required to maintain the same formation geometry $(x_F - x_L, y_F - y_L, z_F - z_L) = (0, 1, 0)$, as with the first flight scenario, in spite of the circular trajectory of the leader quadrotor. The leader quadrotor would be flying at a tangential velocity of 3 m/s on a circular trajectory of radius 10m .

Figure 5.19 presents the leader quadrotor response to the velocity commands. From the figure, it may be observed that the leader quadrotor closely follows the desired velocity commands in spite of the slung load. Figure 5.20 shows the time history of the formation. The follower quadrotor is able to keep up with the leader quadrotor for the duration of the flight. Figure 5.21 shows the time history of the relative position of the follower quadrotor to the leader quadrotor. From the figure, it may be observed that the desired relative distance is closely tracked. Figure 5.22 shows the load rock, swing and heading angles. The two quadrotors are able to carry the load in a smooth fashion with negligible deflection of the load. The load rock angle has a maximum deflection of 6 degrees and settles at 2 degrees for the entire duration of the flight. There is almost no deflection in the swing angle of the load. The load heading angle oscillates between -4 degrees and 2 degrees. Figures 5.23 and 5.24 show the propeller speeds of the two quadrotors. There are no saturations in the speeds of the rotors.

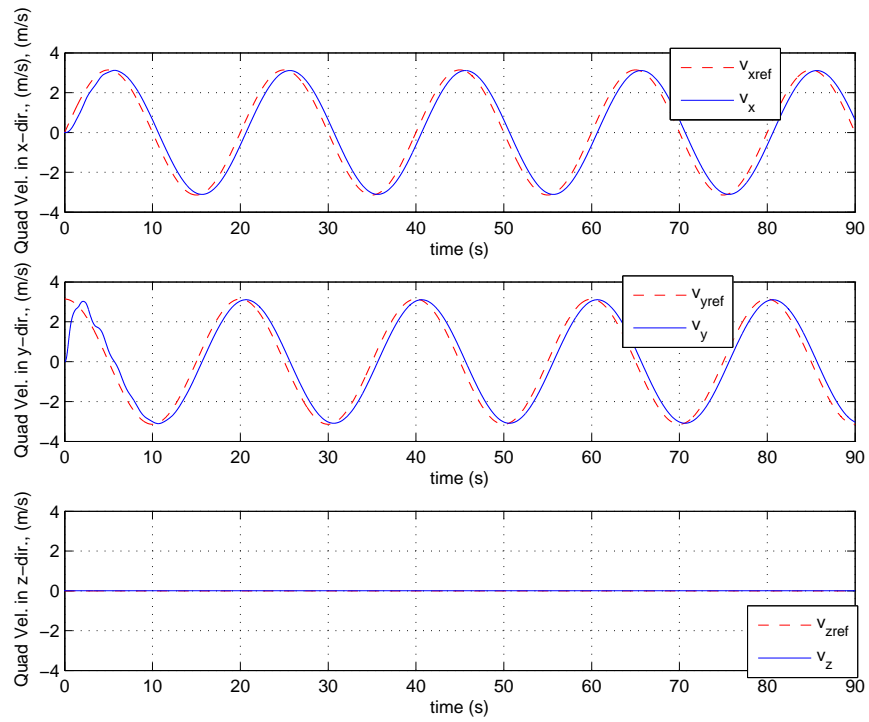


Figure 5.19: Leader Quadrotor Velocity in x, y and z directions respectively (circular trajectory, Alternative Approach)

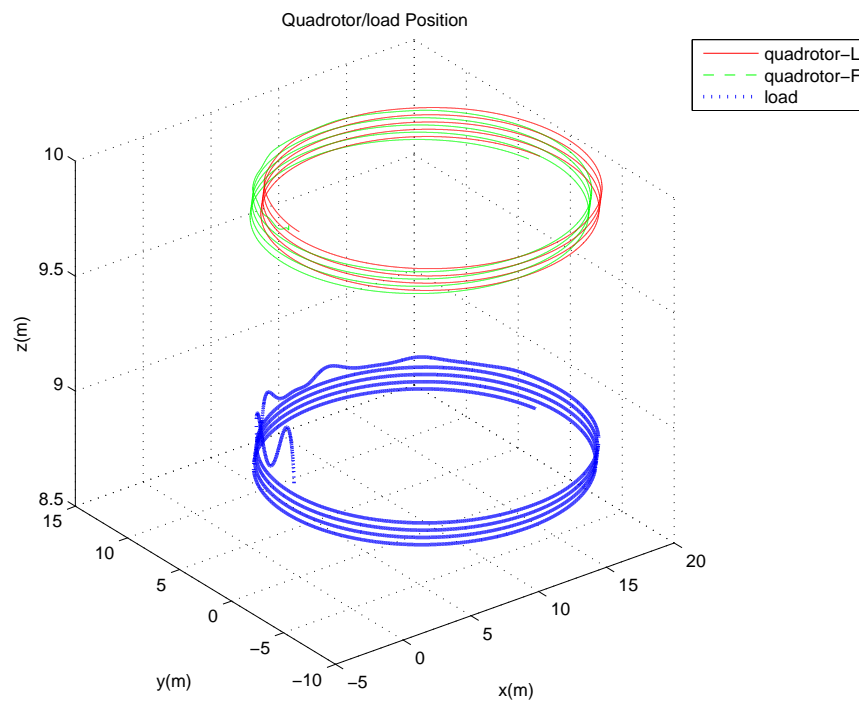


Figure 5.20: Leader and Follower Quadrotor position and Load Position (circular trajectory, Alternative Approach)

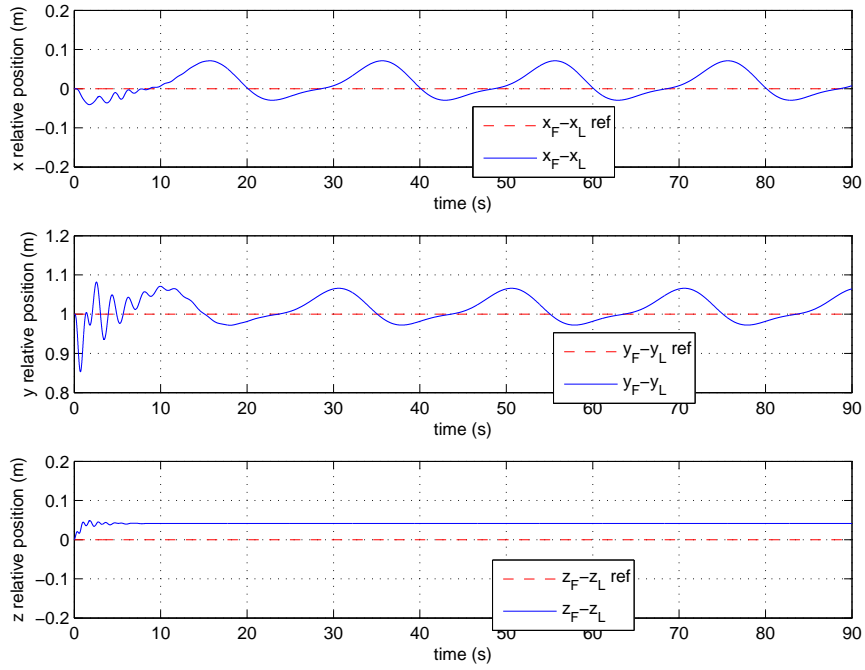


Figure 5.21: Leader and Follower Quadrotor relative positions (circular trajectory, Alternative Approach)

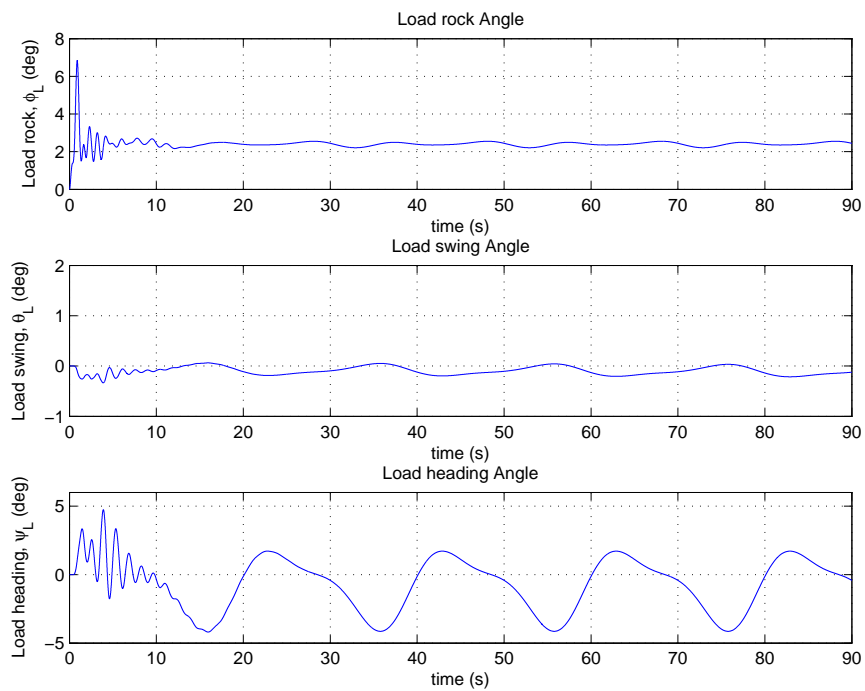


Figure 5.22: Swing, Rock and Heading Angles of the Load (circular trajectory, Alternative Approach)

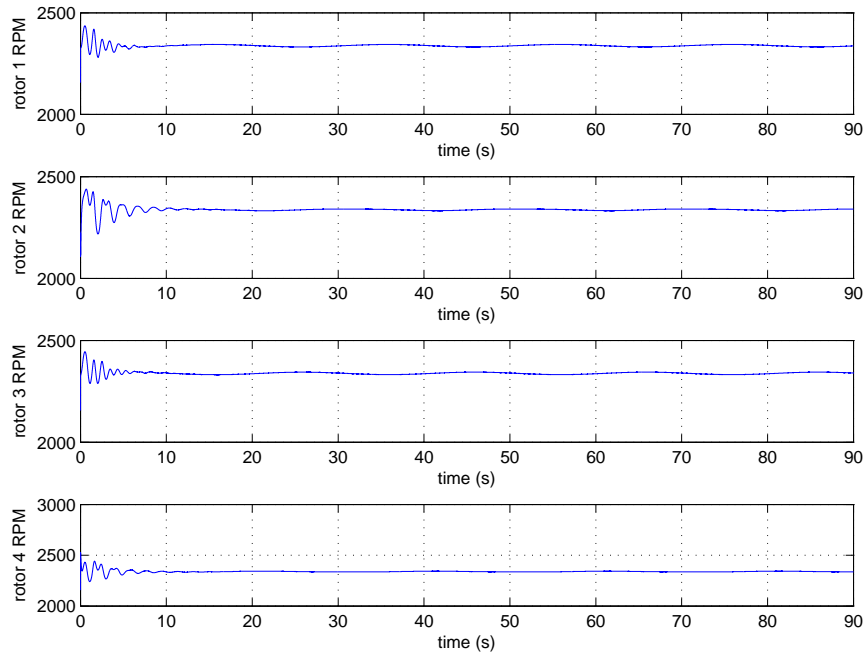


Figure 5.23: Propeller Speeds of the Leader Quadrotor (circular trajectory, Alternative Approach)

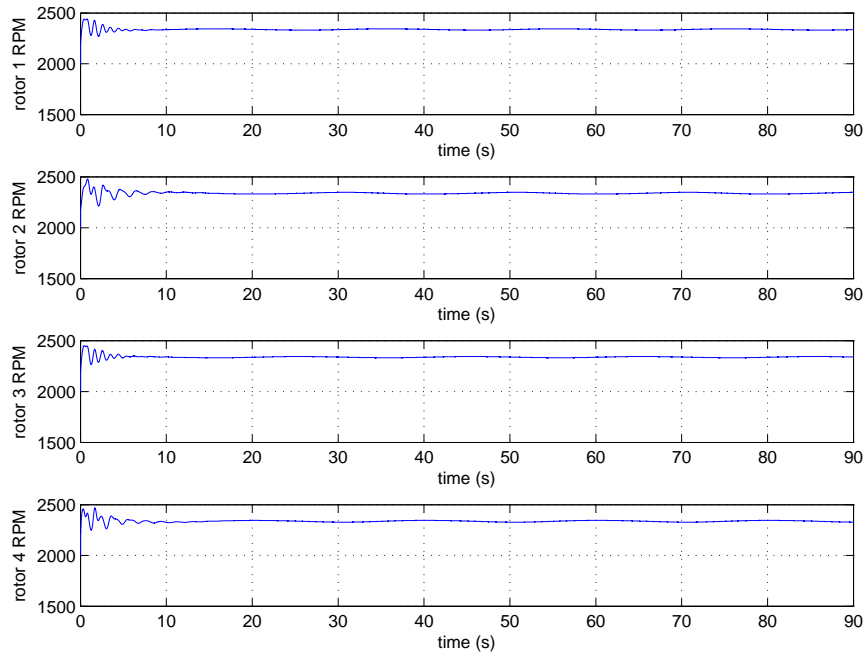


Figure 5.24: Propeller Speeds of the Follower Quadrotor (circular trajectory, Alternative Approach)

CHAPTER 6

ROBUSTNESS TEST FOR THE FULL NONLINEAR CONTROL ALGORITHM DESIGNED IN SECTION 5.3

In this chapter, a stability and performance robustness tests would be performed on the fully nonlinear controller implemented on the follower quadrotor in section 5.3. It is assumed that the leader quadrotor is able to fly without any problems, and we test to see the stability and performance limits of the nonlinear control algorithm implemented on the follower quadrotor in the presence of wind disturbances, sensor noise, varying weights of the load being carried and unmodeled dynamics of the slung load. The simulation results are then analysed and discussed.

6.1 Stability Robustness Test of the Nonlinear Controller

As previously stated in section 5.3, the nonlinear controller has a two loop architecture. The outer and inner loops were designed using Lyapunov functions. In both loops, the dynamical effects of the slung load on the quadrotor were not modelled into the controller design. According to the Lyapunov stability theorem, to guarantee stability, the derivative of the Lyapunov function should be less than zero [35]. Thus, for the stability robustness test we would be investigating the derivative of the Lyapunov functions of the inner and outer loop control architecture designed.

6.1.1 Stability Robustness of the Inner Loop Attitude Controller

The design details of this controller has been given previously in section 5.1.4. In that derivation process, the derivative of the Lyapunov function was obtained as:

$$\dot{V} = \omega_2^T M^{-1} J \dot{\omega}_2 - \omega_2^T \mathbf{t} \quad (61)$$

and from the slung load equations obtained in section 3.1, we have:

$$\dot{\omega}_2 = J_2^{-1} T_2 - J_2^{-1} r_2^\times C_N^2 F_{S_4} - J_2^{-1} \omega_2^\times J_2 \omega_2 \quad (62)$$

A control law to ensure that \dot{V} is negative was then obtained as:

$$U = G^{-1} [J^{-1} (M \mathbf{t} - N \omega) - S] \quad (63)$$

To obtain this control law, $\dot{\omega}_2$ was substituted into \dot{V} in equation 61. However, during the substitution process, the slung load component $-J_2^{-1} r_2^\times C_N^2 F_{S_4}$ was not substituted into the \dot{V} equation. In others words, the torque effect of the slung load on the quadrotor is unmodeled in the controller design. Thus, \dot{V} can now be written as:

$$\dot{V} = \omega_2^T M^{-1} J (S + GU) - \omega_2^T \mathbf{t} \quad (64)$$

where $S = -J_2^{-1} \omega_2^\times J_2 \omega_2$ and $GU = J_2^{-1} T_2$.

To carry out the stability robustness test, we included the torque effect of the slung load into the derivative of our Lyapunov function:

$$\dot{V}_{slung} = \omega_2^T M^{-1} J (S + GU - J_2^{-1} r_2^\times C_N^2 F_{S_4}) - \omega_2^T \mathbf{t} \quad (65)$$

and checked to see whether our control law U that neglects the torque effect of the slung load on the quadrotor still makes $\dot{V}_{slung} < 0$.

Figure 6.1 shows the original derivative of the Lyapunov function, \dot{V} . From the figure, we see that our chosen control law ensures that it is less than zero. Figure 6.2 shows the derivative of the Lyapunov function, \dot{V}_{slung} that was modified to include the torque effect of the slung load. From that figure, we see that with our control law, there are intervals where \dot{V}_{slung} is very slightly greater than zero as the follower quadrotor tries to catch up to the leader quadrotor to maintain formation. However, this does

not cause instability in the quadrotor slug load system. Figure 6.3 shows \dot{V}_{slung} after increasing the gain the innerloop controller. Although, the new control law is obtained with the slung load torque on the quadrotor still being unmodeled in its design, \dot{V}_{slung} becomes less than zero. Thus, we are able to guarantee the stability of our control design.

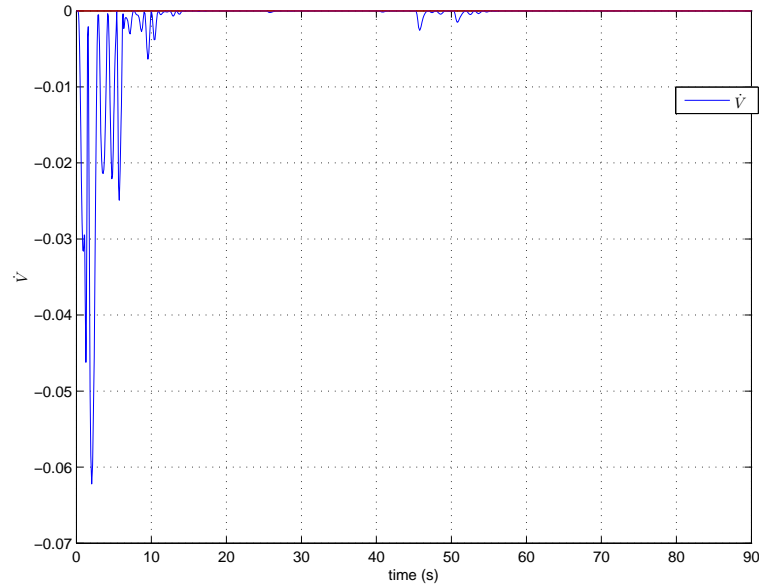


Figure 6.1: Innerloop Lyapunov function derivative without slung load torque effect

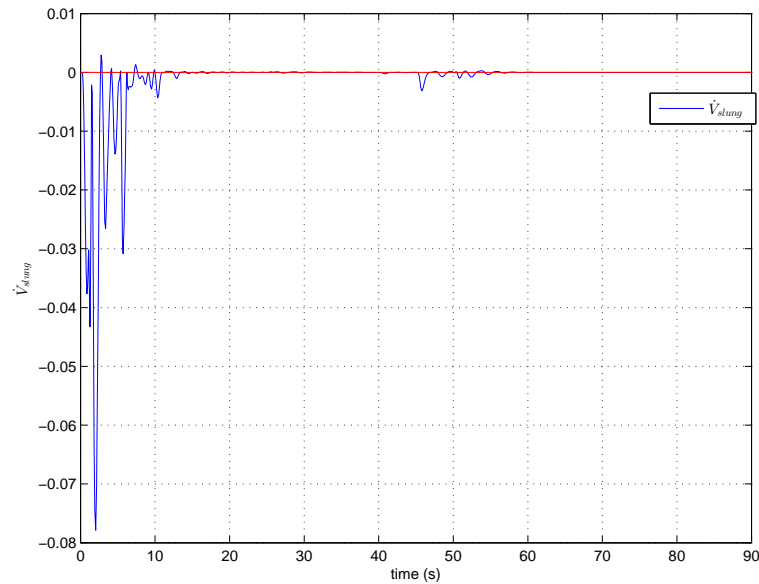


Figure 6.2: Innerloop Lyapunov function derivative with slung load torque effect

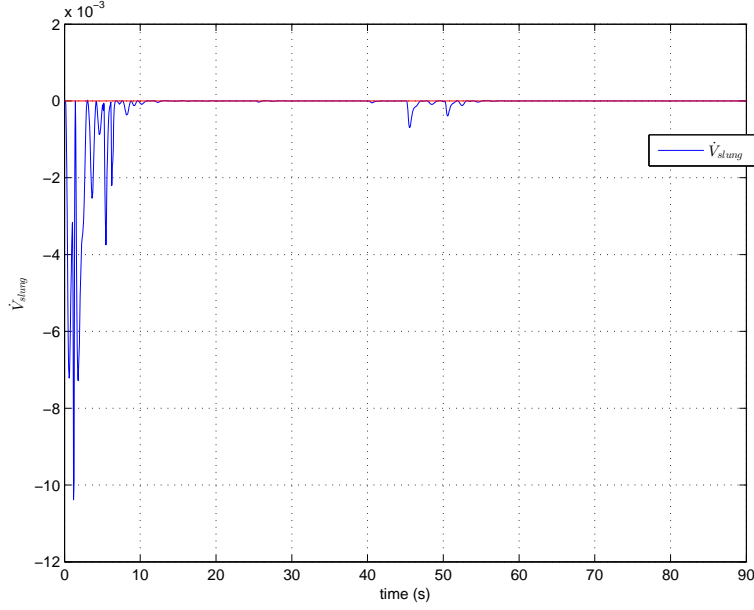


Figure 6.3: Retuned Innerloop Lyapunov function derivative with slung load torque effect

6.1.2 Stability Robustness of the Outer Loop Formation Guidance Controller

The same idea with the inner loop case is employed here as well since the outer loop controller also employs a Lyapunov function. We have a control law that is obtained by ignoring the force effect of the slung load on the quadrotor. We then check to see if this control law makes the derivative of the Lyapunov function that is modified to include the slung load force less than zero.

The details of the outer loop controller design was discussed in section 5.3.2. From that section, the derivative of the Lyapunov function was obtained as:

$$\dot{L} = \Delta V^T m_F \Delta \dot{V} + \Delta V^T R \Delta r \quad (66)$$

and from the slung load translational equations in section 3.1, we have:

$$m_F \dot{v}_F = - \begin{bmatrix} \tilde{k}_x & 0 & 0 \\ 0 & \tilde{k}_y & 0 \\ 0 & 0 & \tilde{k}_z \end{bmatrix} \begin{Bmatrix} v_{x_F}^2 \\ v_{y_F}^2 \\ v_{z_F}^2 \end{Bmatrix} + \begin{Bmatrix} F_x \\ F_y \\ F_z \end{Bmatrix} + \begin{Bmatrix} 0 \\ 0 \\ m_F g \end{Bmatrix} - F s_4 \quad (67)$$

The control law to ensure that \dot{L} is negative definite is then obtained as:

$$\begin{Bmatrix} F_x \\ F_y \\ F_z \end{Bmatrix} = \begin{bmatrix} \tilde{k}_x & 0 & 0 \\ 0 & \tilde{k}_y & 0 \\ 0 & 0 & \tilde{k}_z \end{bmatrix} \begin{Bmatrix} v_{x_F}^2 \\ v_{y_F}^2 \\ v_{z_F}^2 \end{Bmatrix} - \begin{Bmatrix} 0 \\ 0 \\ m_F g \end{Bmatrix} + m_F \dot{v}_L + R\Delta r + S\Delta V \quad (68)$$

As seen from the control law, the slung load force effect, F_{s4} , on the quadrotor, was unmodeled in its derivation process. Substituting this control law and eqn. 67 back into 66, the derivative of the Lyapunov function can be written as:

$$\dot{L} = \Delta V^T \left[m_F \dot{v}_L + \begin{bmatrix} \tilde{k}_x & 0 & 0 \\ 0 & \tilde{k}_y & 0 \\ 0 & 0 & \tilde{k}_z \end{bmatrix} \begin{Bmatrix} v_{x_F}^2 \\ v_{y_F}^2 \\ v_{z_F}^2 \end{Bmatrix} - \begin{Bmatrix} F_x \\ F_y \\ F_z \end{Bmatrix} - \begin{Bmatrix} 0 \\ 0 \\ m_F g \end{Bmatrix} \right] + \Delta V^T R\Delta r \quad (69)$$

To carry out the stability robustness test, the force effect of the slung load on the quadrotor is included in \dot{L} above to obtain a new derivative Lyapunov function \dot{L}_{slung} and then we check to see if our control law that ignores the slung load force effect still makes $\dot{L}_{slung} < 0$.

$$\dot{L}_{slung} = \Delta V^T \left[m_F \dot{v}_L + \begin{bmatrix} \tilde{k}_x & 0 & 0 \\ 0 & \tilde{k}_y & 0 \\ 0 & 0 & \tilde{k}_z \end{bmatrix} \begin{Bmatrix} v_{x_F}^2 \\ v_{y_F}^2 \\ v_{z_F}^2 \end{Bmatrix} - \begin{Bmatrix} F_x \\ F_y \\ F_z \end{Bmatrix} - \begin{Bmatrix} 0 \\ 0 \\ m_F g \end{Bmatrix} + F_{s4} \right] + \Delta V^T R\Delta r \quad (610)$$

Figure 6.4 shows the original derivative of the Lyapunov function, \dot{L} . From the figure, we see that our chosen control law ensures that it is less than zero. Figure 6.5 shows the derivative of the Lyapunov function, \dot{L}_{slung} that was modified to include the force effect of the slung load. From that figure, we see that with our control law, in the first 10 secs \dot{L}_{slung} goes greater than zero as the follower quadrotor initially accelerates to catch up to the leader quadrotor to maintain formation. However, this does not cause instability in the quadrotor slug load system. Figure 6.6 shows \dot{L}_{slung} after increasing the gain of the outerloop controller. Although, the new control law is obtained with the slung load torque on the quadrotor still being unmodeled in its design, \dot{L}_{slung} comes really close to zero. There is a limit to how high we can increase the gain of the outer loop because we have a hierarchical two loop control structure, and its

recommended to have the innerloop much faster than the outer loop. Even though \dot{L}_{slung} is not strictly less than zero, we do not have instability in our quadrotor slung load system.

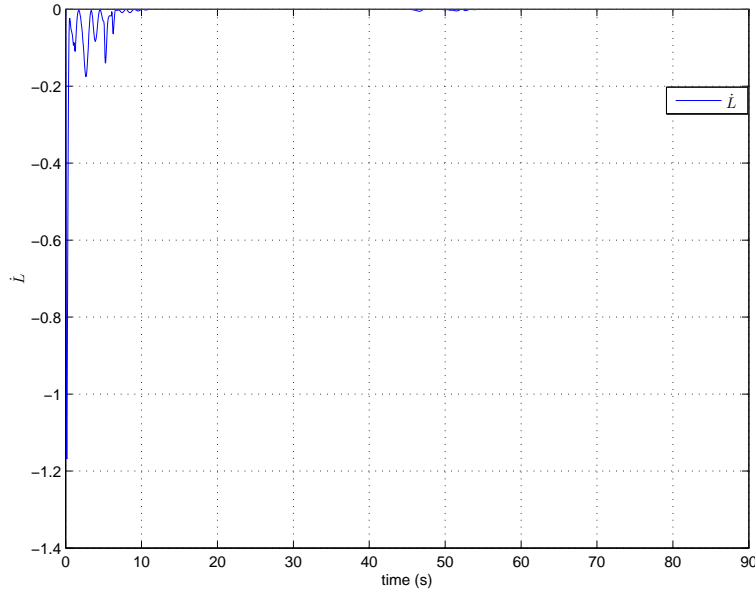


Figure 6.4: Outerloop Lyapunov function derivative without slung load force effect

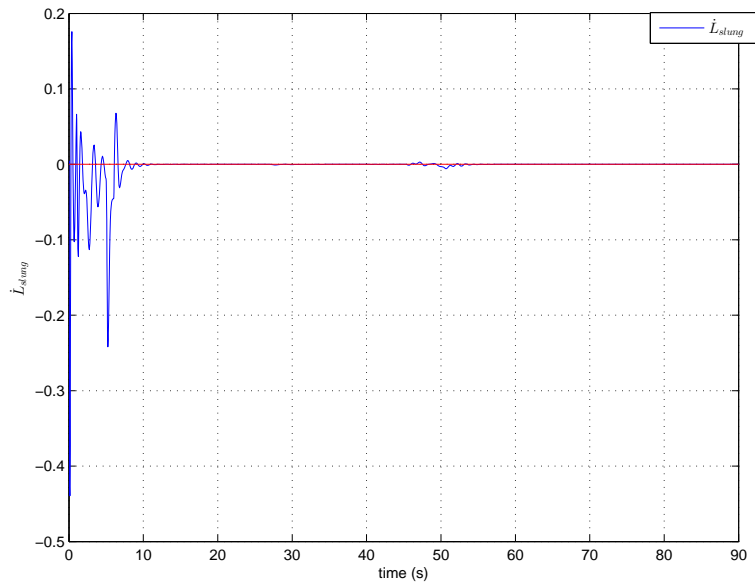


Figure 6.5: Outerloop Lyapunov function derivative with slung load force effect

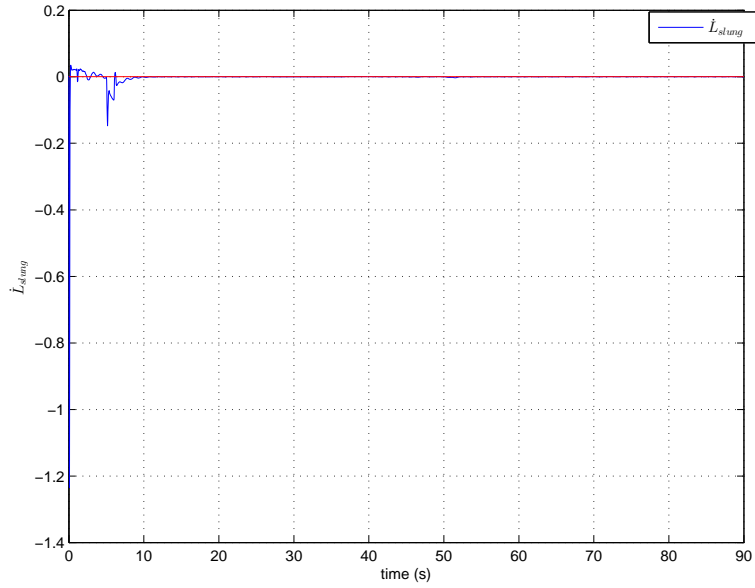


Figure 6.6: Retuned Outerloop Lyapunov function derivative with slung load force effect

6.1.3 Derivative of the Innerloop and Outerloop Lyapunov functions for a range of reaction force and torque

The reaction force and torque used to obtain the plots of the derivative of the Lyapunov functions in fig.6.1 through to fig.6.6 was for a load mass of 0.2 kg . To have a more detailed stability test, different ranges of values for the unmodeled reaction force and torque in the outer loop and inner loop controllers respectively are tested. The reaction force, F_{S_4} and the reaction torque, $r_2^\times C_N^2 F_{S_4}$ are altered by changing the mass of load, as the load mass is proportional to the reaction force. The same stability analysis is then performed for the different reaction forces and torques. The time history of the reaction force and torque for load masses of 0.2 kg , 0.6 kg , 1.0 kg , 1.4 kg , 1.8 kg are gotten through simulation and then used to obtain \dot{L}_{slung} and \dot{V}_{slung} in fig.6.7 and fig.6.8 below. Figure 6.7 shows the time history of the derivative of the outer loop Lyapunov function, \dot{L}_{slung} . As the mass of the load increased, we had a higher magnitude of deflection from zero. This is expected because a higher load mass means a higher unmodeled reaction force. However, in all the cases tested, \dot{L}_{slung} settles to zero as the simulation progressed. Although we had intervals where $\dot{L}_{slung} > 0$, it did not cause instability in our quadrotor slung load system. Figure 6.8

shows the time history of the derivative of the inner loop Lyapunov function. In all the load mass cases considered, the derivative remained negative, thus guaranteeing stability.

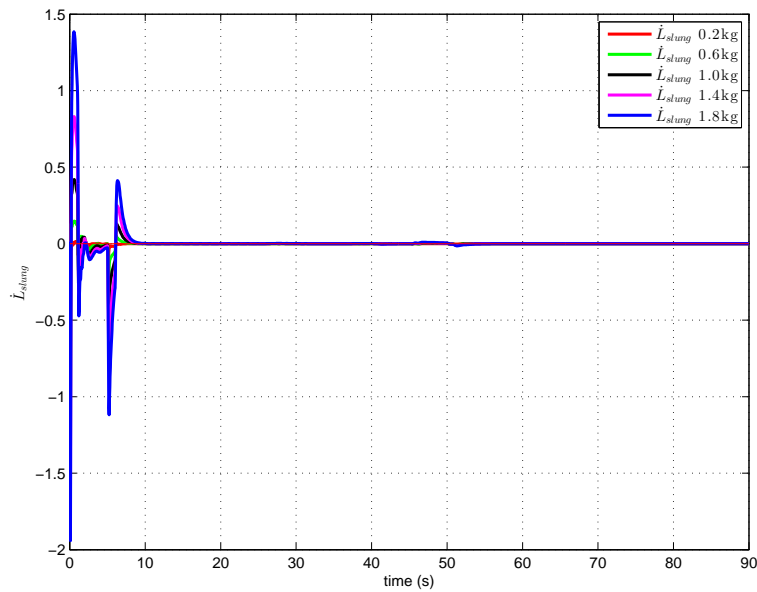


Figure 6.7: Retuned Outerloop Lyapunov function derivative with increasing slung load force effect

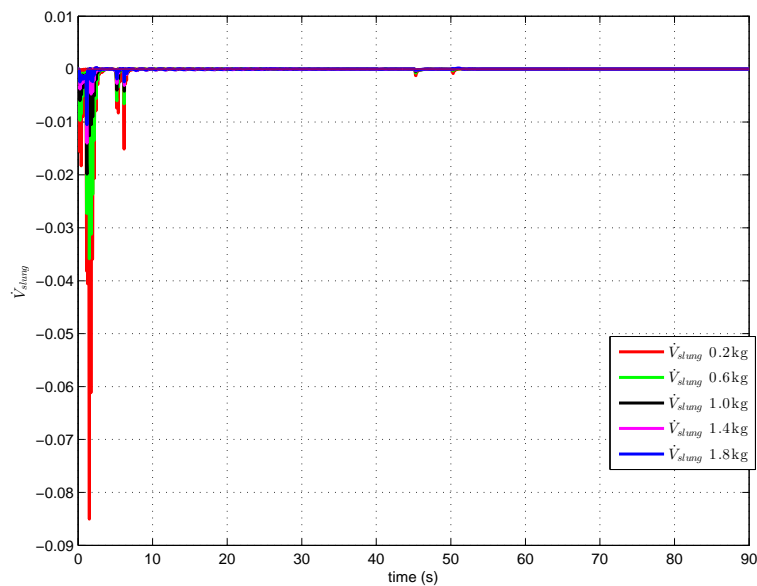


Figure 6.8: Retuned Innerloop Lyapunov function derivative with increasing slung load torque effect

6.2 Performance Robustness Test of the Nonlinear Controller

For the performance robustness test of our controller, two scenarios were considered. For the first scenario, we introduced sensor noise into both the outer loop formation guidance controller and the inner loop attitude controller. We also introduced wind disturbance in the form of wind shear and wind gust into the system to create an atmospheric environment. It is assumed that the leader quadrotor is able to freely fly. Thus, it would not be subjected to the additional drag effects of the wind environment unlike the follower quadrotor and load. Simulations are then carried out to see how the sensor noise and wind disturbance affect the performance of our controllers.

For the second scenario, the weight of the load being carried is varied, we then check to see how the weight change affected the performance of the control system.

6.2.1 Effects of Sensor Noise and Atmospheric Disturbances

The outer loop formation controller receives leader and follower quadrotor velocity and position information, and generates a thrust vector that the follower quadrotor must track to attain a desired reference relative position. Thus, a Gaussian white noise was added into the velocity and position sensor information going to this controller. To model this noise, the datasheet of the LIS302SG 3-axis MEMS accelerometer [39] was employed. From the datasheet, the sensor has a noise density of $200 \mu g/\sqrt{Hz}$. This noise is modeled using the simulink band-limited white noise generation block. The inner loop attitude controller that receives a to-go quaternion generated from the outer loop thrust vector and angular velocity to rotate our quadrotor into the desired attitude. For this attitude controller, noise is added to the angular velocity sensor. The datasheet of the L3GD20H 3-axis MEMS gyroscope is used [40]. This gyroscope has a rate noise density of $0.011 dps/\sqrt{Hz}$ with a selectable output noise frequency of $100 Hz$ and low pass cut-off frequency of $12.5 Hz$.

For the wind disturbance, the wind shear and wind gust simulink model blocks are used. The implementation of the simulink wind shear model block is based on the mathematical representation in the Military Specification MIL-F-8785C [41]. The magnitude of the wind shear is given by the following equation for the mean wind

profile as a function of altitude and the measured wind speed at 20 feet (6 m) above the ground:

$$u_w = W_{20} \frac{\ln\left(\frac{h}{z_0}\right)}{\ln\left(\frac{20}{z_0}\right)}, 3ft < h < 1000ft \quad (611)$$

where u_w is the mean wind speed, W_{20} is the measured wind speed at altitude of 20 ft, h is the altitude and z_0 is a constant equal to 0.15 ft. Using this block, wind shear in the direction of 30 degrees clockwise from north to our quadrotor and W_{20} of 3 m/s is modelled. The implementation of the wind gust simulink model uses the standard "1-cosine" shape. The mathematical representation of the gust is given as [42]:

$$V_{wind} = \begin{cases} 0 & x < 0 \\ \frac{V_m}{2} \left(1 - \cos\left(\frac{\pi x}{d_m}\right)\right) & 0 \leq x \leq d_m \\ V_m & x \geq d_m \end{cases} \quad (612)$$

where V_m is the gust amplitude, d_m is the gust length, x is the distance travelled and V_{wind} is the resultant wind velocity in the body axis frame. using this block, a gust of -5 m/s at different time intervals in the x,y and z direction and lasting for about 5 secs is modelled.

Figure 6.9 shows the wind shear profile used for the performance robustness test. We have about 3 m/s of wind blowing against the quadrotor in the x-direction, -2 m/s of wind blowing against the quadrotor in the y-direction and finally, about 2 m/s of wind initially pushing down on the quadrotor which then settles to about 0.5 m/s. Figure 6.10 shows the wind gust profile in the 3-directions. We have 5 m/s of gust blowing against the quadrotor for about 5seconds at different time intervals. Figure 6.11 shows the wind environment through which our quadrotor flies. This wind profile is used to calculate the additional drag that the follower quadrotor would experience as it flies through that environment.

To carry out the performance robustness test, the same flight scenario used in section 5.2 is used. The leader quadrotor is sent desired velocity commands, and a desired relative distance command is sent to the formation guidance controller to enable the follower quadrotor maintain that distance. It is desired that the initial formation geometry be maintained in spite of the leader quadrotor motion. The reference relative distance sent to the formation guidance controller is: $(x_F - x_L, y_F - y_L, z_F - z_L) =$

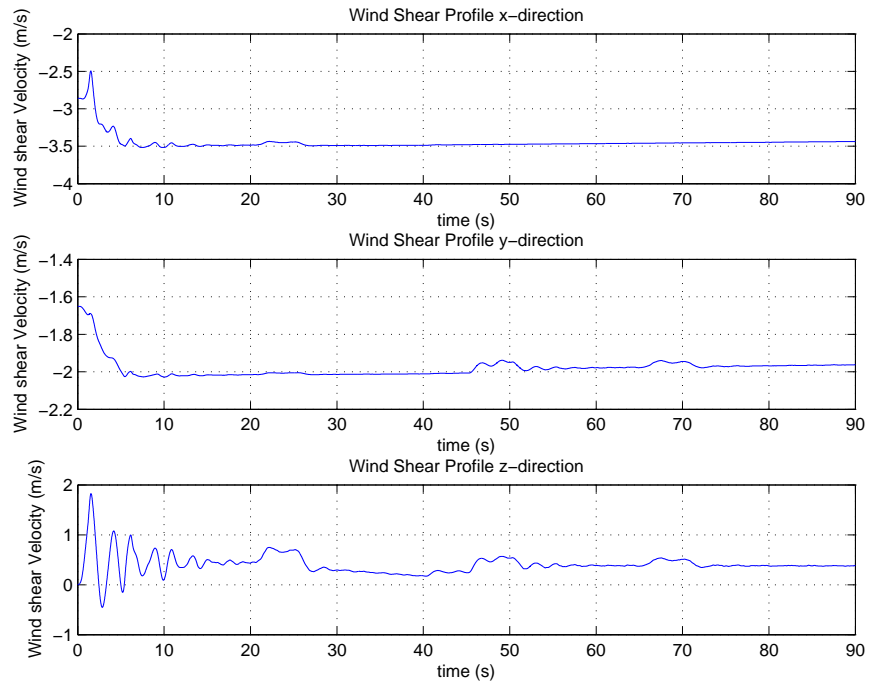


Figure 6.9: Wind shear velocity profile in the 3-directions

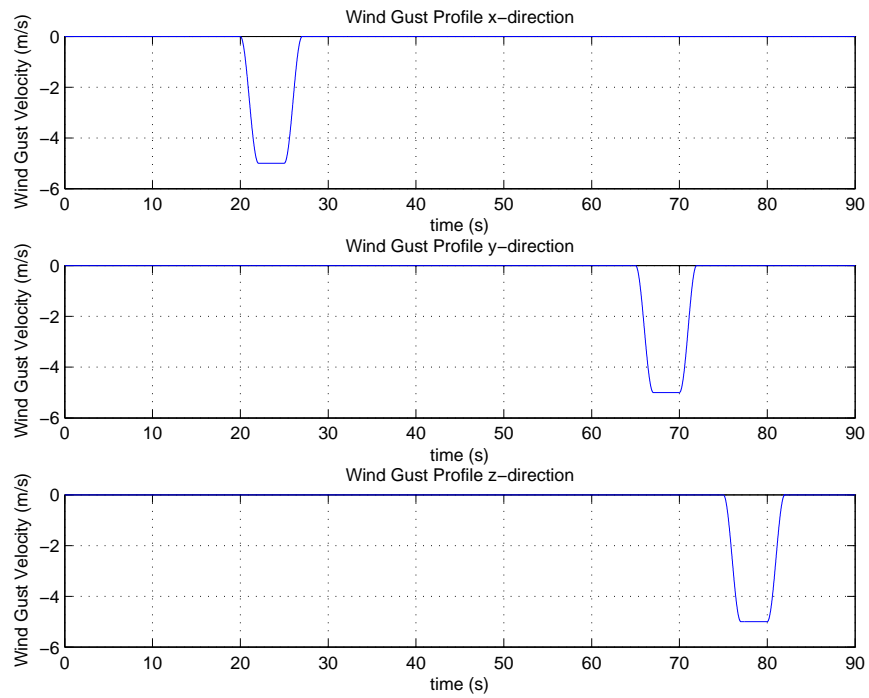


Figure 6.10: Wind Gust velocity profile in the 3-directions

$(0, 1, 0)$. We test to see if the follower can still maintain this formation in the presence of sensor noise and wind disturbances.

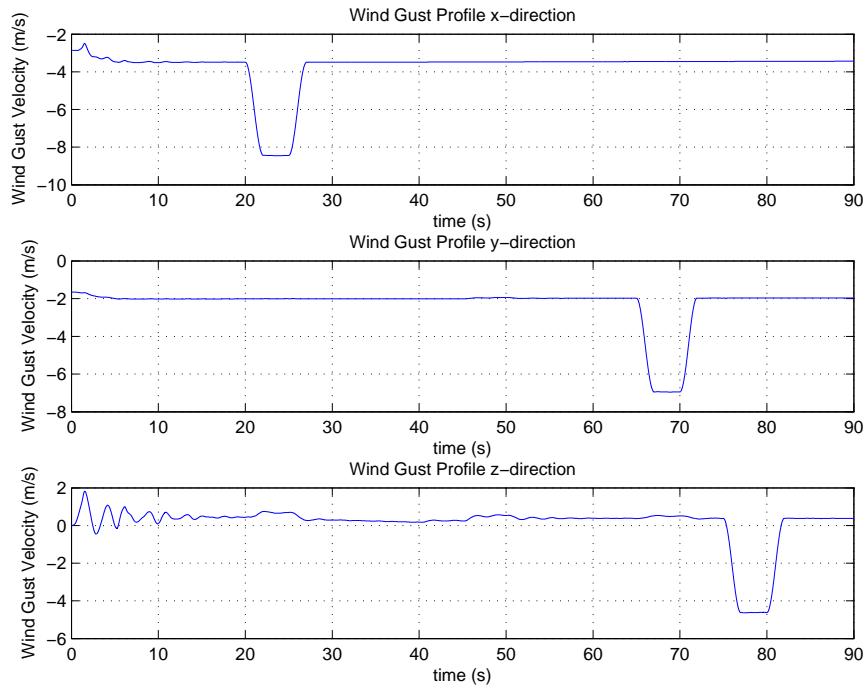


Figure 6.11: Combined Wind Shear and Gust velocity profile in the 3-directions

Figure 6.12 presents the leader quadrotor response to the velocity commands. From the figure, it may be observed that the leader quadrotor closely follows the desired velocity commands in spite of the slung load as expected from previous simulations. Figures 6.13 shows the time history of the formation flight. The follower quadrotor is able to keep up with the leader quadrotor for the duration of the flight. Figure 6.14 shows the time history of the relative position of the follower quadrotor to the leader quadrotor. From the figure, it may be observed that the desired relative distance is closely tracked albeit some slight steady state error. We have a constant wind resistance pushing against the follower quadrotor in all three directions as it tries to maintain its relative position. The effect of the gust can also be seen in these plots. In the relative x-position between 20 and 30 second mark, we see the follower slightly lag behind and swiftly recovers as soon as the gust passed. The effect of the gust on the relative y and z positions can be seen between the 65-75 and 75-80 second mark respectively. Figure 6.15 shows the load rock, swing and heading angles. The two quadrotors are able to carry the load in a smooth fashion. The load rock angle has a maximum deflection of about 12 degrees and settles at 5 degrees for the entire duration of the flight. The load swing angle has a maximum deflection of about -5

degrees and settles at 1 degree for the entire duration of the flight. The load heading angle oscillates between -10 degrees and 30 degrees in the first 10 seconds as a result of the different in x-positions of the leader and follower quadrotors, but settles at 10 degrees as a result of the slight steady state error in relative x-positions of the two quadrotors. Figures 6.16 and 6.17 show the propeller speeds of the two quadrotors. There are no saturations in the speeds of the rotors.

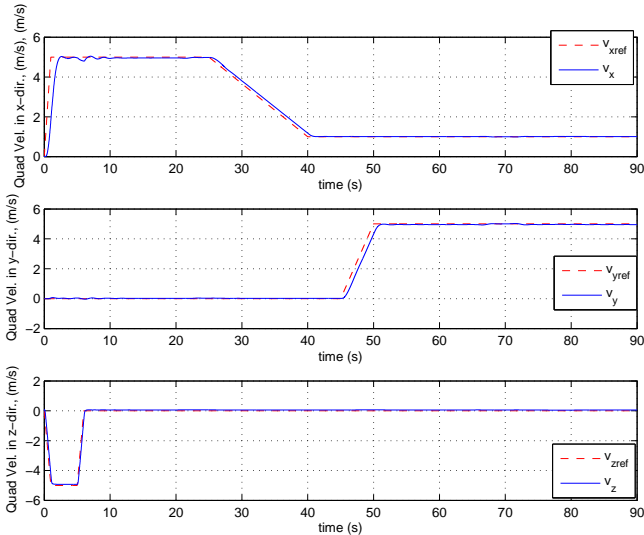


Figure 6.12: Leader Quadrotor Velocity in x, y and z directions respectively (Sensor noise, wind disturbance)

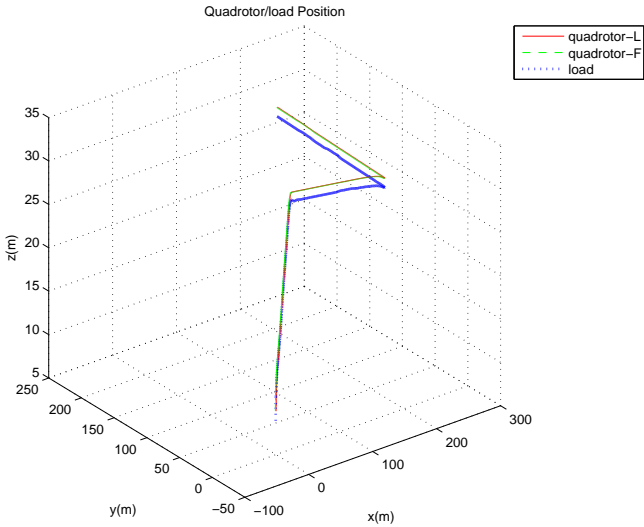


Figure 6.13: Leader and Follower Quadrotor position and Load Position (Sensor noise, wind disturbance)

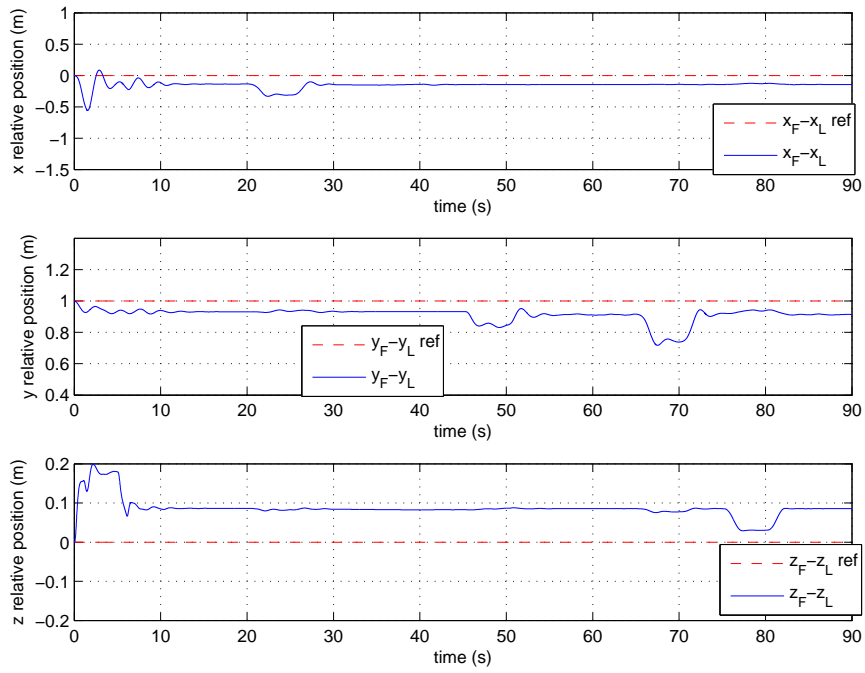


Figure 6.14: Leader and Follower Quadrotor relative positions (Sensor noise, wind disturbance)

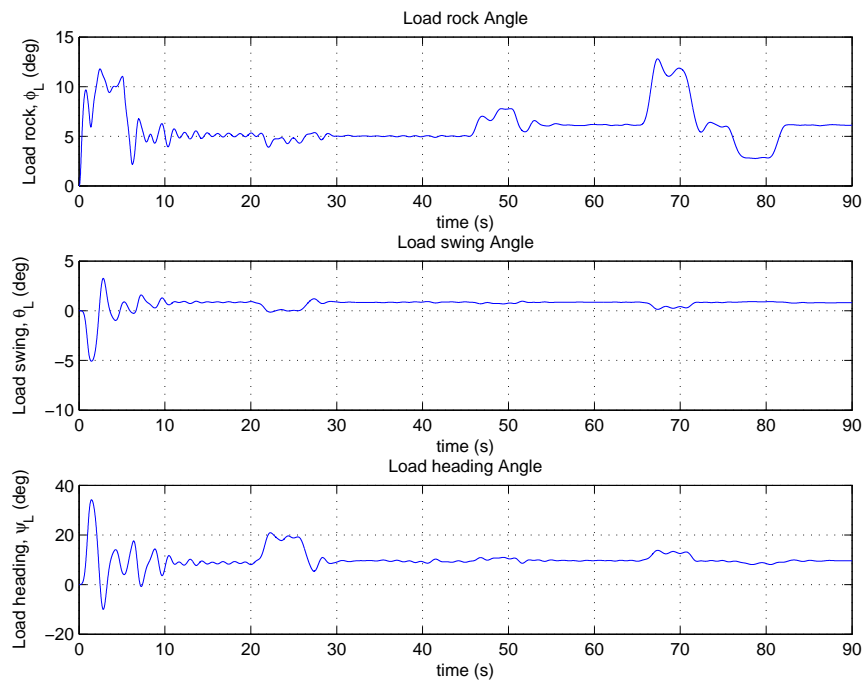


Figure 6.15: Swing, Rock and Heading Angles of the Load (Sensor noise, wind disturbance)

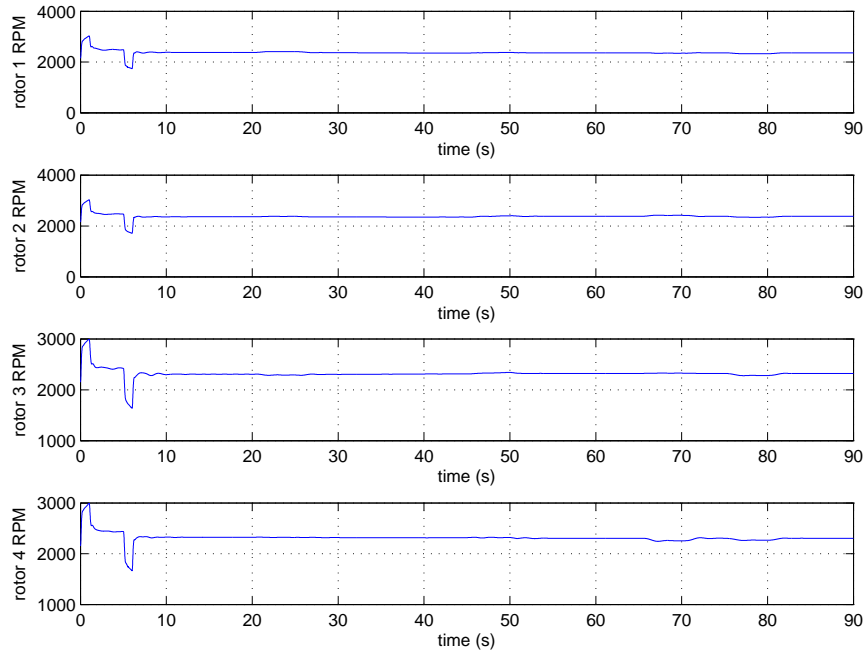


Figure 6.16: Propeller Speeds of the Leader Quadrotor (Sensor noise, wind disturbance)

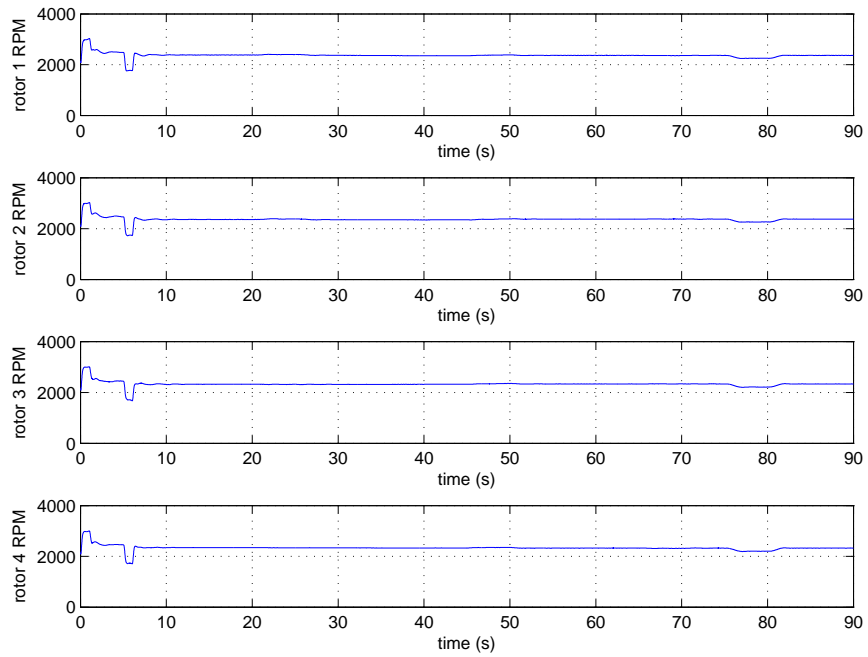


Figure 6.17: Propeller Speeds of the Follower Quadrotor (Sensor noise, wind disturbance)

6.2.2 Effects of Varying Load Weight

In this section, for the performance robustness test, the weight of the load being carried is changed. We then checked to see how robust our control system is to the weight change. Three different weights were considered. The 0.2 kg load that was used for all the previous simulations, a 0.6 kg and a 1 kg load. The same flight scenario used in the previous section is employed for the simulation. Results are presented below.

Figure 6.18 presents the leader quadrotor response to the velocity commands for all the three different load weights. In all three cases, the leader quadrotor closely followed the desired commands. However, as the load weight increased, we have a little bit of steady state error. For the 0.6 kg case, there is steady state error of 0.15 m/s and a steady state error of 0.2 m/s . Figure 6.19 shows the time history of the relative position of the follower quadrotor to the leader quadrotor for all three load weights. The follower is able track the formation geometry in all three cases. However, we have higher overshoots as the weight increased and slightly more sluggish responses. The steady state error in the formation tracking performance increased as the weight increased. The steady state error in the relative y-direction is 3 %, 8 % and 15 % for the 0.2 kg , 0.6 kg , 1.0 kg weights respectively. However, in the relative z-direction, there is a sizeable increase in steady state error as the weight of the load increased. Figure 6.20 shows the load rock, swing and heading angles. The two quadrotors are able to carry the load in a smooth fashion in all three cases. However, the bigger the load, the larger the deflection angle. The oscillation of the angle deflections of the load also reduced as the weight of the load increased. The larger loads also have a higher settling load rock angle because of the increase in the higher relative altitude difference between the leader and follower quadrotor due to the increased steady state error. Figures 6.21 and 6.22 show the propeller speeds of the two quadrotors. There are no saturations in the speeds of the rotors.

The increase in load weight affected the formation tracking performance. Thus, the formation-hold outer loop controller can be retuned for better load weight variation performance. Figures 6.23 and 6.24 show the simulation results when the formation-hold controller is retuned. With this new tuning, the maximum weight we could carry was 1.8 kg without saturating the propellers at 4500 rpm . For the 1.8 kg load, there

is a steady state error of 0.04 m , 0.07 m and 0.15 m is the tracked relative positive of the follower quadrotor to the leader quadrotor.

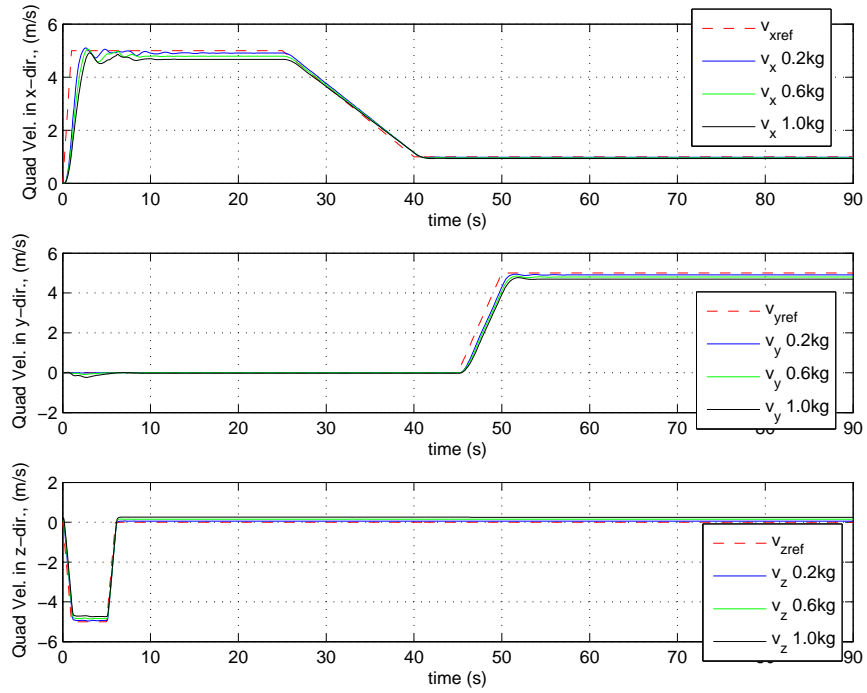


Figure 6.18: Leader Quadrotor Velocity in x, y and z directions respectively (Varying load)

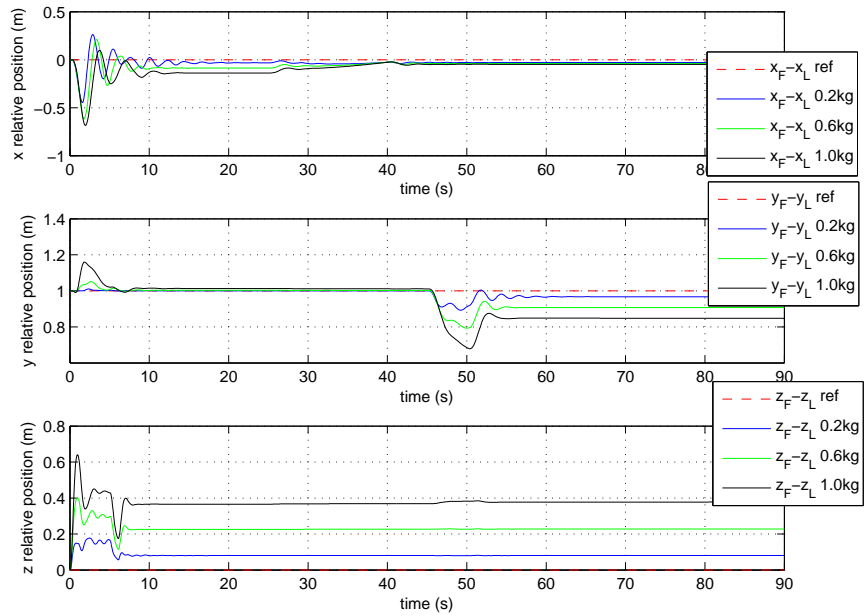


Figure 6.19: Leader and Follower Quadrotor relative positions (Varying load)

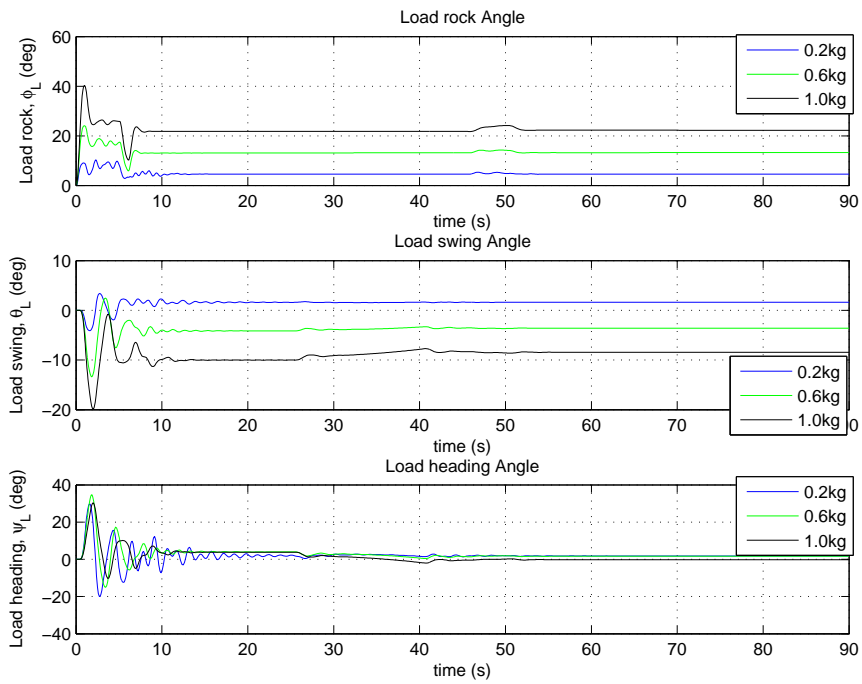


Figure 6.20: Swing, Rock and Heading Angles of the Load (Varying load)

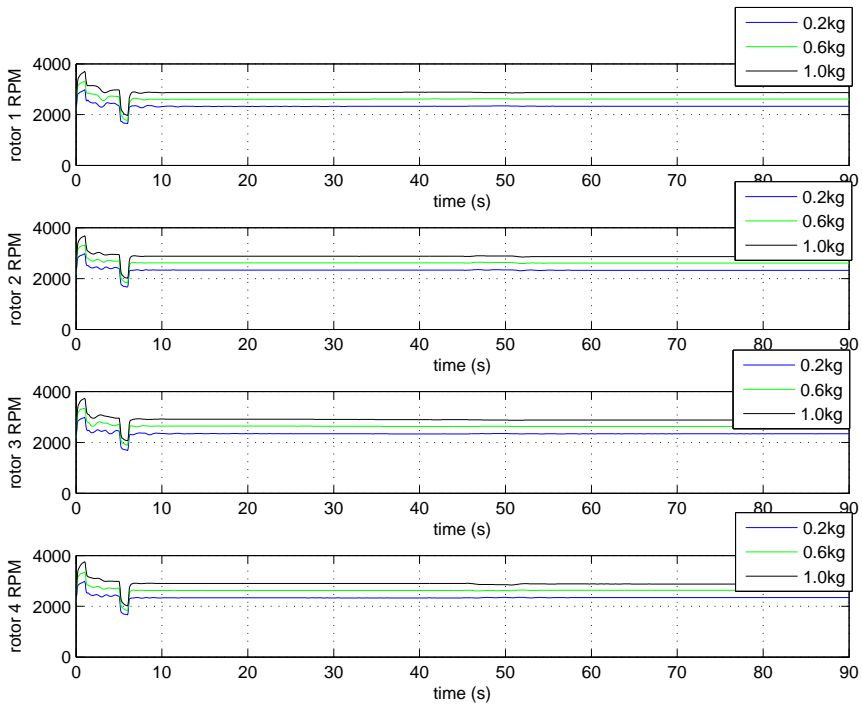


Figure 6.21: Propeller Speeds of the Leader Quadrotor (Varying load)

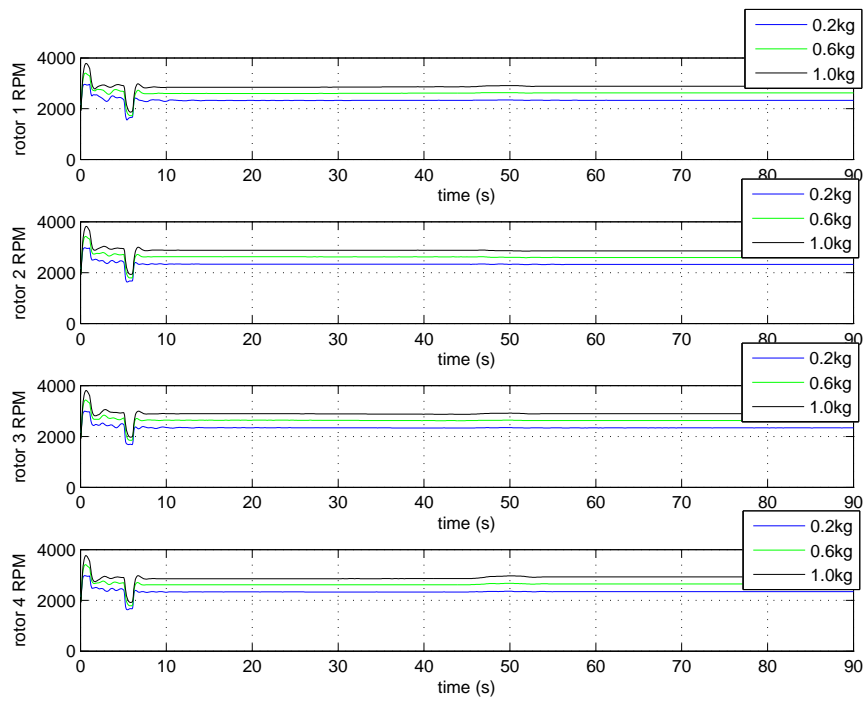


Figure 6.22: Propeller Speeds of the Follower Quadrotor (Varying load)

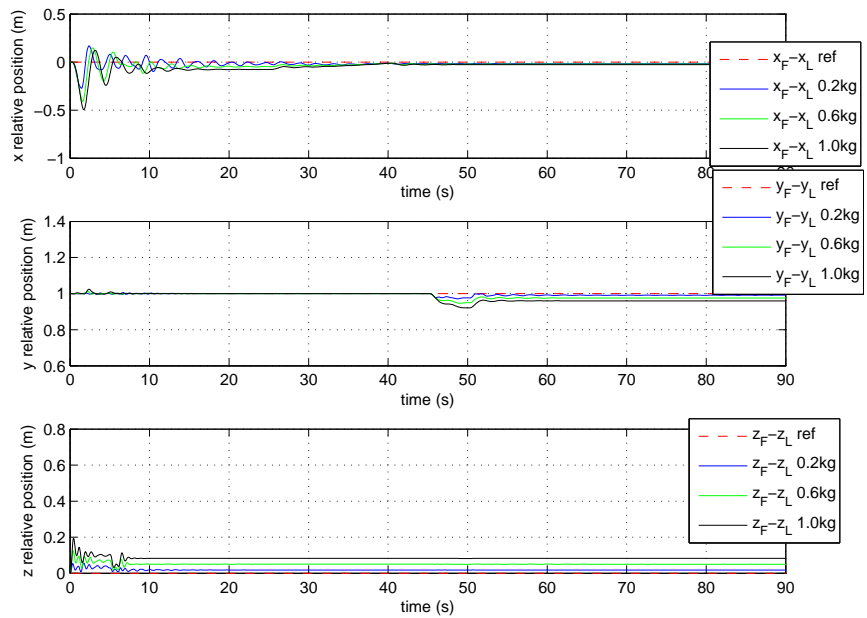


Figure 6.23: Leader and Follower Quadrotor relative positions (Varying load, Re-tuned)

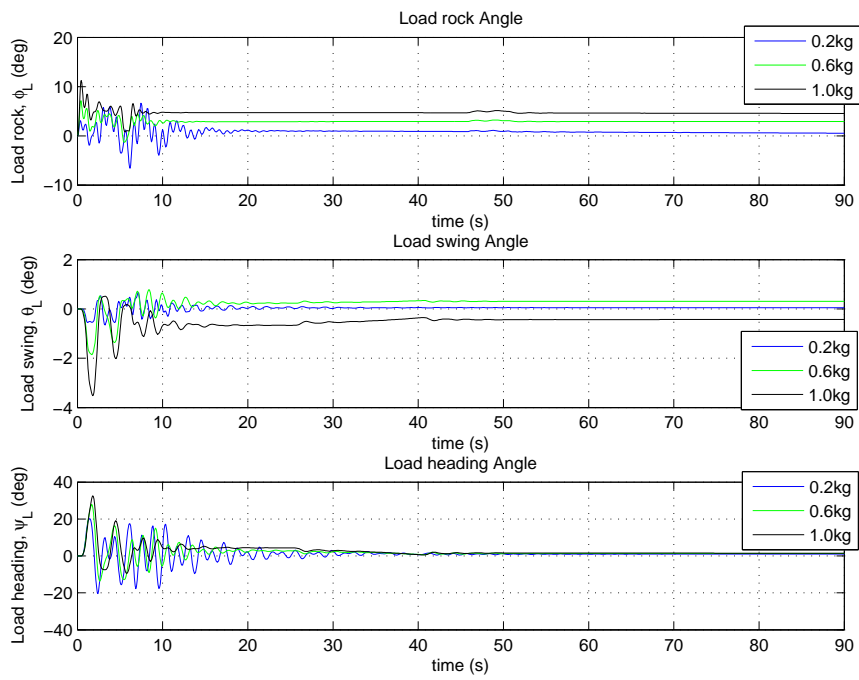


Figure 6.24: Swing, Rock and Heading Angles of the Load (Varying load, Returned)

CHAPTER 7

FULL NONLINEAR CONTROL ALGORITHM FOR A TWO QUADROTOR SLUNG LOAD SYSTEM WITH SLUNG DYNAMICS DISTURBANCE CANCELLATION

In the previous sections, the quadrotor control algorithms implemented did not include the slung load dynamical effects on the quadrotor in the design process. In other words, the additional force and torque acting on the quadrotor as a result of the slung load were treated as disturbances to the control system. In this chapter, the previously designed outer loop formation guidance algorithm designed in section 5.3.2 and the innerloop quaternion based attitude controller designed in section 5.1.4 will both be modified to include the slung load dynamics in obtaining their respective control laws. These modified controllers are then implemented on the follower quadrotor and the simulation results are presented and discussed. A disturbance cancellation scheme was not implemented on the leader quadrotor because the slung load forces acting on the leader quadrotor are not time invariant and the leader quadrotor has a LQT velocity controller implemented in its outerloop. Although, the leader quadrotor has a nonlinear innerloop controller, introducing a disturbance cancellation scheme in its inner loop without balancing out the disturbance in its outer loop led to an over compensation in the controller performance of the leader quadrotor.

7.1 Outer loop Formation Guidance Algorithm with Disturbance Cancellation

Details of the design of this controller have been given in section 5.3.2 albeit some modifications that would be done in this section. Referring to section 5.3.2, the

derivative of the negative definite Lyapunov function was given as:

$$\dot{L} = \Delta V^T m_F \Delta \dot{V} + \Delta V^T R \Delta r = -\Delta V^T S \Delta V \quad (71)$$

simplifying the above equation and solving for the follower quadrotor acceleration, we have:

$$m_F \dot{v}_F = m_F \dot{v}_L + R \Delta r + S \Delta V \quad (72)$$

Using the Newton's equation for translation and including the slung load force on the quadrotor, $m_F \dot{v}_F$ is written in the inertial frame as:

$$m_F \dot{v}_F = - \begin{bmatrix} \tilde{k}_x & 0 & 0 \\ 0 & \tilde{k}_y & 0 \\ 0 & 0 & \tilde{k}_z \end{bmatrix} \begin{Bmatrix} v_{x_F}^2 \\ v_{y_F}^2 \\ v_{z_F}^2 \end{Bmatrix} + \begin{Bmatrix} F_x \\ F_y \\ F_z \end{Bmatrix} + \begin{Bmatrix} 0 \\ 0 \\ m_F g \end{Bmatrix} - F s_4 \quad (73)$$

Substituting eqn. 73 into eqn. 72 and solving for the thrust vector direction, we obtain:

$$\begin{Bmatrix} F_x \\ F_y \\ F_z \end{Bmatrix} = \begin{bmatrix} \tilde{k}_x & 0 & 0 \\ 0 & \tilde{k}_y & 0 \\ 0 & 0 & \tilde{k}_z \end{bmatrix} \begin{Bmatrix} v_{x_F}^2 \\ v_{y_F}^2 \\ v_{z_F}^2 \end{Bmatrix} - \begin{Bmatrix} 0 \\ 0 \\ m_F g \end{Bmatrix} + m_F \dot{v}_L + R \Delta r + S \Delta V + F s_4 \quad (74)$$

The control law obtained in eqn. 74 above, helps the follower quadrotor maintain the prescribed formation geometry and also negate the additional acting force of the slung load on the quadrotor.

7.2 Inner loop Attitude Control Algorithm with Disturbance Cancellation

Details of this controller design have also been given in section 5.1.4. In this section, this previously designed controller would be modified to include the additional torque effect of the slung load on the quadrotor. Referring to section 5.1.4, the derivative of the negative definite Lyapunov function for attitude control was given as:

$$\dot{V} = \omega^T M^{-1} J \dot{\omega} - \omega^T \mathbf{t} = -\omega^T M^{-1} N \omega \quad (75)$$

simplifying the above equation gives:

$$J \dot{\omega} - M \mathbf{t} = -N \omega \quad (76)$$

from the derived slung load equations of motion for the angular acceleration of the follower quadrotor, we have:

$$\dot{\omega}_2 = J_2^{-1}T_2 - J_2^{-1}r_2^\times C_N^2 F_{S_4} - J_2^{-1}\omega_2^\times J_2\omega_2 \quad (77)$$

let $S = -J_2^{-1}\omega_2^\times J_2\omega_2$ and $GU = J_2^{-1}T_2$ in eqn. 77. Substituting eqn. 77 into eqn. 76 and solving for the control law U , we obtain the control law for attitude control as:

$$U = G^{-1}[J_2^{-1}(M\mathbf{t} - N\omega + J_2^{-1}r_2^\times C_N^2 F_{S_4}) - S] \quad (78)$$

This control law also helps negate the additional acting torque of the slung load on the quadrotor.

7.3 Performance Comparison of the Control System with and without Disturbance Cancellation

The same flight scenario in section 5.2 is used to test the performance of our control system with disturbance cancellation. The results are then compared with the previously designed control system without disturbance cancellation. For both cases, the settling times of the controllers are kept the same as in table 5.4. The leader quadrotor is sent desired velocity commands, and a desired relative distance command is sent to the formation guidance controller to enable the follower quadrotor maintain that distance. It is desired that the initial formation geometry be maintained in spite of the leader quadrotor motion. The reference relative distance sent to the formation guidance controller is: $(x_F - x_L, y_F - y_L, z_F - z_L) = (0, 1, 0)$.

Figure 7.1 presents the leader quadrotor response to the velocity commands for the two cases. In both cases, the leader quadrotor closely followed the desired commands as expected. Their responses are identical since we do not have disturbance cancellation implemented on the leader quadrotor for both cases. Figure 7.2 shows the time history of the relative position of the follower quadrotor to the leader quadrotor. For the control system without disturbance cancellation, there is a steady state error of about 3% in the relative y-position. However, this error is gotten rid off in the disturbance cancellation case. Also, in the relative z-position of the quadrotors, there is an offset of 0.08m for the no disturbance cancellation case. This offset is also

gotten rid off in the disturbance cancellation case. Figure 7.3 shows the load rock, swing and heading angles. The two quadrotors are able to carry the load in a smooth fashion in both cases. They both have the very similar load heading angle deflection. The load swing angle of the disturbance cancellation case is less oscillatory and with lower magnitude of angle deflection. The load rock angle with disturbance cancellation also has a smaller magnitude of deflection when compared to the other case. Figures 7.4 and 7.5 show the propeller speeds of the two quadrotors. There are no saturations in the speeds of the rotors.

Overall, countering the additional force and torque effect of the slung load on the follower lead to an improved formation tracking performance and the follower quadrotor becomes more agile.

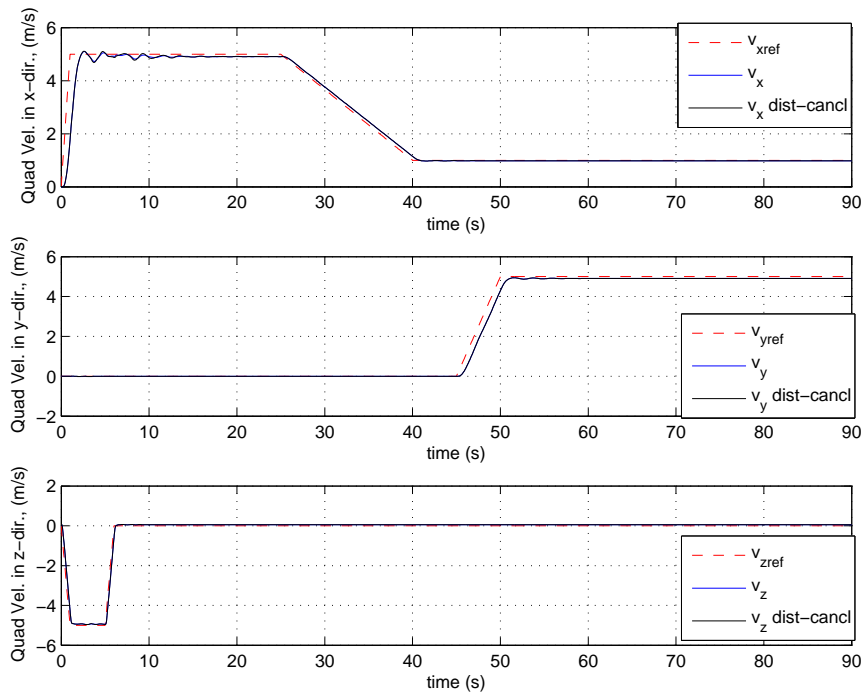


Figure 7.1: Leader Quadrotor Velocity in x, y and z directions respectively (Disturbance Cancellation)

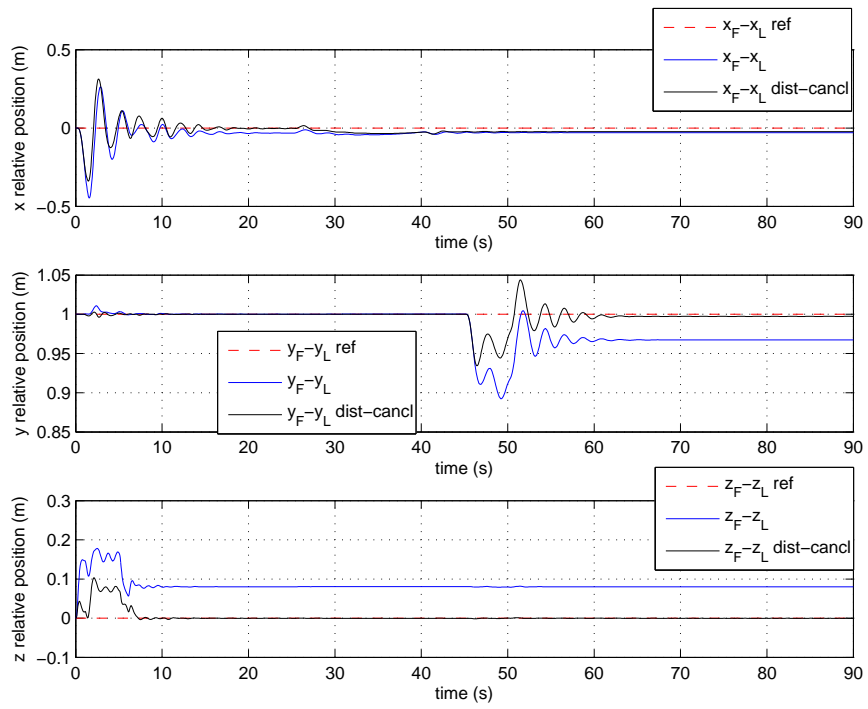


Figure 7.2: Leader and Follower Quadrotor relative positions (Disturbance Cancellation)

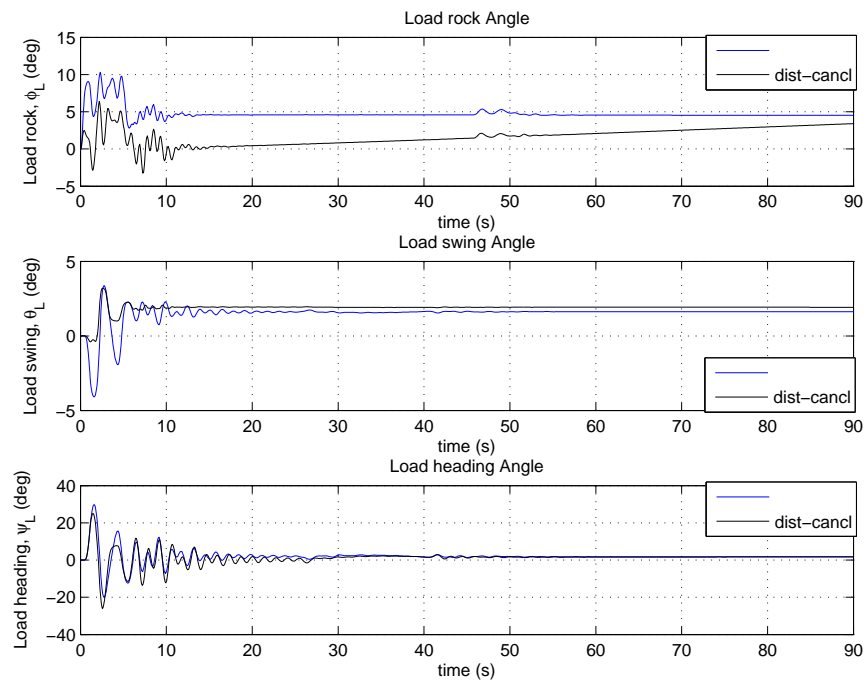


Figure 7.3: Swing, Rock and Heading Angles of the Load (Disturbance Cancellation)

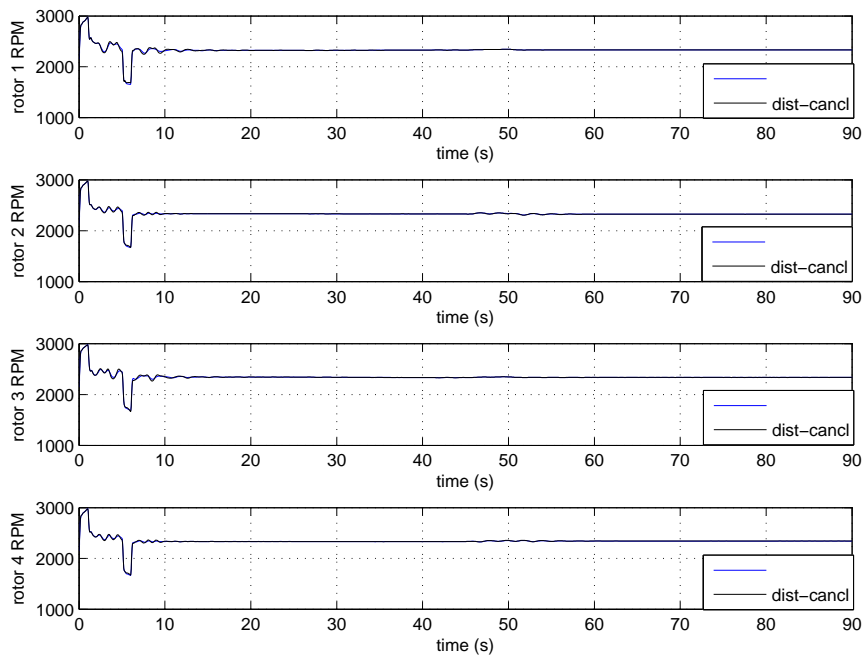


Figure 7.4: Propeller Speeds of the Leader Quadrotor (Disturbance Cancellation)

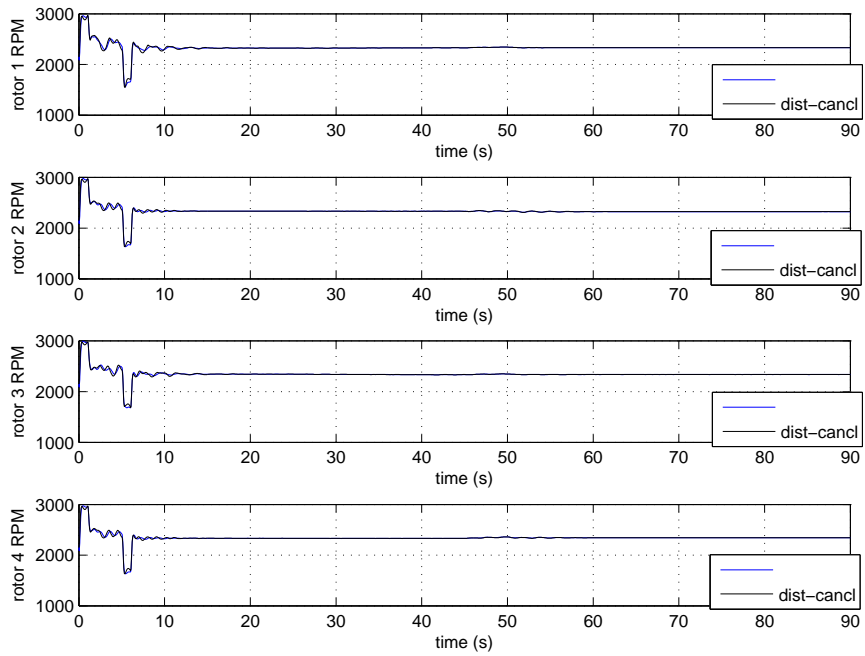


Figure 7.5: Propeller Speeds of the Follower Quadrotor (Disturbance Cancellation)

CHAPTER 8

MODELLING OF A TWO QUADROTOR SLUNG SYSTEM WITH FLEXIBLE BARS USING THE MSC ADAMS SOFTWARE

In the previous chapters, the quadrotor slung load systems were modelled using rigid bars to attach the load to the quadrotors. In this chapter, the rigid bars will be replaced with flexible bars. A two quadrotor slung load system with two flexible bars will be modelled. Two previously designed control systems would then be implemented on this flexible model. The first control system implemented is the control algorithm designed in chapter 3, which featured a two-loop architecture whereby a Lyapunov function based formation guidance loop is on the outer loop and two LQT velocity controllers are in the inner loop. The second control system implemented is the full nonlinear two loop controller designed in section 5.3 that featured a Lyapunov function based scheme both in the outer and inner loops. Simulation results for both cases will be presented and discussed. The results for the first and second control system are presented in section 8.2 and section 8.3 respectively. A performance robustness test for the full nonlinear two loop controller designed in section 5.3 will be done in section 8.4 by changing the stiffness of the flexible bar.

8.1 Two Quadrotor SLung Load System with Flexible Bar with MSC ADAMS

MSC ADAMS is a multibody dynamics simulation software equipped with Fortran and C++ numerical solvers [43]. Using the MSC ADAMS software, Engineers can evaluate and manage the complex interactions between disciplines including motion, structures, actuation, and controls. [43]

The entire two quadrotor slung load system with flexible bar was modelled using

the MSC ADAMS software. The modelled system was then imported to the MATLAB/SIMULINK platform where our control system is tested against this model. The material chosen for the modelling of the flexible bars in the MSC ADAMS software was aluminium. The same model properties used in table 2.2 is used to model our slung load system in the MSC ADAMS platform. However, the modelled aluminium bar has a thickness of 0.4 cm and a mass of 0.034 kg .

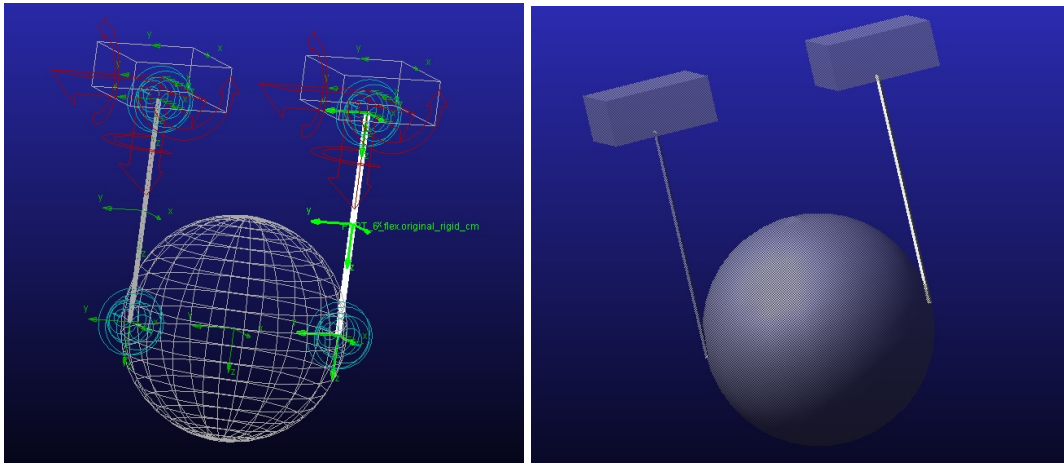


Figure 8.1: Two Quadrotor Slung Load System with Flexible Bar ADAMS Model

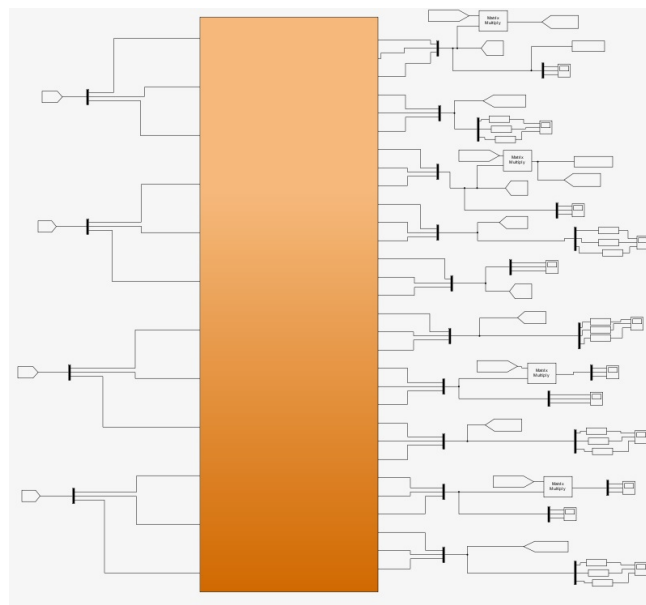


Figure 8.2: Two Quadrotor Slung Load System with Flexible Bar ADAMS to SIMULINK Model

8.2 Two Quadrotor Slung Load System with Flexible Bar: Result and Discussion For the Control System designed in chapter 3

The same formation flight scenario employed in all the previous works presented in this thesis is also employed in testing the flexible model. We tested to see how robust our control system is in handling a two quadrotor slung load system with flexible beams. The leader quadrotor is sent desired velocity commands, and a desired relative distance command is sent to the formation guidance controller to enable the follower quadrotor maintain that distance. It is desired that the initial formation geometry be maintained in spite of the leader quadrotor motion. The reference relative distance sent to the formation guidance controller is: $(x_F - x_L, y_F - y_L, z_F - z_L) = (0, 1, 0)$.

From fig. 8.3, we see that the leader quadrotor is able to closely follow the desired velocity reference. Figures 8.4 and 8.5 show the trajectory of the two quadrotors and load. Figure 8.6 shows the time history of the relative position of the follower quadrotor to the leader quadrotor. The desired relative distances are being tracked. Figures 8.7 and 8.8 shows the rock, swing and heading angles of the load with the flexible bar and rigid bar respectively. The plot of fig. 8.8 was obtained from the simulations in section 3.3. Comparing these two figures, We see considerably higher angle deflections in the rock and swing angles of the load in the flexible bar case as compared with the rigid bar case for the same control approach. From these figures, we see the load rock angle settling at around 17 degrees and being oscillatory for the flexible bar case, while the load rock angle returns to 0 degrees in the rigid bar case. The load swing angle initially oscillates between -25 and -2 degrees with the angles through which it oscillates gradually reducing as the simulation progressed in the flexible bar case. However, for the rigid bar, we see a much smoother swing angle with no oscillations. Figures 8.9 and 8.10 show the propeller speeds of the quadrotors. Overall, we have more oscillations and bigger load angle deflections in the flexible case. However, the formation tracking performances are identical.

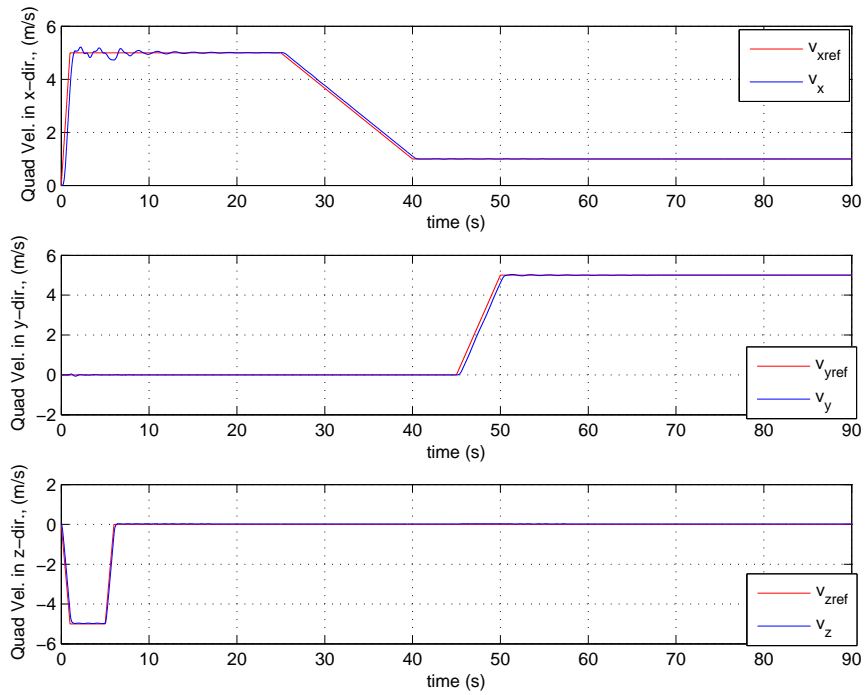


Figure 8.3: Leader Quadrotor Velocity in x, y and z directions respectively (Two Quadrotor, Flexible Bar)

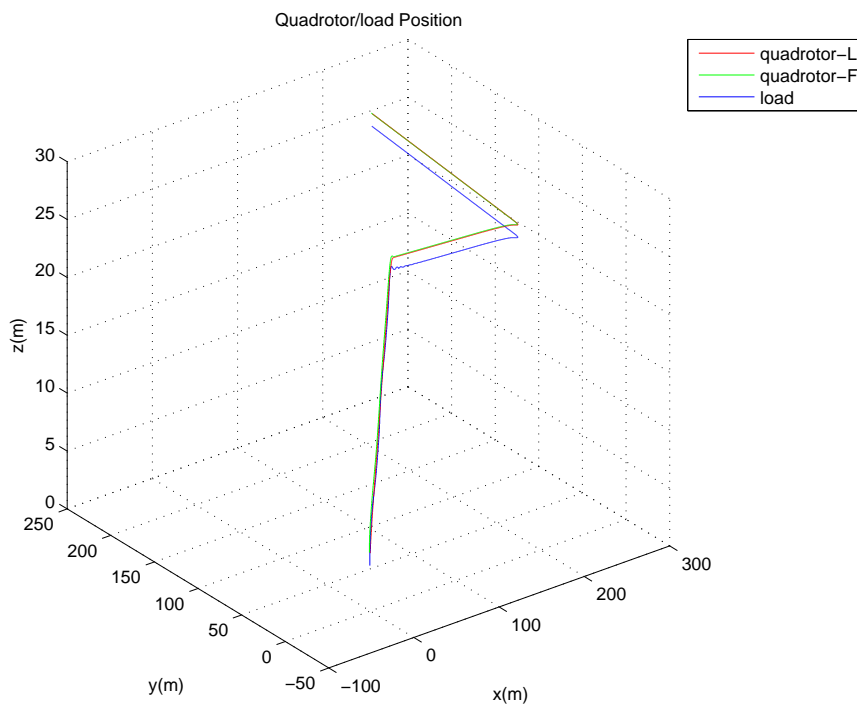


Figure 8.4: Leader and Follower Quadrotor position and Load Position (Two Quadrotor, Flexible Bar)

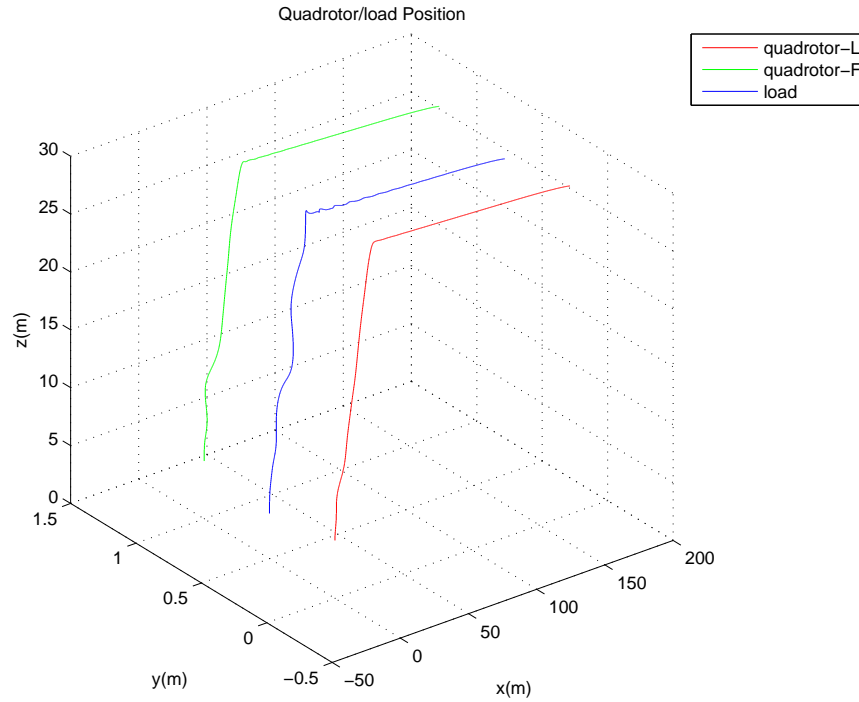


Figure 8.5: Leader and Follower Quadrotor position and Load Position (Two Quadrotor, Flexible Bar, 40 secs simulation)

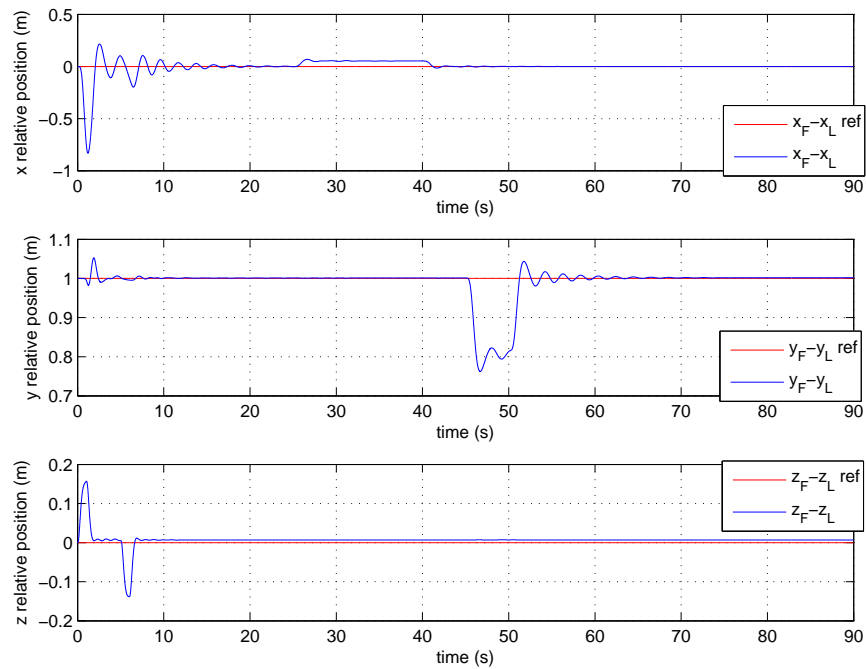


Figure 8.6: Leader and Follower Quadrotor relative positions (Two Quadrotor, Flexible Bar)

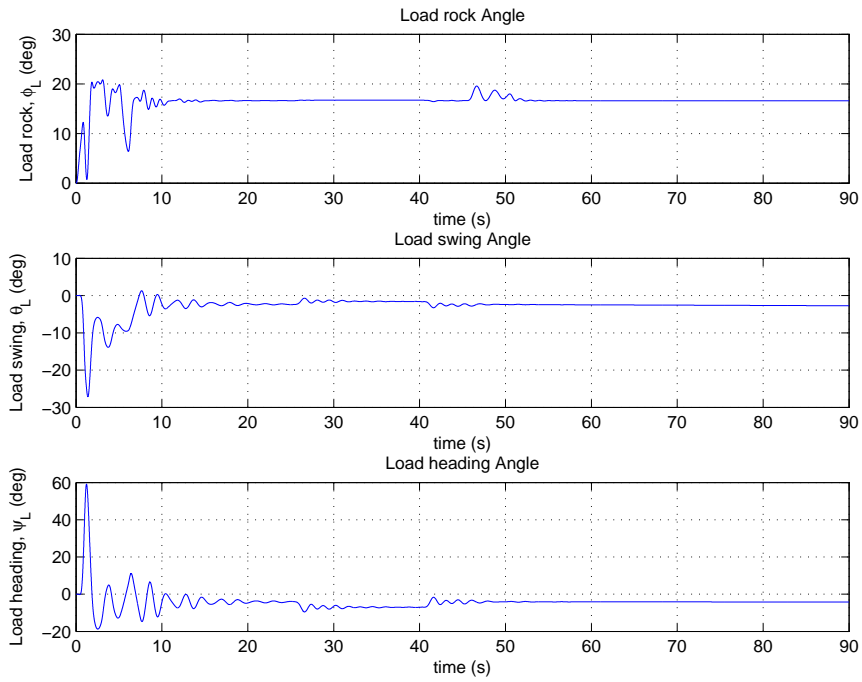


Figure 8.7: Swing, Rock and Heading Angles of the Load (Two Quadrotor, Flexible Bar)

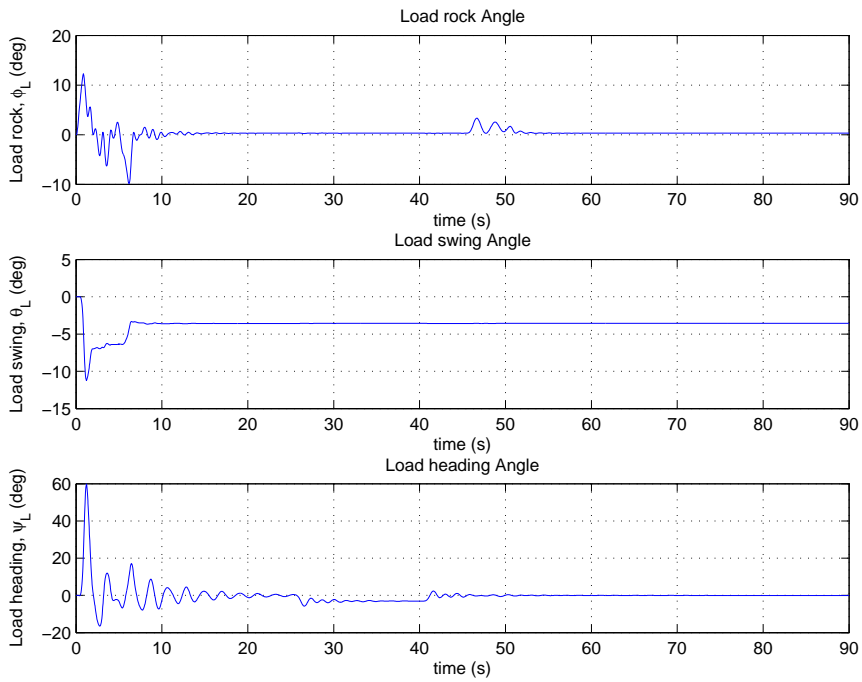


Figure 8.8: Swing, Rock and Heading Angles of the Load (Two Quadrotor, Rigid Bar)

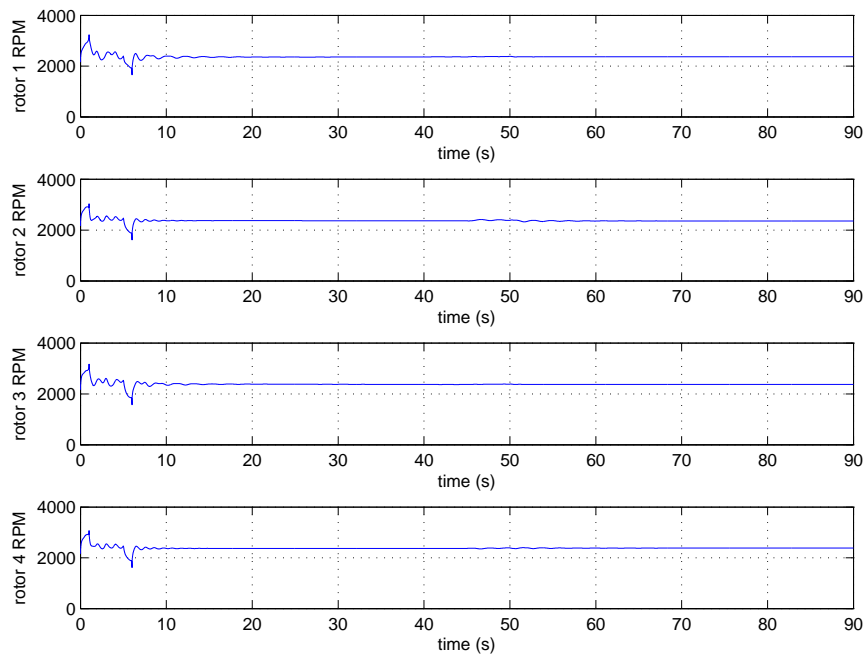


Figure 8.9: Propeller Speeds of the Leader Quadrotor (Two Quadrotor, Flexible Bar)

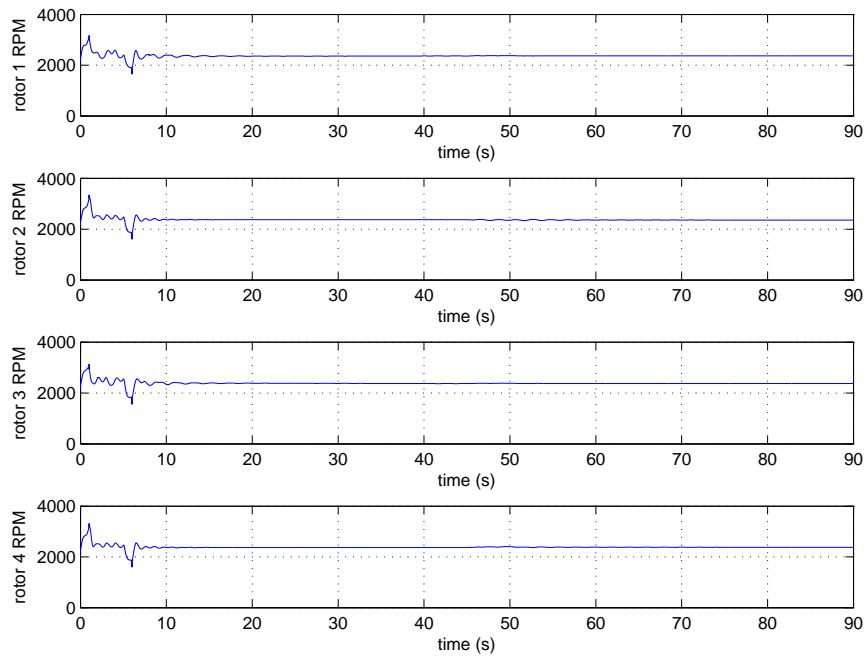


Figure 8.10: Propeller Speeds of the Follower Quadrotor (Two Quadrotor, Flexible Bar)

8.3 Two Quadrotor Slung Load System with Flexible Bar: Result and Discussion For the Control System designed in section 5.3

The same formation flight scenario as with section 8.2 is also employed in testing the flexible model against the full nonlinear controller designed in section 5.3. However, this controller is retuned to have a faster outer loop as compared to the rigid bar case in table 5.4. The new controller settling times are given in the table below:

Table 8.1: Controller Settling Times (Full Nonlinear, Flexible Bar)

Lyapunov Formation Guidance/Thrust Vector controller (Outer Loop)	Quaternion based Attitude Controller (Inner Loop)
1.38 Sec	0.38 Sec
0.69 Sec	0.38 Sec
0.69 Sec	0.38 Sec

The leader quadrotor is sent desired velocity commands, and a desired relative distance command is sent to the formation guidance controller to enable the follower quadrotor maintain that distance. It is desired that the initial formation geometry be maintained in spite of the leader quadrotor motion. The reference relative distance sent to the formation guidance controller is: $(x_F - x_L, y_F - y_L, z_F - z_L) = (0, 1, 0)$.

From fig. 8.11, we see that the leader quadrotor is able to closely follow the desired velocity references. Figures 8.12 and 8.13 show the time history of the formation flight. The follower quadrotor is able to keep up with the leader quadrotor for the duration of the flight. Figure 8.14 shows the time history of the relative position of the follower quadrotor to the leader quadrotor. The desired relative distances are closely tracked. Figure 8.15 shows the rock, swing and heading angles of the load with the flexible bar. The two quadrotors are able to carry the load in a smooth fashion. From these figures, we see oscillations in the load angles for the first 10 secs of simulation, and the load angles then settle to about 4 degrees, 2 degrees and 0 degrees for the rock, swing and heading angles respectively afterwards. Figures 8.16 and 8.17 show

the propeller speeds of the quadrotors. There are no saturations in the speeds of the rotors.

Comparing the two control approaches implemented for the flexible bar case in this chapter, the full nonlinear approach has a faster formation geometry tracking performance but at the cost of more oscillations in the load angle deflections, albeit with smaller angular magnitude.

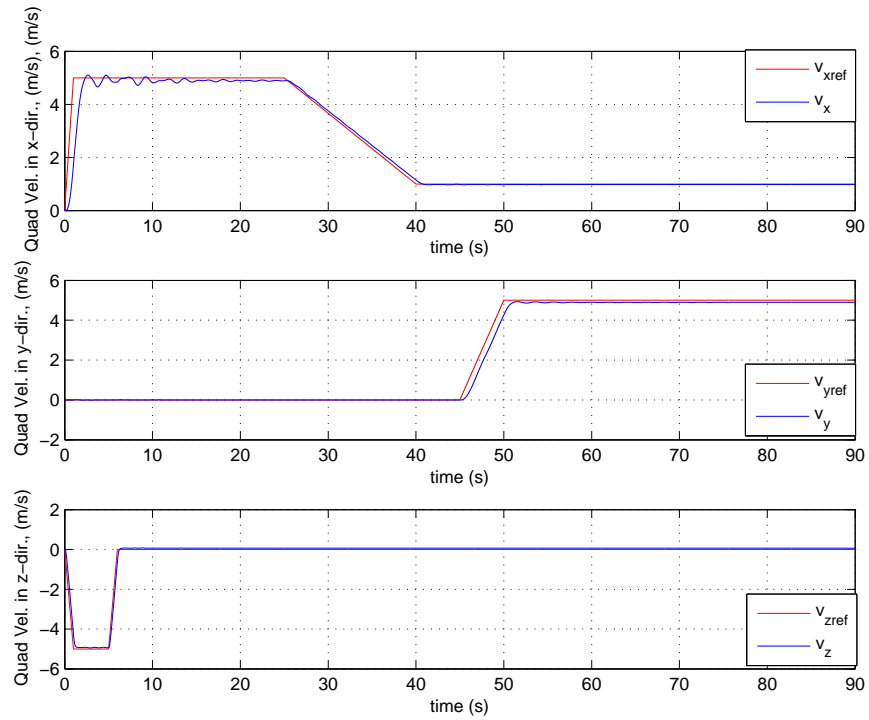


Figure 8.11: Leader Quadrotor Velocity in x, y and z directions respectively (Flexible Bar, Alternative Approach)

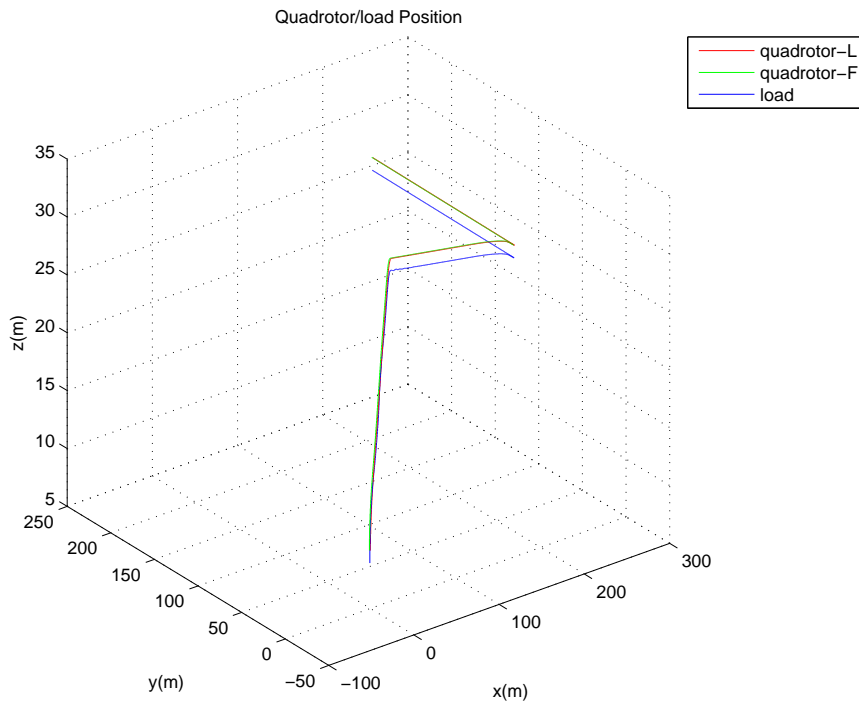


Figure 8.12: Leader and Follower Quadrotor position and Load Position (Flexible Bar, Alternative Approach)

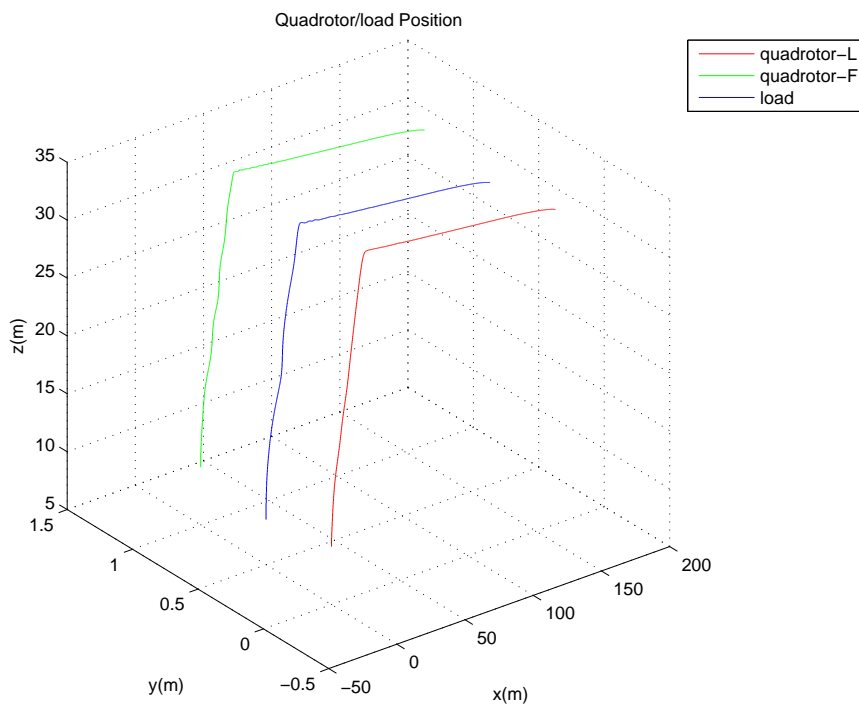


Figure 8.13: Leader and Follower Quadrotor position and Load Position (Flexible Bar, Alternative Approach, 40 secs simulation)

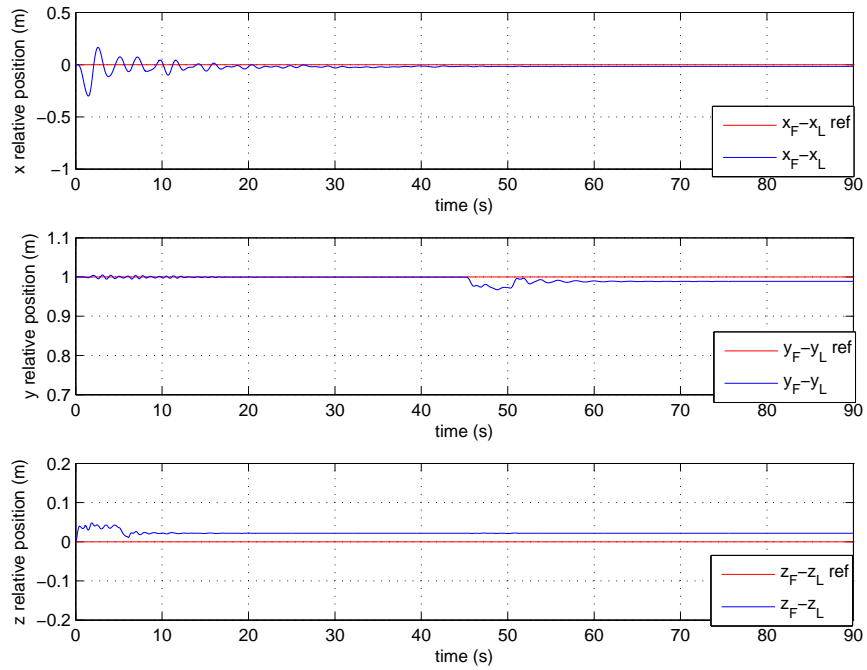


Figure 8.14: Leader and Follower Quadrotor relative positions (Flexible Bar, Alternative Approach)

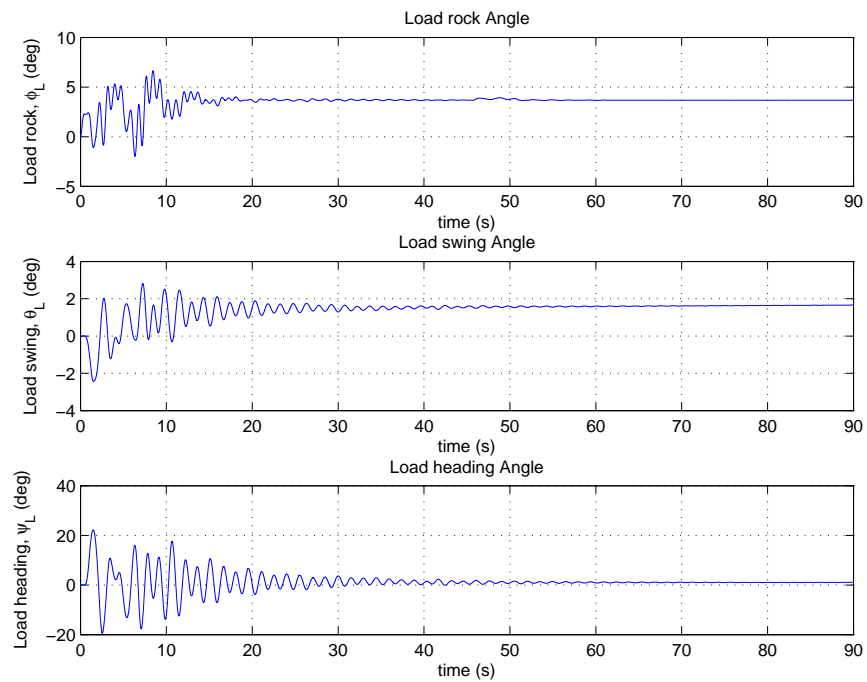


Figure 8.15: Swing, Rock and Heading Angles of the Load (Flexible Bar, Alternative Approach)

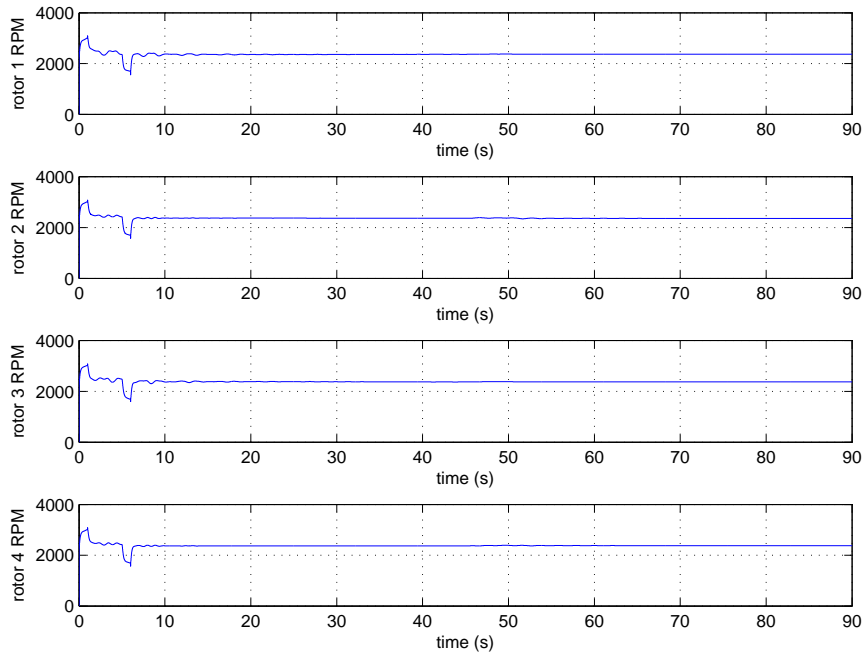


Figure 8.16: Propeller Speeds of the Leader Quadrotor (Flexible Bar, Alternative Approach)

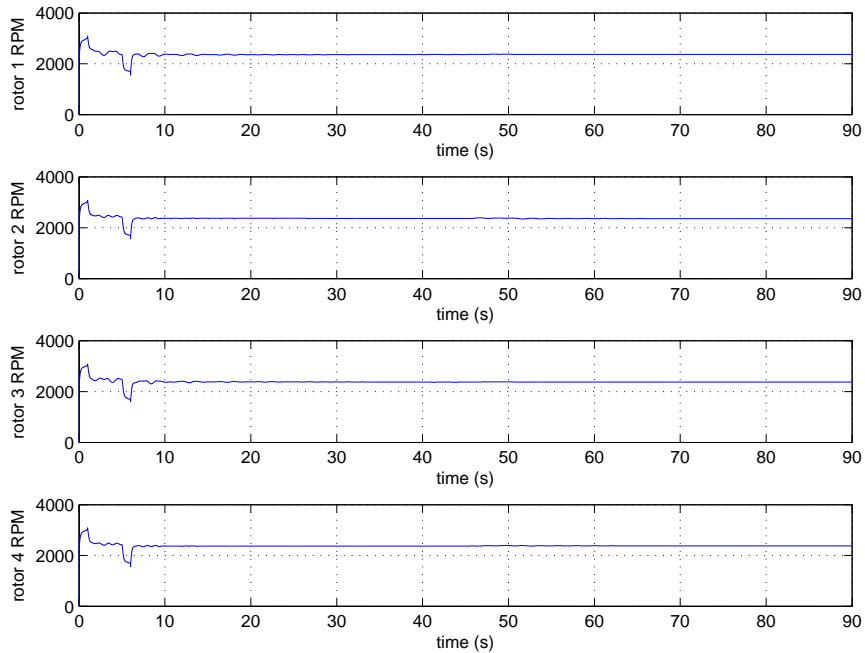


Figure 8.17: Propeller Speeds of the Follower Quadrotor (Flexible Bar, Alternative Approach)

8.4 Performance Effects of Different Beam Stiffness on the Control System in section 8.3

In this section, a performance robustness test was done by changing the stiffness of the aluminium beam to see how the flexibility of the beam affects the control system. This was done through the MSC ADAMS software by changing the thickness of the aluminium beam, as thickness is inversely proportional to flexibility, and importing the model to the MATLAB/SIMULINK environment. Three aluminium beams of thickness 0.4cm , 0.6cm and 0.8cm were used. The properties of the aluminium beam are presented in the table below.

Table 8.2: Aluminium Beam Properties

Aluminium Beam Thickness	Density	Weight
0.4 cm	2.7 g/cm^3	0.034 kg
0.6 cm	2.7 g/cm^3	0.076 kg
0.8 cm	2.7 g/cm^3	0.136 kg

8.4.1 Results and Discussion For Varying Beam Stiffness

The simulation results for a beam with 0.4cm thickness as been presented in section 8.3. The results would be compared with simulation results for 0.6 cm and 0.8 cm aluminium beams. Thus, the same flight scenario as used in section 8.3 is used for all three cases.

Figure 8.18 presents the leader quadrotor response to the velocity commands for the three beams. The leader is able to closely follow the desired command in all three cases. 8.19 shows the time history of the relative position of the follower quadrotor to the leader quadrotor. In all three cases, the desired formation geometry is tracked. However, there is a slight increase in steady state error as the beam becomes less flexible. There is a steady state error of 1% in the relative y position of the two quadrotors, and an offset of 0.02 m in the relative z direction for the 0.4 cm beam.

The steady state error in relative y-direction increased to 1.5% for the 0.6 cm and 2% for the 0.8 cm beam. The offset in relative z-direction also increased to 0.03m and 0.04m for the 0.6 cm and 0.8 cm beams respectively. Figure 8.20 shows the load rock, swing and heading angles for the three beams. They have similar angle deflection range in the three cases. However, we have more oscillations but smaller angle deflection as the beam gets more flexible.

Overall, the more flexible the beam, the faster the formation tracking performance, leading to smaller angle deflections of the load angles but at the cost of more oscillations in the load angles.

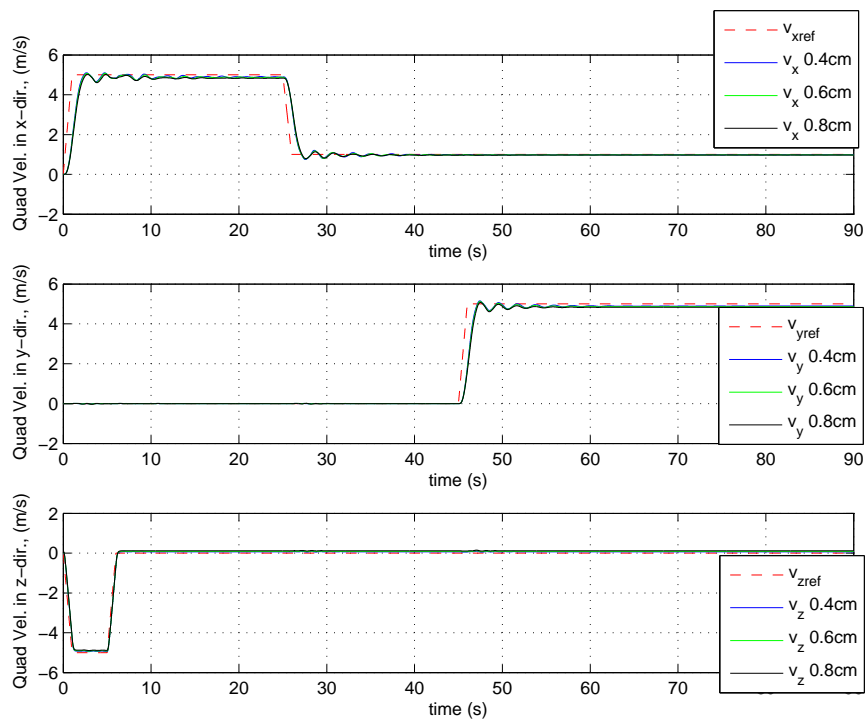


Figure 8.18: Leader Quadrotor Velocity in x, y and z directions respectively (Flexible Bar, Stiffness Variation)

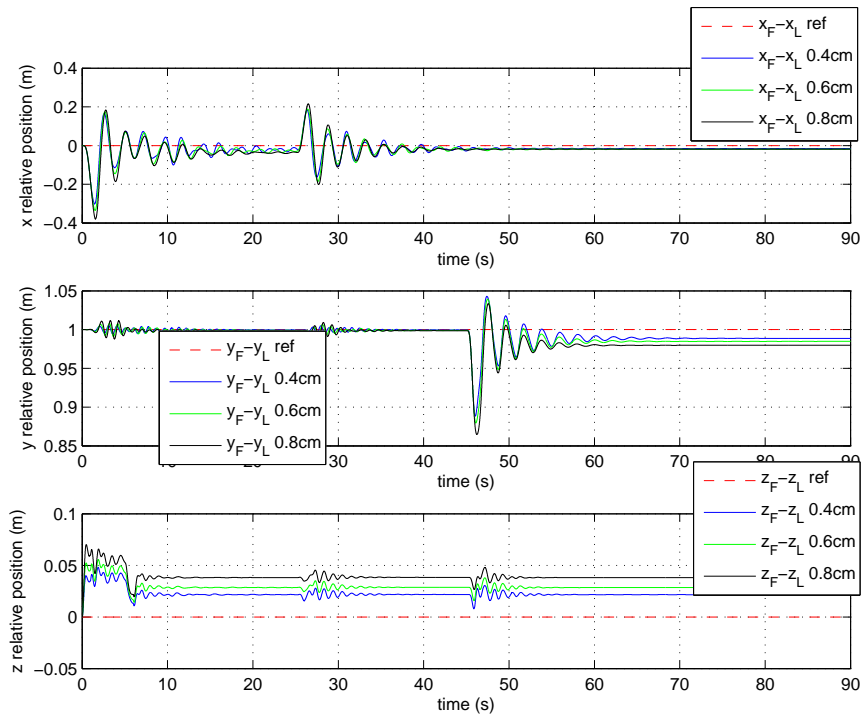


Figure 8.19: Leader and Follower Quadrotor relative positions (Flexible Bar, Stiffness Variation)

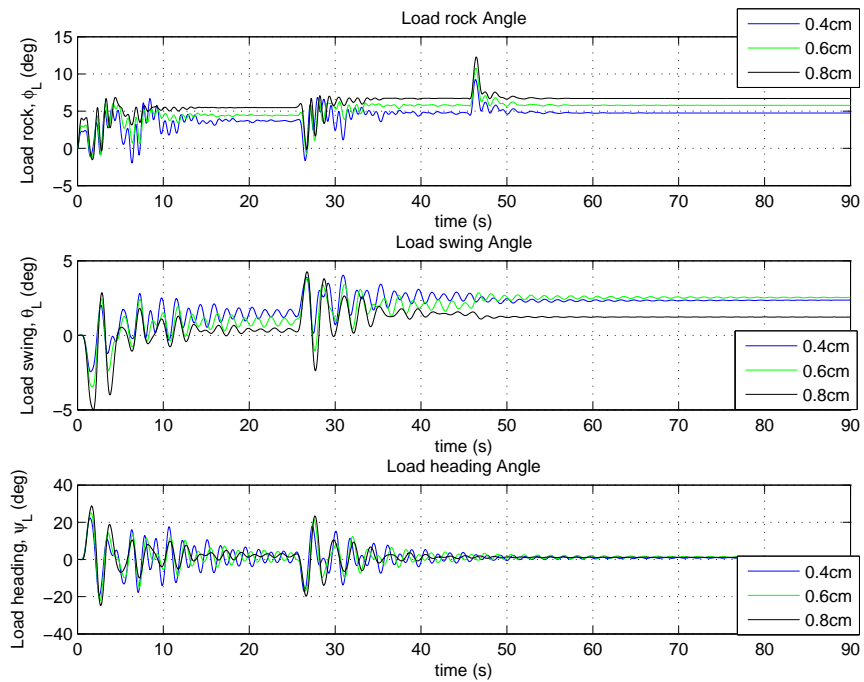


Figure 8.20: Swing, Rock and Heading Angles of the Load (Flexible Bar, Stiffness Variation)

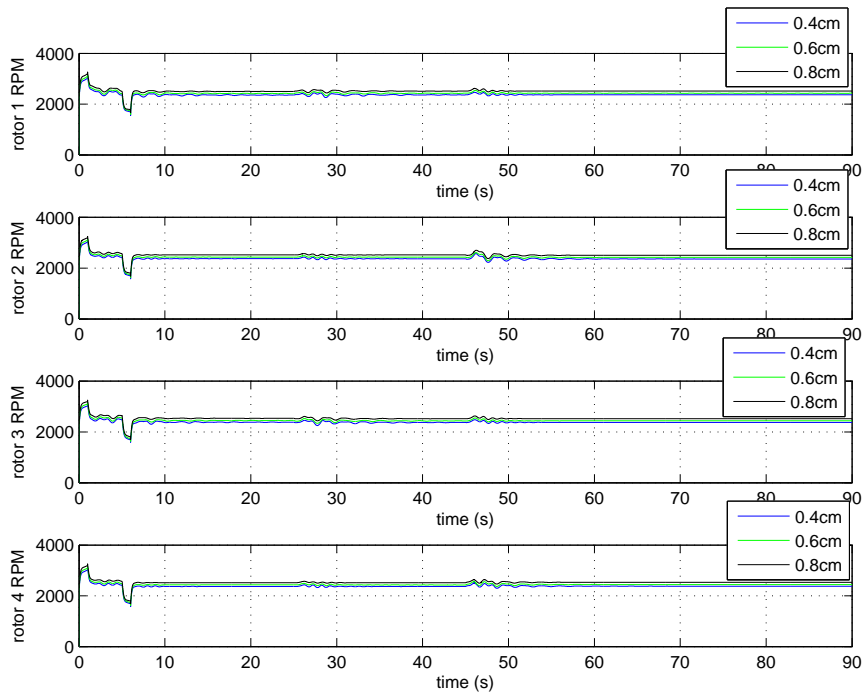


Figure 8.21: Propeller Speeds of the Leader Quadrotor (Flexible Bar, Stiffness Variation)

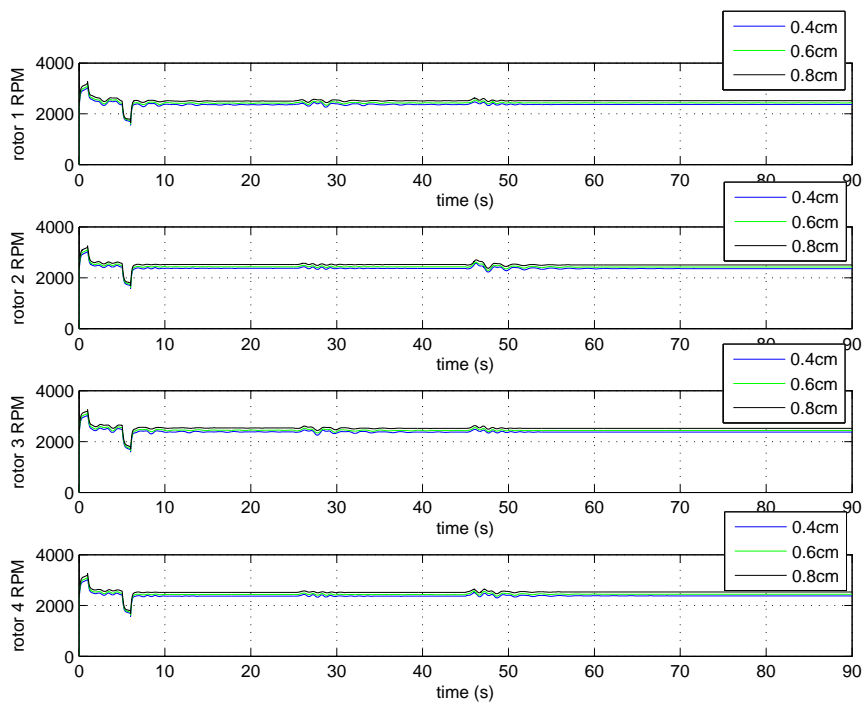


Figure 8.22: Propeller Speeds of the Follower Quadrotor (Flexible Bar, Stiffness Variation)

CHAPTER 9

SUMMARY AND CONCLUSIONS

9.1 Conclusion

In this thesis, the modelling and control of quadrotor slung load systems is investigated. Full nonlinear dynamical models of a single quadrotor slung load system, a two quadrotor slung load system and a three quadrotor slung load system is designed and modelled on the MATLAB/SIMULINK platform. For the two and three quadrotor case, the leader-follower control approach to formation flight was employed to enable the quadrotors fly in a fixed geometrical formation. In the Leader-follower approach to formation flight, the leader maintains a prescribed trajectory while the followers track a fixed relative distance from the neighboring aircraft. A two quadrotor slung load model with flexible bars was also modelled using the MSC ADAMS software.

To control the single quadrotor slung load system, two LQT controllers were designed on the quadrotor to track velocities in all three directions as well as the heading. The dynamics of the rigid bar and load were not included in the controller design. However, the LQT controller was robust enough to accommodate the disturbance from the bar and load when implemented on the nonlinear one quadrotor slung load model. However, there were considerably deflections in the load rock and swing angles as the quadrotor flew.

For the two quadrotor case, it is desired that the quadrotors fly in the prescribed formation as they carried the load. To achieve this, four control system algorithms were investigated:

- The first control system employed a two-loop architecture in which the two LQT controllers designed for the single quadrotor case was implemented in its inner loop. The outer loop contained a Lyapunov function based nonlinear formation guidance controller. This formation guidance controller used the leader quadrotor velocity and position, follower quadrotor position and the relative distance that the follower and leader quadrotor must maintain, to determine the velocities that follower quadrotor must track to maintain the formation geometry. These determined velocities are then sent to the innerloop. This control system worked quite nicely to fly the quarotors in a formation in spite of the slung load dynamics. The rock and swing angles of the load were considerably reduced when compared to the single quadrotor case.
- The second control approach involved a hierarchical three-loop architecture. The same Lyapunov function based formation guidance controller in the first approach is used in the outermost loop of this control system. The middle loop contained a LQT controller that uses the velocity commands coming from the outermost loop to generate a thrust vector direction. This thrust vector direction is then sent to the innermost loop which contained another Lyapunov function and quaternion based nonlinear attitude controller. This nonlinear attitude controller uses the thrust vector direction from the middle loop as well as a to-go quaternion to match the quadrotor's thrust vector with the thrust vector direction from the middle loop. This control system also worked nicely to fly the quarotors in a formation in spite of the slung load dynamics. The rock and swing angles of the load were also considerably reduced when compared to the single quadrotor case.
- The third control approach is fully nonlinear with a two loop control architecture. It features a Lyapunov function based algorithm in both its outer and inner loops. The inner loop is exactly the same with the inner loop of the second control approach, where attitude control is achieved through a to-go quaternion and thrust vector direction. Formation guidance and thrust vector command generation is achieved in the outer loop. This control system flies the quadrotors nicely as well in spite of the slung load.
- The fourth control approach is a modification of the previously designed con-

trol scheme developed in the third approach. In this approach, the additional force and torques of the slung load acting on the quadrotor are factored into the controller design as opposed to treating the slung dynamics as disturbances to the system. This scheme gave the smallest deflections in the load swing and rock angles.

The control approaches with the hierarchical two-loop architecture were more responsive than the control approach with a hierarchical three loop architecture.

For the three quadrotor case, the first control approach used for the two quadrotor case is implemented here. This control system also worked nicely to fly the quadrotors in a formation in spite of the slung load dynamics. The three quadrotors carried the load with the least amount of deflection in the rock and swing angles. We can thus conclude that each additional quadrotor in the slung load system introduces additional constraints on the load thereby limiting the rock and swing angles of the load.

The two controllers with the two-loop control architecture were also implemented on a two quadrotor slung load system with flexible bars. Our control systems were robust enough to fly the quadrotor slung load system in the desired trajectory and formation. However, they were considerably larger deflections in the load rock and swing angles as well as oscillations in the responses of the quadrotor slung load model when compared to the rigid bar case.

9.2 Future Work

The dynamics of the slung load were included in the nonlinear controller implemented on the follower quadrotor for the fourth control approach. However, they were not included in the controller implemented on the leader quadrotor. This is because the leader quadrotor controller had a linear outer loop. A future work could be to make the leader quadrotor controller fully nonlinear and also include the slung load dynamics in its design.

An obstacle avoidance scheme could also be added to the control system to enable the quadrotors avoid obstacles in their flight path as they carry the load.

Due to the fact that the leader-follower approach to formation control is not robust to leader failure and that the likelihood of higher error propagation increases with an increasing number of aircrafts in the formation, a different formation control approach may be investigated for cases with more than three quadrotors in the slung load system.

All the tests carried out were all software based. In the future, this algorithm may be implemented on actual quadrotor slung load systems to experimentally validate the efficacy of the control system.

REFERENCES

- [1] D. Glade, “Unmanned aerial vehicles: Implications for military operations,” tech. rep., Air Univ Press Maxwell Afb Al, 2000.
- [2] Z. Sarris and S. Atlas, “Survey of uav applications in civil markets,” in *IEEE Mediterranean Conference on Control and Automation*, p. 11, 2001.
- [3] J. M. Fowler and R. D’Andrea, “Distributed control of close formation flight,” in *Decision and Control, 2002, Proceedings of the 41st IEEE Conference on*, vol. 3, pp. 2972–2977, IEEE, 2002.
- [4] R. Ray, B. Cobleigh, M. Vachon, and C. St. John, “Flight test techniques used to evaluate performance benefits during formation flight,” in *AIAA Atmospheric Flight Mechanics Conference and Exhibit*, p. 4492, 2002.
- [5] U. O. Committee, “Formation flying.” http://www.unitedoperations.net/wiki/Formation_flying, 2018. [Last Visited 25-October-2018].
- [6] SHT-IHA, “İnsansız hava aracı sistemlerinin ayrılmış hava sahalarındaki operasyonlarının usul ve esaslarına İlişkin talimat,” 2013.
- [7] M. Chiaramonti, F. Giulietti, and G. Mengali, “Formation control laws for autonomous flight vehicles,” in *Control and Automation, 2006. MED’06. 14th Mediterranean Conference on*, pp. 1–5, IEEE, 2006.
- [8] M. Pachter, J. D’Azzo, and J. Dargan, “Automatic formation flight control,” *Journal of guidance, control, and dynamics*, vol. 17, no. 6, pp. 1380–1383, 1994.
- [9] K.-H. Tan and M. A. Lewis, “Virtual structures for high-precision cooperative mobile robotic control,” in *Intelligent Robots and Systems’ 96, IROS 96, Proceedings of the 1996 IEEE/RSJ International Conference on*, vol. 1, pp. 132–139, IEEE, 1996.

- [10] Z. Chao, L. Ming, Z. Shaolei, and Z. Wenguang, "Collision-free uav formation flight control based on nonlinear mpc," in *Electronics, Communications and Control (ICECC), 2011 International Conference on*, pp. 1951–1956, IEEE, 2011.
- [11] F. Giulietti, M. Innocenti, and L. Pollini, "Formation flight control-a behavioral approach," in *AIAA Guidance, Navigation, and Control Conference and Exhibit*, p. 4239, 2001.
- [12] T. H. Van den Broek, N. van de Wouw, and H. Nijmeijer, "Formation control of unicycle mobile robots: a virtual structure approach," in *Decision and Control, 2009 held jointly with the 2009 28th Chinese Control Conference. CD-C/CCC 2009. Proceedings of the 48th IEEE Conference on*, pp. 8328–8333, IEEE, 2009.
- [13] Y. Zou, P. R. Pagilla, and R. T. Ratliff, "Distributed formation flight control using constraint forces," *Journal of guidance, control, and dynamics*, vol. 32, no. 1, pp. 112–120, 2009.
- [14] T. Paul, T. R. Krogstad, and J. T. Gravdahl, "Uav formation flight using 3d potential field," in *Control and Automation, 2008 16th Mediterranean Conference on*, pp. 1240–1245, IEEE, 2008.
- [15] D. Galzi and Y. Shtessel, "Uav formations control using high order sliding modes," in *AIAA Guidance, Navigation, and Control Conference and Exhibit*, p. 6367, 2005.
- [16] R. Sattigeri, A. Calise, and J. Evers, "An adaptive approach to vision-based formation control," in *AIAA Guidance, Navigation, and Control Conference and Exhibit*, p. 5727, 2003.
- [17] O. Tekinalp and S. Ariyibi, "Nonlinear guidance of unmanned aircraft formations," in *AIAA Guidance, Navigation, and Control Conference*, p. 2007, 2015.
- [18] I. Palunko, R. Fierro, and P. Cruz, "Trajectory generation for swing-free maneuvers of a quadrotor with suspended payload: A dynamic programming approach," in *Robotics and Automation (ICRA), 2012 IEEE International Conference on*, pp. 2691–2697, IEEE, 2012.

- [19] E. Stoneking, “Newton-euler dynamic equations of motion for a multi-body spacecraft,” in *AIAA Guidance, Navigation and Control Conference and Exhibit*, p. 6441, 2007.
- [20] A.-R. Merheb, H. Noura, and F. Bateman, “Active fault tolerant control of quadrotor uav using sliding mode control,” in *Unmanned Aircraft Systems (ICUAS), 2014 International Conference on*, pp. 156–166, IEEE, 2014.
- [21] R. Xu and U. Ozguner, “Sliding mode control of a quadrotor helicopter,” in *Decision and Control, 2006 45th IEEE Conference on*, pp. 4957–4962, IEEE, 2006.
- [22] T. Madani and A. Benallegue, “Control of a quadrotor mini-helicopter via full state backstepping technique,” in *Decision and Control, 2006 45th IEEE Conference on*, pp. 1515–1520, IEEE, 2006.
- [23] S. Bouabdallah, A. Noth, and R. Siegwart, “Pid vs lq control techniques applied to an indoor micro quadrotor,” in *Proc. of The IEEE International Conference on Intelligent Robots and Systems (IROS)*, pp. 2451–2456, IEEE, 2004.
- [24] Z. T. Dydek, A. M. Annaswamy, and E. Lavretsky, “Adaptive control of quadrotor uavs: A design trade study with flight evaluations,” *IEEE Transactions on control systems technology*, vol. 21, no. 4, pp. 1400–1406, 2013.
- [25] M. H. Amoozgar, A. Chamseddine, and Y. Zhang, “Fault-tolerant fuzzy gain-scheduled pid for a quadrotor helicopter testbed in the presence of actuator faults,” *IFAC Proceedings Volumes*, vol. 45, no. 3, pp. 282–287, 2012.
- [26] B. Wie, H. Weiss, and A. Arapostathis, “Quaternion feedback regulator for spacecraft eigenaxis rotations,” *Journal of Guidance, Control, and Dynamics*, vol. 12, no. 3, pp. 375–380, 1989.
- [27] C. A. Arellano-Muro, B. Castillo-Toledo, A. G. Loukianov, L. F. Luque-Vega, and L. E. González-Jiménez, “Quaternion-based trajectory tracking robust control for a quadrotor,” in *System of Systems Engineering Conference (SoSE), 2015 10th*, pp. 386–391, IEEE, 2015.
- [28] E. Reyes-Valeria, R. Enriquez-Caldera, S. Camacho-Lara, and J. Guichard, “Lqr control for a quadrotor using unit quaternions: Modeling and simulation,” in

- Electronics, Communications and Computing (CONIELECOMP), 2013 International Conference on*, pp. 172–178, IEEE, 2013.
- [29] A. Tayebi and S. McGilvray, “Attitude stabilization of a vtol quadrotor aircraft,” *IEEE Transactions on control systems technology*, vol. 14, no. 3, pp. 562–571, 2006.
- [30] J. Carino, H. Abaunza, and P. Castillo, “Quadrotor quaternion control,” in *Unmanned Aircraft Systems (ICUAS), 2015 International Conference on*, pp. 825–831, IEEE, 2015.
- [31] E. Suiçmez, *Trajectory tracking of a quadrotor unmanned aerial vehicle (uav) via attitude and position control*. PhD thesis, Master’s thesis, MIDDLE EAST TECHNICAL UNIVERSITY, 2014.
- [32] M. J. Sidi, *Spacecraft dynamics and control: a practical engineering approach*, vol. 7. Cambridge university press, 2000.
- [33] D. S. Naidu, *Optimal control systems*. CRC press, 2002.
- [34] K. Ogata and Y. Yang, *Modern control engineering*, vol. 4. Prentice hall India, 2002.
- [35] H. K. Khalil, “Nonlinear systems,” *Prentice-Hall, New Jersey*, vol. 2, no. 5, pp. 5–1, 1996.
- [36] S. Ariyibi and O. Tekinalp, “Modeling and control of quadrotor formations carrying a slung load,” in *2018 AIAA Information Systems-AIAA Infotech@ Aerospace*, p. 0250, 2018.
- [37] O. Tekinalp and O. Atas, “Attitude control mechanization to de-orbit satellites using solar-sails,” in *Proceedings of the 2nd International Academy of Astronautics Conference on Dynamics and Control of Space Systems*, pp. 24–26.
- [38] B. Wie, *Space vehicle dynamics and control*. American Institute of Aeronautics and Astronautics, 2008.
- [39] S. Microelectronics, “Lis302sg.” <https://www.st.com/resource/en/datasheet/cd00187369.pdf>, 2019. [Last Visited 6-June-2019].

- [40] S. mircoelectronics, “L3gd20h.” <https://www.st.com/en/mems-and-sensors/l3gd20h.html>, 2019. [Last Visited 6-June-2019].
- [41] Matlab, “Wind shear block model.” <https://www.mathworks.com/help/aeroblks/windshear.html>, 2019. [Last Visited 6-June-2019].
- [42] Matlab, “Wind gust block model.” <https://www.mathworks.com/help/aeroblks/discretewindgust.html>, 2019. [Last Visited 6-June-2019].
- [43] M. S. Corporation, “Msc adams software.” <http://www.mscsoftware.com/product/adams>, 2018. [Last Visited 27-July-2018].

APPENDIX A

PERFORMANCE COMPARISON BETWEEN THE MSC ADAMS MODEL AND THE SIMULINK MODEL DESIGNED USING EQUATIONS OF MOTION

Comparison of the simulation codes developed in simulink using rigid bar slung load model obtained using the equations of motion derived in section 3.1 and a rigid bar slung load model using the ADAMS software is presented in this appendix to give some level of verification to the simulation codes developed. The full nonlinear controller developed in section 5.3 is used in both simulation models. The results are presented in figures A.1-A.3. The leader quadrotor is commanded to follow a prescribed velocity vector. The results given in fig. A.1 shows that the simulated leaders follow the command closely in both simulations. Their responses are also quite close to each other.

Follower velocities are presented in fig. A.2. It may be observed that the follower velocities obtained from both codes are also close to each other. The load angle deflections obtained from these two simulations are also presented in fig A.3. This figure also demonstrates that the simulation codes are giving similar results. It may be concluded that the ADAMS code embedded simulation is giving similar results to that of the simulation based on the equations presented in section 3.1.

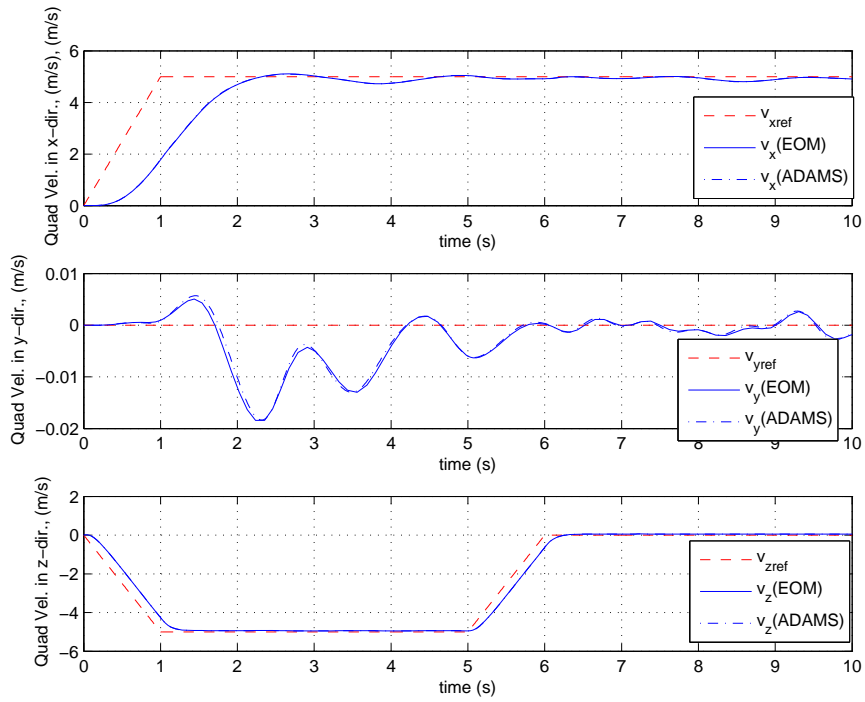


Figure A.1: Comparison between leader quadrotor velocities

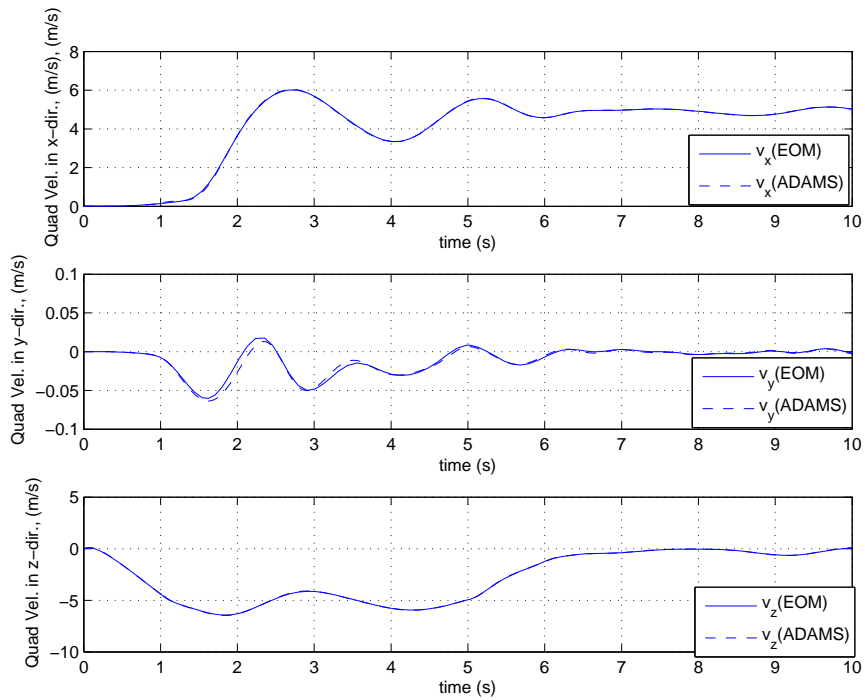


Figure A.2: Comparison between follower quadrotor velocities

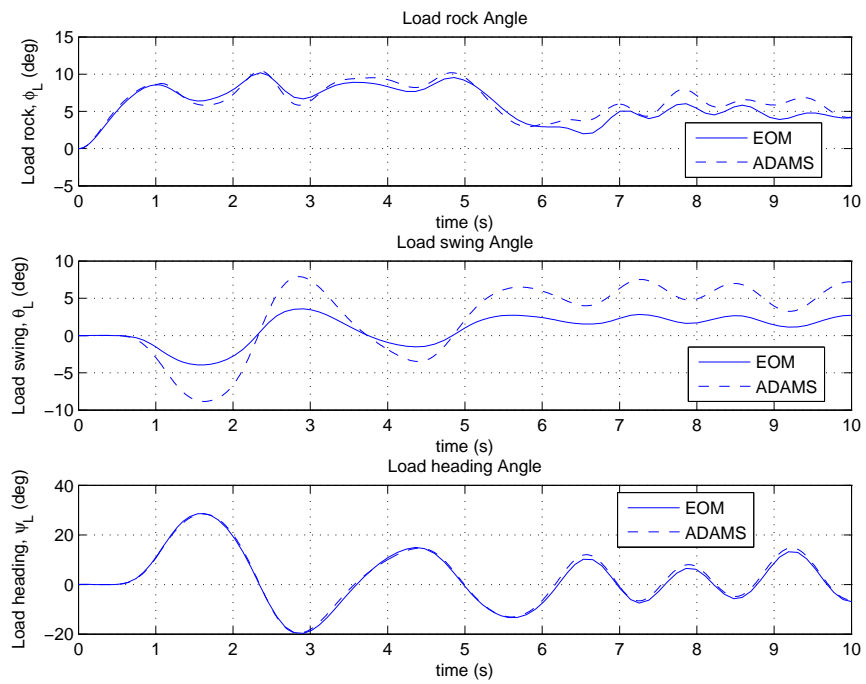


Figure A.3: Comparisons between load angle deflections

APPENDIX B

TWO QUADROTOR SLUNG LOAD SYSTEM EQUATION OF MOTION DERIVATION

A more detailed derivation process of the equation of motion of a two quadrotor slung load system is given in this appendix.

The two quadrotor slung load system is a multi-body system consisting of two quadrotors, two rigid bars and a load (5 Bodies). Consider the free body diagram of the 5-body system given below:

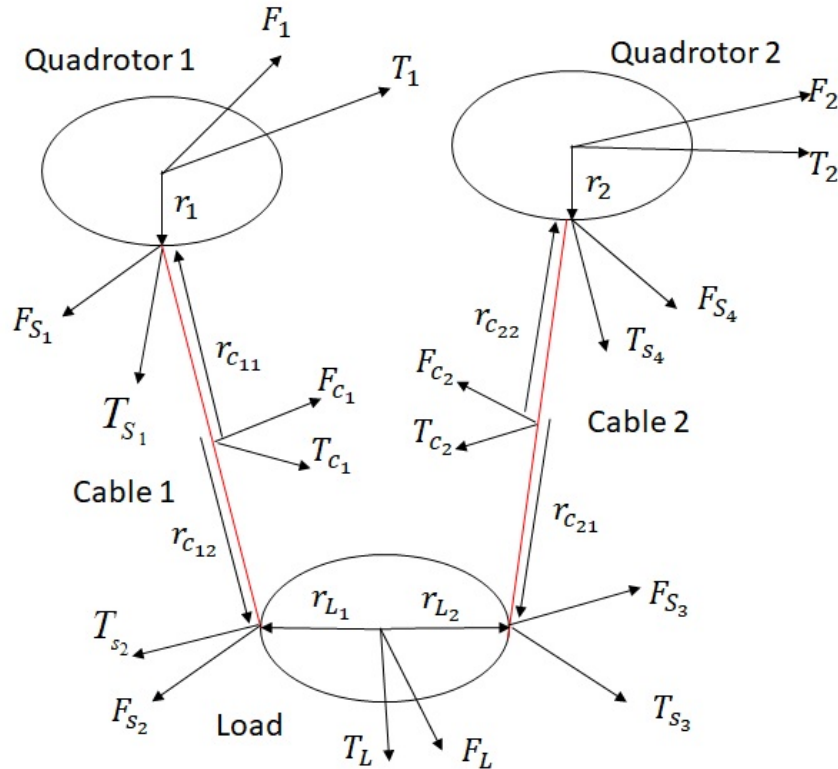


Figure B.1: Two Quadrotor Slung Load System Free Body Diagram

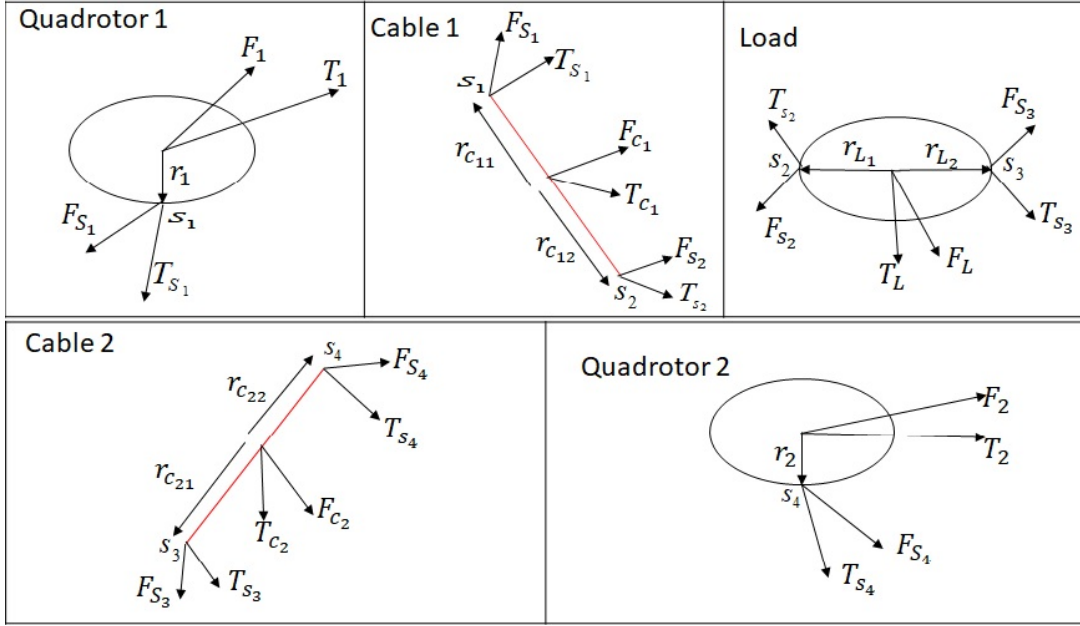


Figure B.2: Free body Diagram of the Individual dynamic entities

Let B_1, B_2, B_{c1}, B_{c2} and B_L be the body fixed reference frames on quadrotor 1, quadrotor 2, cable 1, cable 2 and the load respectively. Let the inertial frame be denoted as N . Then, all the vectors in the free body diagram expressed in their respective reference frames is given in table B.1 .

Table B.1: Reference frames for the expression of components of dynamic entities

Items expressed in B_1	$T_1, T_{s1}, \omega_1, \dot{\omega}_1, r_1$
Items expressed in B_2	$T_2, \omega_2, \dot{\omega}_2, r_2$
Items expressed in B_{c1}	$T_{c1}, T_{s2}, \omega_{c1}, \dot{\omega}_{c1}, r_{c11}, r_{c12}$
Items expressed in B_{c2}	$T_{c2}, T_{s4}, \omega_{c1}, \dot{\omega}_{c1}, r_{c21}, r_{c22}$
Items expressed in B_L	$T_L, T_{s3}, \omega_L, \dot{\omega}_L, r_{L1}, r_{L2}$
Items expressed in N	$F_1, F_2, F_{c1}, F_{c2}, F_L, F_{s1}, F_{s2}$ $F_{s3}, F_{s4}, \dot{v}_1, \dot{v}_2, \dot{v}_{c1}, \dot{v}_{c2}, \dot{v}_L$

The Newton-Euler equations can now be written for each body in the slung load system. The rotational equations of motion written in reference frame B_1 for quadrotor 1 is:

$$J_1 \dot{\omega}_1 = T_1 + T_{s1} - \omega_1^\times J_1 \omega_1 + r_1^\times C_N^1 F_{s1} \quad (\text{B1})$$

For cable 1 in reference frame B_{c1} :

$$J_{c1}\dot{\omega}_{c1} = T_{c1} - C_1^{c1}T_{S1} - r_{c11}^\times C_N^{c1}F_{S1} + T_{s2} + r_{c12}^\times C_N^{c1}F_{S2} - \omega_{c1}^\times J_{c1}\omega_{c1} \quad (\text{B2})$$

For the load in reference frame B_L :

$$J_L\dot{\omega}_L = T_L - C_{c1}^L T_{s2} - r_{L1}^\times C_N^L F_{S2} + T_{s3} + r_{L2}^\times C_N^L F_{S3} - \omega_L^\times J_L \omega_L \quad (\text{B3})$$

For cable 2 in reference frame B_{c2} :

$$J_{c2}\dot{\omega}_{c2} = T_{c2} - C_L^{c2}T_{S3} - r_{c21}^\times C_N^{c2}F_{S3} + T_{s4} + r_{c22}^\times C_N^{c2}F_{S4} - \omega_{c2}^\times J_{c2}\omega_{c2} \quad (\text{B4})$$

and finally for quadrotor 2 in reference frame B_2 :

$$J_2\dot{\omega}_2 = T_2 - C_{c2}^2 T_{S4} - r_2^\times C_N^2 F_{S4} - \omega_2^\times J_2 \omega_2 \quad (\text{B5})$$

The translational equations of motion for the bodies in the slung load system written in reference frame N are:

$$\begin{aligned} m_1\dot{v}_1 &= F_1 + F_{S1} \\ m_{c1}\dot{v}_{c1} &= F_{c1} + F_{s2} - F_{S1} \\ m_L\dot{v}_L &= F_L + F_{S3} - F_{S2} \\ m_{c2}\dot{v}_{c2} &= F_{c2} + F_{S4} - F_{S3} \\ m_2\dot{v}_2 &= F_2 - F_{S4} \end{aligned} \quad (\text{B6})$$

The constraint equations for the slung load systems can be obtained by equating the joint accelerations of the connecting bodies at joints s_1, s_2, s_3, s_4 .

At these connection points, we have:

$$\begin{aligned} v_{S1} &= v_1 + \omega_1^\times r_1 = v_{c1} + \omega_{c1}^\times r_{c11} \\ v_{S2} &= v_{c1} + \omega_{c1}^\times r_{c12} = v_L + \omega_L^\times r_{L1} \\ v_{S3} &= v_L + \omega_L^\times r_{L2} = v_{c2} + \omega_{c2}^\times r_{c21} \\ v_{S4} &= v_{c2} + \omega_{c2}^\times r_{c22} = v_2 + \omega_2^\times r_2 \end{aligned}$$

Differentiating these four velocities give the joint accelerations.

At joint s_1 , we have:

$$\dot{v}_1 + C_1^N \dot{\omega}_1^\times r_1 + C_1^N \omega_1^{\times \times} r_1 = \dot{v}_{c_1} + C_{c_1}^N \dot{\omega}_{c_1}^\times r_{c_{11}} + C_{c_1}^N \omega_{c_1}^{\times \times} r_{c_{11}}.$$

Then the relative acceleration of cable 1 to quadrotor 1 is:

$$\dot{v}_{c_1} - \dot{v}_1 = C_1^N \dot{\omega}_1^\times r_1 + C_1^N \omega_1^{\times \times} r_1 - C_{c_1}^N \dot{\omega}_{c_1}^\times r_{c_{11}} - C_{c_1}^N \omega_{c_1}^{\times \times} r_{c_{11}} \quad (\text{B7})$$

At joint s_2 , we have:

$$\dot{v}_{c_1} + C_{c_1}^N \dot{\omega}_{c_1}^\times r_{c_{12}} + C_{c_1}^N \omega_{c_1}^{\times \times} r_{c_{12}} = \dot{v}_L + C_L^N \dot{\omega}_L^\times r_{L_1} + C_L^N \omega_L^{\times \times} r_{L_1}$$

Then the relative acceleration of the load to cable 1 is:

$$\dot{v}_L - \dot{v}_{c_1} = C_{c_1}^N \dot{\omega}_{c_1}^\times r_{c_{12}} + C_{c_1}^N \omega_{c_1}^{\times \times} r_{c_{12}} - C_L^N \dot{\omega}_L^\times r_{L_1} - C_L^N \omega_L^{\times \times} r_{L_1} \quad (\text{B8})$$

At joint s_3 , we have:

$$\dot{v}_L + C_L^N \dot{\omega}_L^\times r_{L_2} + C_L^N \omega_L^{\times \times} r_{L_2} = \dot{v}_{c_2} + C_{c_2}^N \dot{\omega}_{c_2}^\times r_{c_{21}} + C_{c_2}^N \omega_{c_2}^{\times \times} r_{c_{21}}$$

Then the relative acceleration of cable 2 to the load is:

$$\dot{v}_{c_2} - \dot{v}_L = C_{c_2}^N \dot{\omega}_{c_2}^\times r_{c_{21}} + C_{c_2}^N \omega_{c_2}^{\times \times} r_{c_{21}} - C_L^N \dot{\omega}_L^\times r_{L_2} - C_L^N \omega_L^{\times \times} r_{L_2} \quad (\text{B9})$$

At joint s_4 , we have:

$$\dot{v}_{c_2} + C_{c_2}^N \dot{\omega}_{c_2}^\times r_{c_{22}} + C_{c_2}^N \omega_{c_2}^{\times \times} r_{c_{22}} = \dot{v}_2 + C_2^N \dot{\omega}_2^\times r_2 + C_2^N \omega_2^{\times \times} r_2$$

Then the relative acceleration of cable 2 to the load is:

$$\dot{v}_2 - \dot{v}_{c_2} = C_{c_2}^N \dot{\omega}_{c_2}^\times r_{c_{22}} + C_{c_2}^N \omega_{c_2}^{\times \times} r_{c_{22}} - C_2^N \dot{\omega}_2^\times r_2 - C_2^N \omega_2^{\times \times} r_2 \quad (\text{B10})$$

Equations B1 to B10 give the equations of motion for a two quadrotor slung load system. These equations can be put in a vector-matrix form and further simplified for faster computation in the MATLAB/SIMULINK Environment. Refer to sec. section 3.1 for the details.

CURRICULUM VITAE

PERSONAL INFORMATION

Surname, Name: Ariyibi, Segun

Nationality: Nigerian (NG)

Date and Place of Birth: 27.02.1990, Lagos State

Marital Status: Single

Phone: +90 551 407 0851

EDUCATION

Degree	Institution	Year of Graduation
Ph.D.	Middle East Technical University	2019
M.S.	Middle East Technical University	2014
B.S.	Fatih University	2010

PUBLICATIONS

International Conference Publications

S. Ariyibi and O. Tekinalp. "Nonlinear Guidance of Unmanned Aircraft Formations" AIAA Scitech, Orlando FL. January 5-9, 2015.

S. Ariyibi and O. Tekinalp. "Modeling and Control of Quadrotor Formations Carrying a Slung Load" AIAA Scitech, Kissimmee Florida, January 8-12, 2018.

S. Ariyibi and O. Tekinalp. "Control of a Quadrotor Formation Carrying a Slung Load Using Flexible Bars" AIAA Aviation and Aeronautics Forum and Exposition,

Dallas Texas. June 17-21, 2019.